Title
CORRELATIONS BETWEEN HIGH-TEMPERATURE CREEP BEHAVIOR AND STRUCTURE

Authors
Bird, James E.
Mukherjee, Amiya K.
Dorn, John E..

Publication Date
1969-07-01

A Review and Analysis - Prepared for The International Conf. on Quantitative Relation Between Properties and Microstructure, Haifa, Israel, July 27-August 1, 1969

UCRL-19056
Preprint

c.2

CORRELATIONS BETWEEN HIGH-TEMPERATURE CREEP BEHAVIOR AND STRUCTURE

James E. Bird, Amiya K. Mukherjee, and John E. Dorn

July 1969

AEC Contract No. W-7405-eng-48

LAWRENCE RADIATION LABORATORY
UNIVERSITY of CALIFORNIA BERKELEY

DISCLAIMER

CORRELATIONS BETWEEN HIGH-TEMPERATURE CREEP BEHAVIOR AND STRUCTURE

By

James E. Bird*, Amiya K. Mukherjee**, and John E. Dorn***

A Review and Analysis:

Prepared for The International Conference

on

Quantitative Relation

Between

Properties and Microstructure.

To be presented at

Haifa, Israel, July 27-Aug. 1, 1969

*Research Assistant, I.M.R.D. of Lawrence Radiation Laboratory, Berkeley, California

**Associate Professor Department of Mechanical Engineering, University of California, Davis, California.

***Professor of Materials Science, Department of Materials Science and Engineering, and Senior Research Metallurgist, Inorganic Materials Research Division, Lawrence Radiation Laboratory, University of California, Berkeley.

CORRELATIONS BETWEEN HIGH-TEMPERATURE CREEP BEHAVIOR AND STRUCTURE

Inorganic Materials Research Division, Lawrence Radiation Laboratory
Department of Materials Science and Engineering, and
College of Engineering University of California, Berkeley, California

ABSTRACT

Creep of metals and alloys at high temperatures is usually diffusion-controlled. Nevertheless, the creep behavior is often sensitive to various structural and substructural details. The secondary creep rates, $\dot{\varepsilon}_s$, of all coarse-grained fcc metals are given by

$$\dot{\varepsilon}_s = 2.5 \times 10^6 \frac{DGb}{kT} \left(\sigma/G\right)^n$$

where D = the diffusivity, G = the shear modulus of elasticity, b = the Burgers vector, kT = the Boltzmann constant times the absolute temperature, and σ = the applied tensile stress. The constant n increases from 4.4 for Al, to 5.3 for Ag in a consistent manner with increasing value of Gb/Γ where Γ is the stacking fault energy. Whereas, many alloys give the same trends, others in which the velocity of glide of dislocations is limited by solute atom diffusion, give

$$\dot{\varepsilon}_s \simeq 0.5 \frac{DGb}{kT} \left(\frac{\sigma}{G}\right)^3$$

At the steady state the substructure consists of subgrains demarked by low-angle boundaries and more or less randomly meandering dislocations within the subgrains. The density, ρ, of dislocations during steady state creep depends only on the applied stress and is given by the same relationship that applies to metals during low-temperature strain hardening, namely

$$\frac{\sigma}{2} = 0.6\ Gb\sqrt{\rho}$$

The subgrain diameter increases almost linearly with G/σ for examples of creep controlled by the dislocation climb mechanism.

Alloys that do not undergo initial straining do not exhibit the usual primary stage of transient creep. The decreasing creep rate that is observed after initial straining seems to arise as a result of dispersal of dislocation entanglements rather than to a decrease in the mobile dislocation density. Recent advances in developing a theory for transient stage of creep will be discussed.

The effects of grain size, grain boundary shearing, and dispersions on high temperature creep will be reviewed. Consideration will be given to the implications of creep behavior for understanding the phenomenon of superplasticity.

I. INTRODUCTION

Whereas some mechanical properties of crystalline solids, such as their moduli of elasticity, are only modestly influenced by the microstructural details, other mechanical properties, particularly those that relate to plastic behavior, are often quite sensitive to even small variations in grain size, orientation, types of substructures, and other microstructural features. High-temperature creep constitutes an outstanding example of a highly structure-sensitive phenomen; the creep rates of materials can easily be changed up to 10^6 times or more by introduction of microstructural and substructural modifications. It is wholly appropriate, therefore, that this subject be reported in a symposium that is devoted to the "Quantitative Relation Between Properties and Microstructure".

Creep refers to the continued deformation of materials under constant stress. Although it can take place over all temperatures above the absolute zero, it assumes major importance in the high-temperature range; namely above about one-half of the melting temperature. Even over this limited range of conditions, several different mechanisms of creep are known to be operative. It appears appropriate to limit the following discussion in this review to those examples for which rather definitive correlations can be made between the creep rate, the substructure and microstructure. As will be illustrated, a number of different diffusion-controlled mechanisms are known to determine high-temperature creep rates and each is influenced in its own unique way by substructural and microstructural modifications. It appears that those mechanisms are common to all crystalline materials. In this report,

however, emphasis will be placed on the creep of metals and alloys because more data is currently available on these systems.

It is the plan of this report to discuss the somewhat simpler case of steady-state creep followed by an analysis of transient creep. The mechanical behavior will be presented as concisely as possible, and major emphasis will be given to the substructural and microstructural correlations with the creep behavior.

II. TYPICAL CREEP CURVES

Several common types of high-temperature creep curves are illustrated schematically in Fig. 1, and documented in Table I. Most metals and alloys exhibit a reasonably extensive range of steady-state creep, Stage II, followed by an increasing creep rate, Stage III, characterized by micro-fissuring, local plastic deformation and creep rupture. Major differences between the creep curves of various materials, however, are noted over the initial creep period, Stage I. Type B, which enters the steady-state almost immediately, is typical of materials in which the substructure pertinent to creep remains substantially constant[1-6]. In contrast, the usual creep curves of Type A, obtained for all annealed metals[1] and some alloys, exhibit a decelerating primary creep rate, illustrating the continued formation of a more creep resistant substructure during the transient stage. These same metals and alloys give creep curves of Type C when they have been previously crept at a higher applied stress[7], or cold worked[1]. The increasing creep rate over Stage I denotes the recovery of the pertinent substructure to a steady-state condition. The same steady-state creep rate is obtained in these metals and alloys regardless of their previous mechanical treatment[8]. It is clear, therefore, that the secondary creep rate is obtained when a balance is reached between the rate of generation of the creep-resistant substructure and the rate of its thermal recovery under the applied stress. The sigmoidal type of creep curve over Stage I shown by Type D suggests[9] the nucleation and spread of slip zones until the steady-state is achieved. It has been observed in certain special dispersed phase alloys[10]. More complicated types of creep curves than those shown in

TABLE I. Metals which display creep curves similar to those illustrated in Fig. 1.

Type of Curve	Metal	Thermomechanical History	Reference
A	Ni	Annealed	1
B_1	Au	Annealed	2
B_1	AgMg	Annealed	3
B_2	Al	Annealed	4
B_2	Al-3.1%Mg	Annealed	5
B_3	Ag_2Al	Annealed	6
B_3	Ni	Cold Worked to $\varepsilon = 0.031$	1
C	Ni	Cold Worked to $\varepsilon = 0.034$	1
C	Al	Crept at Higher Stress	7
D	Nimonic Alloy	Annealed	9

Fig. 1, however, are obtained as a result of periodic recrystallization[11], or as a result of microstructural changes attending precipitation hardening, overaging, etc[12]. In order to limit this paper to tractable dimensions, the latter types of creep behavior will not be covered here.

III. NABARRO CREEP

Nabarro creep[13] results from the diffusion of vacancies from regions of high chemical potential at grain boundaries subjected to normal tensile stresses to regions of lower chemical potential where the average tensile stresses across the grain boundaries are zero. Atoms migrating in the opposite direction account for the creep strain. When volume diffusion controls, the tensile creep rate, $\dot{\varepsilon}_s$, is given by

$$\dot{\varepsilon}_s = A_n \frac{Db^3\sigma}{d^2kT} \tag{1}$$

where b is the Burgers vector, σ the applied stress, d the mean grain diameter, and kT the Boltzmann constant times the absolute temperature. The diffusivity, D, is obtained from the tracer diffusivity D^*. For pure metals

$$D = \frac{D^*}{f} \tag{2a}$$

and for binary solution alloys[11]

$$D = \frac{D_A^* D_B^*}{(N_B D_A^* + N_A D_B^*)f} \tag{2b}$$

where N_A and N_B are the atomic fractions of A and B atoms, and f is the correlation factor. The dimensionless constant A_n depends insensitively on the geometry of grains, but is generally estimated to have a value of from 8[13] to 5[15].

Nabarro creep does not involve the motion of dislocations. It predominates over high-temperature dislocation-dependent mechanisms only at low stress levels and then, only for fine-grained materials. Since it is unaffected by substructural changes, Nabarro creep gives curves of Type B_2 in which small transients are occasionally observed. Nabarro creep is characterized by creep rates that increase linearly with the stress and inversely with the square of the grain diameter, and have an activation energy that is nearly equal to that for self diffusion.

Nabarro creep has been studied in several investigations on pure metals and on a few alloy systems: Au[2,16] Ag[17,18], Cu[19,20], Ni[21], austenite[22], delta-Fe[22,23], Be[24], Mg[25], Fe-Si alloys[23,26], Ni-Cu alloys[27], dilute Fe-N[23], and dilute Fe-P alloys[23]. Investigations from which quantitative data could be extracted are listed in Table II and the data recorded in Fig. 2. In order to provide a ready comparison of Nabarro creep with other mechanisms to be discussed later, the data have been plotted in accordance with a reformulation of Eq. 1, namely

$$\frac{\dot{\varepsilon}_s\, kT}{DGb} = A_n \left(\frac{b}{d}\right)^2 \left(\frac{\sigma}{G}\right)^1 \qquad (3)$$

where G is the shear modulus of elasticity. The accuracy of the theoretical expression for Nabarro creep can be judged directly from the figure or Table II. The values predicted by Eq. 3, using the reported grain geometry information and the appropriate A_n, are shown in the

TABLE II: Experimental Investigations of Nabarro Creep in Metals

Theoretically predicted values of $\frac{\dot{\varepsilon}_s kT}{DGb}$ are given by $\frac{12.37}{\sqrt{2}}\left(\frac{b^2}{Dd}\right)\left(\frac{\sigma}{G}\right)$ for wire creep test specimens and by $\frac{7.48}{\sqrt{2}}\left(\frac{b^2}{Dd}\right)\left(\frac{\sigma}{G}\right)$ for thin foil and polycrystalline specimens.

Metal and Code	Data Source Ref.	Homologous Temperature Range of Creep Tests	Activation Energy in Kcal/mole for: Creep	Activation Energy in Kcal/mole for: Diffusion	Grain Size of Specimens (in mm.) Test Specimens	Wire Dia. or foil Thickness, D or t*	Average Grain Dimension, d**	Ratio of $\frac{\dot{\varepsilon}\ \text{exptl.}}{\dot{\varepsilon}\ \text{predicted}}$
Au(a)	2	0.89-0.97	48	44.2	Wire	0.028	0.028	
Au(b)	13	0.96-0.08	51	44.2	Wire	0.131	0.16	
Ag(a)	14	0.936			Wire	0.13	0.17	
Ag(b)	15	0.967			Wire	0.203	0.17 0.100	
Cu	16	0.91-0.98	56.8	47.1	Foil	0.203	0.051	
Ni	18	0.88-0.99	49.5	66.8	Wire	0.122	0.16	
Austenite	19	0.904		67.8	Wire	0.122	0.16	
Delta Fe	19	0.990	61	56.5	Wire	0.122	1.1	
Fe-6% Si	23	0.87-0.99	87	55.1	Wire	0.127	0.47	
Be	21	0.66-0.72	42±2	38	Rod	0.27**	0.27	

*Wire or foil test specimens generally develop grains which extend completely across their smallest dimension, the wire diameter, D or foil thickness, t.

**Equal to the grain size in thin foils or polycrystalline aggregates; equal to the average grain length in wire specimens which develop a "bamboo" structure.

figure for each creep investigation by dashed lines*. The "best fit" of the experimental data to Eq. 3 is shown by solid lines. The agreement between theory and experiment is generally quite good in view of the difficulties of accurately characterizing grain size and geometry, and in estimating A_N.

Further confirmation of Nabarro creep theory is provided by observations on the effect of grain size on creep rates. Investigations on Cu[19] and Be[24] have shown the predicted $1/d^2$ grain size dependence. Investigations on Ag[18] and Cu[19] have shown that negligible creep rates are produced in single crystals under test conditions which result in significant creep rates for fine-grained polycrystals. The evidence for Nabarro creep, at low stresses and high temperature, is often convincing. Limitations of Nabarro creep will be discussed in more detail later in this report.

IV. STEADY-STATE CREEP

A. General Aspects of Mechanical Behavior.

At high temperatures the rate of creep of most metals and many solid solution alloys is controlled by recovery of the dislocation substructure. When the temperature is high enough, in excess of from 0.55 to 0.7 of the

---

*Experimental information on secondary creep rates by other mechanisms will be summarized in figures identical with that of Fig. 2. The sources of the supplementary data needed for these figures, such as values for diffusivity, shear modulus, and stacking fault energy, are given in the Appendix. Pertinent details of the experimental creep investigations are summarized in tables usually located adjacent to the figures. Creep data obtained from tests performed with single crystals are distinguished from the more common polycrystalline test data by the symbol [S]. Alloy compositions are stated in terms of atomic percent unless otherwise noted. Table II summarizes information for the Nabarro creep investigations.

melting point, T_m, dislocation climb appears to be the rate-controlling recovery process and consequently the rate-controlling step of creep.

The rate of dislocation-climb creep depends sensitively upon the dislocation substructure that is present in the metal. Creep curves of types A, B_1, C and D are observed, dependent upon the initial condition of the metal and subsequent substructural changes. Eventually, a steady-state is achieved in which both the creep rate and the rate-controlling substructural details remain constant. As will be shown later, the steady-state creep rates and dislocation structure are independent of previous creep history and are reasonably reproducible. Consequently, steady-state creep is more readily analyzable than transient creep which also depends on the initial substructure.

In a recent survey[28], it was shown that many aspects of steady-state climb-controlled creep can be correlated by the semi-empirical equation

$$\frac{\dot{\varepsilon}_s kT}{DGb} = A_C \left(\frac{\sigma}{G}\right)^n \qquad (4)$$

where A_C and n are dimensionless quantities and the diffusivity, D, is given by Eqs. 2a or 2b. For climb-controlled creep of pure metals and solid solution alloys, n generally ranges in value from 4.2 to 7. Since Eq. 4 is based upon the assumption that steady-state creep is diffusion controlled, its use is restricted to temperatures where the activation enthalpy for creep, H_c, is equal to that for self-diffusion, H_d. Care has been exercised in the selection of data reported here to exclude creep tests where this condition is not fulfilled. More will be said about apparent activation energies for high-temperature creep later in this report.

B. Climb-Controlled Creep in FCC Metals.

All available data on the high-temperature steady-state creep rates of nominally pure FCC metals are correlatable in terms of Eq. 4, as documented in Fig. 3 and Table III. This compilation of secondary creep rates is based on more accurate values of D and G, as outlined in the Appendix, than was possible in previous surveys[28,46,47]. In addition, many new data have been added to provide a more complete picture of this correlation.

The trends shown in Fig. 3 confirm the validity of Eq. 4 for individual FCC metals. In fact, for a given value of σ/G, the values of $\dot{\varepsilon}_s kT/DGb$ for the different metals do not deviate more than about 60 times from the mean of the band.

If all factors pertinent to steady-state creep of FCC metals at high temperatures had been correctly incorporated into Eq. 4, all reliable data given in Fig. 3 should have clustered about a single straight line within experimental accuracy of determining $\dot{\varepsilon}_s$, T, D, G and σ. The fact that such a unique correlation is not obtained reveals that additional factors, not included in Eq. 4, are also pertinent for correlations of secondary creep rates.

In the case of FCC metals it appears that the major factor arises from effects of stacking-fault width on the dislocation climb mechanism. Feltham[48] and McLean[49] have suggested that, discounting a few exceptions, the creep rates of FCC metals seem to increase as the stacking-fault energy increases. Barrett and Sherby[38] interpreted this as an effect of stacking fault energy on A_c of Eq. 4. This concept was extended recently[28] by the authors of this present review who emphasized

Table III: Experimental Investigations of Climb-Controlled Creep in FCC Nominally Pure Metals

Data are taken from constant stress creep tests, with the exception of the Al(b), Ni(a), Pt(a), Ag(a), and Ag(d) tests which were conducted under constant load. n* is taken from the best fit line of Fig. 4. Creep rates are predicted from Eq. 5 using n*.

Metal	Ref.	Homologous Temperature Range of Creep tests	n, Determined from: Isothermal Creep tests	n, Determined from: Fig. 3	n*	A, Determined from: n,Exptl†	A, Determined from: n*	Average value of $\frac{\dot{\epsilon}\ \text{exptl}}{\dot{\epsilon}\ \text{predicted}}$
Al(a)	29	0.57-0.93	4.5	4.5	4.43	6×10^{6}	3×10^{6}	1.3
Al(b)	30	0.56-0.88	4.5	4.5	4.43	4×10^{6}	2×10^{6}	0.85
Al(c)	8	0.51-0.57		4.4	4.43	2×10^{6}	2×10^{6}	0.78
Al(d)[S]	31	0.55-0.96		4.4	4.43	1×10^{6}	1×10^{6}	0.54
Ni(a)	32	0.62-0.80	~4.7	4.7	4.74	8×10^{5}	1×10^{6}	0.45
Ni(b)	33	0.657	5.3	5.3	4.74	2×10^{7}	2×10^{5}	0.096
Ni(c)	34	0.62-0.80	~4.9	4.7	4.74	1×10^{7}	4×10^{6}	1.4
Pb[S]	35	0.62-0.99	4.7	~4.7	4.69	4×10^{6}	4×10^{6}	1.7
γ-Fe	36	0.67-0.86	~5.1	5.0	4.87	2×10^{7}	4×10^{6}	1.7
Cu(a)	37	0.717	~4.7	4.9	4.99	3×10^{5}	3×10^{6}	1.1
Cu(b)	38	0.72-0.90	4.8		4.99	5×10^{5}	3×10^{6}	1.1
Cu(c)	39	0.75-0.87		4.9	4.99	3×10^{6}	5×10^{6}	2.1

Table III - Cont.

Metal	Ref.	Homologous Temperature Range of Creep tests	n, Determined from: Isothermal Creep tests	n, Determined from: Fig. 3	n*	A, Determined from: n, Exptl†	A, Determined from: n*	Average value of $\frac{\dot{\epsilon}\ \text{exptl}}{\dot{\epsilon}\ \text{predicted}}$
Au	33	0.849	5.5	5.5	4.95	5×10^{8}	3×10^{6}	1.1
Pt(a)	40	0.59-0.63	5.0	5.0	5.08	3×10^{7}	7×10^{7}	2.7
Pt(b)	41	0.61-0.76	6.8	7.0	5.08	5×10^{13}	4×10^{7}	~14
Ag(a)	42	0.72-0.82	-	5.3	5.30	2×10^{6}	2×10^{6}	0.69
Ag(b)	43	0.707	-		5.30	7×10^{6}	7×10^{6}	2.9
Ag(c)	44	0.70-0.77	-		5.30	3×10^{5}	3×10^{5}	0.13
Ag(d)	45	0.66-0.70	-		5.30	2×10^{6}	2×10^{6}	0.69

†n determined from isothermal creep tests whenever data available.

that this approach assumes n to be the same constant for all FCC metals. The alternate possibility, however, is that A_c is a universal constant and that the remaining parameter, n of Eq. 4, increases with the dimensionless quantity Gb/Γ where Γ is the stacking-fault energy.

The nominal validity of the concept that n depends on the stacking-fault energy is shown in Fig. 4, where the datum points refer to average reported values* of n and Gb/Γ and the vertical and horizontal bars give the range of error estimated for these values. Excluding the data of Pt(b), Ni(b) which are obviously inconsistent with other investigations on the same metals, n increases systematically with Gb/Γ. Deviations from the "best-fit" solid line are within the range of scatter of the experimental data. As shown in summary in Table III all FCC metals exhibiting normal creep trends have about the same values of $A_c \simeq 2.5 \times 10^6$ when the "best-fit" value of n is adopted. Excluding the metal Pt, for which Gb/Γ is not well-established, the secondary creep rates of all FCC metals (17 confirming examples) are given by

$$\frac{\dot{\varepsilon}_s kT}{DGb} = 2.5 \times 10^6 \left(\sigma/G\right)^n \qquad (5)$$

within a factor of about two when n is selected from the "best-fit" curve of Fig. 4. Such predicted curves are shown in Fig. 5, which can be compared directly with Fig. 3.

---

*The sources of Gb/Γ data are described in the appendix; values of n were taken from Table III.

TABLE IV: Experimental Investigations of Climb-Controlled Creep in Nominally Pure BCC Metals

Creep data for α-Fe, β-Tl, V, and Mo(a) are from constant stress tests. Other data are from constant load tests.

Metal	Ref.	Homologous Temperature Range of Creep Tests	n, Determined from: Isothermal Creep Tests	A, Determined from Exptl. n
α-Fe (a)	50	0.486-0.568	6.9	7×10^4
α-Fe (b)	51	0.428-0.636	4*, 5-7**	4×10^5
α-Fe (c)	52	0.515	4.5	8×10^4
α-Fe (d)†	52	0.538	4.0	4×10^5
Mo (a)[S]‡	53, 235	0.582	~6	1×10^{13}
Mo (b)	54	0.665-0.958	~5.5	3×10^9
Ta	55	0.600-0.895	4.2	1×10^6
β-Tl	56	0.88-0.96	~5.4	2×10^9
W (a)	57	0.694-0.844	7.0	8×10^{14}
W (b)	58	0.694-0.735	5.5	6×10^{10}
W (c)	59	0.605-0.681	6.0 and 4.2	5×10^{12}
W (d)	59	0.605	6.0	1×10^{13}

Metal	Ref.	Homologous Temperature Range of Creep Tests	n, Determined from: Isothermal Creep Tests	A, Determined from Exptl. n
W (e)	60	0.570-0.900	4.6	4×10^{7}
V	61	0.552-0.862	~4 ℘	3×10^{5}

*$T \geq 700°C$ and $\sigma/G < 3 \times 10^{-4}$

**$T < 700°C$ and $\sigma/G > 3 \times 10^{-4}$

†Determined from creep and stress relaxation tests.

‡$\dot{\epsilon}$ values are estimated from tests which closely approached steady-state creep.

℘Isothermal data unavailable.

C. Climb Controlled Creep in BCC Metals.

All available data on the high-temperature steady-state creep rates of BCC metals (for which $H_c \simeq H_d$) are summarized in Fig. 6 and Table IV. As for FCC metals, the effects of stress and temperature on the steady-state creep rates in any test series seems to agree reasonably well with that suggested by Eq. 4. In contrast to the FCC metals, the values of n for BCC metals seem to vary much more widely, from 4 to 7. This might suggest that some additional factors, not documented in Eq. 4, influence the steady-state creep rates of BCC metals. Unlike the case of FCC metals, however, no systematic variations in either n or A_c with respect to obvious variables, are discernable. In fact, the variations in n appear to be as great from one investigator to another on the same metal as they appear to be from one metal to another. This fact is illustrated by the range of n values reported by different investigators for α-Fe and for W as shown in Table IV. Discounting the Mo(b) and W(a) data, which appear to be somewhat suspect in terms of questionable experimental control, all of the BCC data fall in a band of $\dot{\varepsilon}_s kT/DGb$ values that has a variation of less than about 10 times from the median of the band:

$$\frac{\dot{\varepsilon}_s kT}{DGb} = 2.5 \times 10^6 \left(\frac{\sigma}{G}\right)^{4.4} \qquad (6)$$

It is significant that this variance is substantially less than that noted for the FCC metals. It may also be significant that the creep rates of the BCC metals, when plotted in accordance with Eq. 4, are similar in magnitude to those of Al, a metal in which dislocations are also substantially unextended. Although there is no firm evidence at present as to what factors might be responsible the variance in n or the steady-

state creep rates of BCC metals, it appears likely that purity might have some effect.

D. Climb Controlled Creep in HCP Metals

All pertinent data for dislocation climb controlled steady-state creep in HCP metals are summarized in Fig. 5, and Table V. Discounting α-Tl, which undergoes a phase transformation at slightly higher temperatures, the creep rates of the remaining HCP metals can be represented by the average relationship.

$$\frac{\dot{\varepsilon}_s kT}{DGb} = 2.5 \times 10^6 \left(\frac{\sigma}{G}\right)^{5.25} \qquad (7)$$

to within a factor of about 5 times. This equation agrees quite well with that for creep of FCC metals with low stacking-fault energies.

The creep of HCP metals at temperatures greater than 0.6 to 0.7 T_m appears to be governed by a separate mechanism which is characterized by a distinctly higher activation energy, given approximately by 27 RT_m[67], where R is the gas constant and T_m is the melting point of the metal. The mechanism is as yet unidentified and will not be considered here.

E. Climb-Controlled Creep of Solid-Solution Alloys

At sufficiently high temperatures some solid-solution alloys creep in accord with Weertman's viscous drag[68] mechanism and others creep in nominal agreement with Weertman's dislocation climb mechanism[69,70]. Only alloys in the second group will be considered in this section.

All known examples of creep in binary alloys for which D and G are also available are correlated in Fig. 8 and Table VI. Examples for which D and G are unavailable are listed in Table VII. Most of the analyzed

TABLE V: Experimental Investigations on Climb-Controlled Creep in Nominally Pure HCP Metals

All data are from constant stress tests. Creep data obtained at high temperatures where $H_c > H_d$ have been excluded from the analysis.

Metal	Ref.	Homologous Temperature Range of Creep Tests	n, Determined from: Isothermal Creep Tests	n, Determined from: Fig. 7	A, Determined from n of Fig. 7
Cd	62	0.576-0.710	~4.3	4.3	1×10^3
Mg (a)	63	0.497-0.604	~5.7	~5.7	6×10^6
Mg (b)	64	0.59 and 0.757	4.2	~5.7	8×10^7
α-Tl	56	0.582-0.847	~5.0	5.0	1×10^8
Zn (a)	65	0.596-0.782	~4.5	4.6	3×10^4
Zn (b)	66	0.597-0.735	~7	4.6	3×10^4

TABLE VI: Experimental Investigations of Climb-Controlled Creep in Binary Solid Solution Alloys

All data obtained from constant stress creep tests, except for AgMg which was tensile-tested at a constant rate of strain.

Alloy	Ref.	Homologous Temperature Range of Creep Tests	n, Determined from: Isothermal Creep Tests	n, Determined from: Fig. 8	n*, Selected from Fig. 4	A, Determined from Exptl. n	Average value and exptl. of predicted
Cu-10.3 % Zn	71	0.68-0.75	4.8	4.8	5.19	1×10^4	0.070
Cu-20.3 % Zn	71	0.68-0.75	5.3	5.4	5.68†	2×10^5	0.90
Cu-30.7 % Zn	71	0.69-0.75	5.2	5.4	5.87†	8×10^4	3.6
Ni-13.0 % Cu	39	0.58-0.83	~5.3	~5.2	4.89	4×10^7	0.70
Ni-45.6 % Cu	39	0.62-0.83	~5.0	~5.3	4.98	8×10^4	0.029
Ni-78.5 % Cu	39	0.68-0.89	~4.7	~4.9	4.88	8×10^4	0.049
Ni-10.0 % Cr	34	0.59-0.85	~5	5.0	4.81	4×10^6	0.43
Ni-19.9 % Cr	34	0.65-0.71	-	-	4.87	-	0.38
Ni-24.2 % Cr	34	0.65-0.71	-	-	4.95	-	0.47
Ni-29.7 % Cr	34	0.62-0.85	~5.0	~5.0	5.05	1×10^6	0.75
Ni-12.0 % Fe	72	0.68-0.74	5.5	5.5	4.89	2×10^8	0.65
Ni-20.7 % Fe	72	0.65-0.74	4.9	5.1	4.88	5×10^5	0.17

Alloy	Ref.	Homologous Temperature Range of Creep Tests	n, Determined from: Isothermal Creep Tests	n, Determined from: Fig. 8	n*, Selected from Fig. 4	A, Determined from Exptl. n	Average value and exptl. of predicted
Ni-25.8 % Fe	72	0.69-0.75	5.4	5.4	4.96	3×10^7	0.51
Ni-31.0 % Fe	72	0.69-0.75	5.5	5.5	4.93	3×10^7	0.19
Ni-40.7 % Fe	72	0.69-0.75	~6	5.5	4.98	1×10^9	0.37
Ni-61.1 % Fe	72	0.69-0.74	5.2	5.2	5.29	1×10^7	11
Ni-80.3 % Fe	72	0.65-0.73	4.5	4.8	5.02	3×10^5	5.1
Fe-5.8 % Si (3 wt. % Si)	73	0.510	5.3	5.3	-	1×10^7	-
AgMg [S] (50.7% Mg)	3	0.67-0.76	5.7	5.7	-	5×10^8	-

† Obtained from linear extrapolation of "best fit" line in Fig. 4.

Table VII: Experimental Investigations of Climb-Controlled Creep in Binary Solid Solutions

Alloy (at.%)	Crystal Structure	n	Ref.
Ni - 10 to 30% W	FCC	4-7	74
Austenitic Stainless Steels	FCC	4.2	75
		4	76
		4.75	77
Pb - 0 to 16% Bi	FCC	4.5	35
Fe - 2 to 11% Si	BCC	4-10	78
Fe - 7.5% Si	BCC	6.3	79
Fe - 0 to 4.5% Si	BCC	-	80
Fe - 11 to 28% Al	BCC	4.6-6.8	81
Fe - 15 to 20% Al	BCC	4.7-6	82
Fe - 0.3 to 5.2% Mo	BCC	-	80
Fe - 0 to 4.2% Mo	BCC	4-10	83
Fe - 1.9 to 9.6% Co	BCC	-	80
Fe - Cr	BCC	4.0	84
Nb - 0 to 10% Mo	BCC	4.2-6.2	85
Mg - 12% Li	HCP	4.8,4.9	86,87
FeCo - 2% V	BCC CsCl *	4.8	88

*Undergoes a order-disorder reaction at $T \simeq 0.82\ T_m$

data are for FCC alloys, although one BCC alloy is included, Fe-5.8% Si. AgMg, which is an intermetallic compound with a CsCl lattice type, has been included in the data analysis but will be discussed later.

The steady-state creep rates of the FCC alloys that obey the dislocation-climb mechanism fall into a wide band similar to that of the FCC metals. A comparison of Fig. 8 with Fig. 3, shown schematically in Fig. 9, shows that the band for the alloys is displaced towards lower creep rates than that of the metals. In all cases examined, the value of $\dot{\varepsilon}_s kT/DGb$ was reduced by solid solution alloying, in some cases only slightly but in others by over an order of magnitude.

It seems likely that Gb/Γ has the same effect on the steady-state creep rates of FCC alloys which undertake the dislocation climb mechanism as it does for the FCC metals. This effect may be responsible for the slightly lower creep rates of the alloys, as it is generally observed in most metals that stacking fault width increases with alloying. Alloying of such metals should thus be accompanied by a decrease in creep rate and a small increase in n.

Experimental uncertainties in the values of both n and Gb/Γ make a direct comparison of n versus Gb/Γ for alloys, such as was done for pure metals in Fig. 6, almost valueless. As Fig. 9 shows the stress range covered by the creep investigations of the FCC alloys is rather narrow in comparison to that used for FCC metals. The experimental uncertainties in n are consequently much greater for the alloys than those of the pure metals. Furthermore, as pointed out in the Appendix, the available Gb/Γ values for several of the alloys may represent just first approximations to the true value. For this reason, an indirect method was used to check the possible dependence of creep rate and n on stacking-fault energy. The "best fit" line of Fig. 6, which was deduced from the more

reliable pure metal values, was used to obtain n for each alloy from Gb/Γ data. Both this value and the experimentally determined values of n are listed in Table VI. Then values of $\dot{\varepsilon}_s kT/DGb$ were calculated using Eq. 5 and compared to those obtained experimentally. Agreement between the two rates to within a factor of five was obtained for all but two FCC alloys.

On this basis, it is suggested that the steady-state creep rates of FCC alloys undertaking the dislocation-climb mechanism can be correlated reasonably well with those for FCC metals assuming the validity of $n \equiv n\left\{Gb/\Gamma\right\}$ given in Fig. 6 and Eq. 5. Whereas $\dot{\varepsilon}_s bT/DGb$ could have been correlated almost equally well with σ/G by assuming that n is constant and that $A_c \equiv A_c\left\{Gb/\Gamma\right\}$ for the alloys, such a correlation appears inferior to the one that is adopted here for the FCC metals themselves.

Dislocation climb-controlled creep is frequently observed in BCC alloys as Table VII shows. It is also observed in HCP alloys, although few data for HCP alloys have yet been generated. Because of the sparcity of diffusivity data on these alloys, most of the available data cannot be correlated using Eq. 4. Data for one alloy, Fe-5.8% Si, has been analyzed by making the assumption that the diffusivity can be extrapolated for high temperatures without being significantly lowered in value by ferromagnetic ordering. The correlated creep rate is similar to those of the FCC alloys as Fig. 8 shows, and the creep rate of the alloy can be predicted to within a factor of four if the experimentally determined value of n is used in Eq. 5. No conclusions should be drawn from this isolated example. However, it seems probable that the creep behavior of BCC and HCP alloys is not unlike that of the pure metals and FCC alloys whenever the climb mechanism is rate-controlling.

F. Viscous Glide Creep of Solid Solution Alloys.

The climb mechanism is rate-controlling in solid solution alloys whenever dislocation glide is rapid. As previously shown, it is characterized by values of n which range from 4.2 to 7. But some solid solution alloys display values of n during creep which are much lower, $3 \leq n \leq 3.6$. This type of behavior is obtained whenever the creep rate is controlled by viscous glide of dislocations, as Weertman first demonstrated[68].

A number of different dislocation-solute atom mechanisms may be responsible for producing viscous glide creep in solid solution alloys. Any interaction mechanism that can reduce the rate of gliding dislocations to a value which is so low that glide becomes slower than dislocation-climb recovery can produce such creep behavior. In principle several mechanisms can do this. When solute atoms are bound to dislocations through the Cottrell[89], Suzuki[90], or other analogous interaction mechanisms[91,92], glide can proceed no faster than the rate of solute atom diffusion. When disorder is introduced into a crystal by glide of a dislocation, the steady-state glide velocity is limited by the rate at which chemical diffusion can reinstate order behind the gliding dislocation. In such alloys glide is diffusion-controlled, and is consequently much slower than glide in pure metals. In some metals, at least, this can lead to glide-controlled creep.

A straightforward derivation for the rate of glide-controlled creep, which does not invoke fixed dislocation sources or glide of dislocation arrays, can be made for the simple case where all dislocations within a crystal drag Cottrell atmospheres. Because steady-state creep is

restricted to high temperatures we need consider only dilute solute atom atmospheres, where each extra solute atom of the atmosphere subtends a distance λ of the dislocation. Under steady-state conditions the force acting on the dislocation segment λ due to a tensile stress σ, namely $\frac{\sigma}{2} \lambda b$, equals the force exerted on each additional atmosphere atom. As each atom jumps forward one Burgers vector under the action of this force, the dislocation also moves forward one Burgers vector. Therefore, as shown by Friedel[93], the steady-state tensile strain rate can be approximated by

$$\dot{\varepsilon}_s \simeq 2/3\, \rho b v \simeq 2/3\, \rho b \left(\frac{\nu b}{\lambda}\right) b \exp\left(\frac{-g_d}{kT}\right) \left\{\exp\left(\frac{+\sigma\lambda b^2}{2kT}\right) - \exp\left(\frac{-\sigma\lambda b^2}{2kT}\right)\right\} \quad (8)$$

where v is the mean dislocation velocity, ρ the dislocation density, ν the Debye frequency and g_d is the free energy of activation for solute atom diffusion. Since $\sigma\lambda b^2 << 2kT$ and the diffusivity is given by

$$D \simeq \nu b^2 \exp(-g_d/kT) \quad (9)$$

the viscous drag equation reduces to

$$\dot{\varepsilon}_s = 2/3\, \rho D \frac{\sigma b^3}{kT} \quad (10)$$

The diffusivity for these cases differs from that given for the climb mechanism since it refers to the chemical interdiffusivity of the alloy, $\tilde{D}$, or equivalently to the Darken[94] expression for interdiffusivity

$$\tilde{D} = \left(N_A D_B^* + N_B D_A^*\right)\left(1 + \frac{\partial \ln \gamma_A}{\partial \ln N_A}\right) \quad (11)$$

for binary solutions where γ_A is the activity coefficient of the A species.

As will be demonstrated later, the density of dislocations, ρ, is given by

$$\sigma/_2 \simeq \alpha\, Gb\sqrt{\rho} \tag{12}$$

where α is a constant equal to about 0.6. Consequently, the tensile strain rate is given by

$$\dot{\varepsilon}_s \simeq \frac{1}{6\alpha^2}\,\frac{DGb}{kT}\left(\sigma/_G\right)^3 \tag{13}$$

or equivalently by

$$\frac{\dot{\varepsilon}_s kT}{DGb} = A_g\left(\frac{\sigma}{G}\right)^n \tag{14}$$

which is analogous to Eq. 4. For the simple case of viscous glide creep that has been considered

$$\frac{\dot{\varepsilon}_s kT}{DGb} = 0.5\left(\frac{\sigma}{G}\right)^3 \tag{15}$$

This result is similar to that originally derived by Weertman. The only difference is that the pre-exponential term A_g is independent of solute concentration and independent of the details of the Cottrell interaction mechanism. This latter difference is significant, for it suggests that the rate of glide-controlled creep should be given approximately by Eq. 15 regardless of the mechanism which restricts glide in the alloy.

A review of the literature shows that viscous glide creep is rate-controlling in the solid solution alloys that are documented in Tables VIII and IX. For the alloys of Table IX insufficient data are presently available on the values of D and G to permit a test of Eq. 15. Fortunately, reasonable values for these quantities can be estimated for a number of other solid solution alloys as described in the Appendix. The creep rates

Table VIII: Experimental Investigations of Viscous Drag Creep of Binary Solid Solutions and Intermetallic Compounds

Data for Au-Ni, β-CuZn, and Ag_2Al alloys have been obtained from constant stress creep tests, data for Al - 3.1% Mg from constant load creep tests. Steady-state creep rates for other Al-Mg alloys were obtained from constant strain-rate tensile tests; data from these tests were reported in terms of shear stress, τ, and shear strain rate $\dot{\gamma}$, but have been converted to tensile data assuming that $\sigma = 2\tau$ and $\dot{\epsilon} = 2/3\ \dot{\gamma}$.

Alloy	Ref.	Homologous Temperature Range of Creep Tests	n, Determined from: Isothermal Creep Tests	n, Determined from: Fig. 11	A, Determined from Exptl. n
Au - 10% Ni	33	0.878	3.4	3.4	2.2
Au - 25% Ni	33	0.918	3.4	3.4	3.2
Au - 50% Ni	33	0.917	3.1	3.1	0.63
Au - 66% Ni	33	0.88	2.9	2.9	3.3
Au - 78% Ni	33	0.82	3.0	3.0	1.8
Au - 87% Ni	33	0.76	3.8	3.8	71.
Al - 5.5% Mg	95	0.62 - 0.77	2.8 - 3.3	3.1	0.28
Al - 3.3% Mg [S]	96	0.67 - 0.77	3.5	~3.5	18
Al - 3.3% Mg	95	0.62 - 0.78	3.5	3.5	15
Al - 3.1% Mg	5	0.53 - 0.85	3.5	3.5	12
Al - 1.1% Mg [S]	96	0.67 - 0.72	4.2	4.2	4×10^4
Al - 1.1% Mg	95	0.62 - 0.77	-	~3.6	1.2×10^2
NiAl (54% Al) [S]	97	0.56 - 0.88	3.3	3.3	4.6
β - CuZn (47.5% Zn)[S]	98	0.65 - 0.72	-	3.4	2.6
β'-CuZn (47.5% Zn)[S]	98	0.58 - 0.65	-	~3.0	0.005
Ag_2Al [S]	6	0.53 - 0.65	3.6	3.6	1×10^2

Table IX. Experimental Investigations of Viscous Drag Creep of Binary Solid Solutions and Intermetallic Compounds.

Alloy	n	Ref.
In - 0.9 to 12% Pb	4.5 to 3.0	35
In - 1 to 5.1% Cd	4.6 to 3	35
In - 0.4 to 6.0% Hg	4.5 to 3.6	35
In - 4.7 to 36% Tl	4.3 to 3.2	35
In - 1.6 to 7.9% Sn	4.4 to 3.5	35
Pb - 4.4 to 19.4% Sn	4.5 to 3.1	35
Pb - 1.8 to 4.8% Cd	3.8	35
Pb - 3.5 to 64% In	5.0 to 3.1	35
W - 25 to 30 Wt % Re	3.8	99
Au - 27% Cu	3.4	100
MgCd	3.4	101
TiNi	3.0	102
Ni - 20% Al - 10% Fe	3.2	103

of these alloys which have been correlated with Eq. 14, are presented in Fig. 10 and documented in Table VIII.

The most striking aspect of Fig. 10 is the close agreement found between the experimentally measured steady-state creep rates and those predicted from Eq. 15. Only two of the alloys investigated, Au - 66% Ni and ordered β'-CuZn, have creep rates which are substantially different from the predicted values; examination* of the original Au-Ni creep data suggests that the rates of the Au - 66% Ni alloy may be too high by a factor of about 10.

The other interesting aspect of Fig. 10 is that n is often greater than the theoretically suggested value of 3. The Au-Ni and Al-Mg alloys demonstrate the usually observed effect of solute concentration on n[35]. As alloying content increases n veers from values characteristic of climb-controlled creep towards the limiting value of 3 that is predicted from simple models of viscous glide creep. This indicates that the mechanism of viscous glide creep is sensitive to solute atom concentration. Presently formulated models of viscous glide creep are not yet sophistocated enough to predict such behavior. It is perhaps best to think of them as representative of the limiting case of viscous glide creep.

Up to the present it has not been possible to predict which solid solution alloys should creep by the viscous glide mechanism and which

*A plot of log $\dot{\varepsilon}_s$, obtained under the same stress, vs % Ni parallels a similar plot of log $\tilde{D}$ vs % Ni, except for Au - 66%Ni.

should creep by dislocation climb. In attempting such predictions it should be kept in mind that two criteria must be simultaneously satisfied before viscous glide creep can replace dislocation climb as the rate-controlling mechanism during high-temperature creep:

1. Solute atoms must be bound to gliding dislocations through some solute atom-dislocation interaction or ordering mechanism.

2. The resulting rate of dislocation glide must be slow enough to be rate-controlling during steady-state creep. This criterion is met only when $\dot{\varepsilon}_s$ (Eq. 4) > $\dot{\varepsilon}_s$ (Eq. 14).

In the past it has not been possible to accurately formulate the second criterion. With the correlations developed in this report it may be possible to formulate this criterion with sufficient accuracy to make predictions on the creep mechanisms of solid solution alloys feasible.

G. Climb-Controlled Creep of Intermetallic Compounds.

Very few reliable data are available on the high-temperature creep of intermetallic compounds[104,105]. In a large number of compounds significant creep strain is not observed until a temperature of as high as 0.6-0.7 of the melting temperature is reached[106]. Furthermore, the reported activation energies for high-temperature creep of intermetallic compounds do not always agree well with those for diffusion. The only unqualified example of steady-state creep by the dislocation-climb mechanism is that for AgMg shown in Fig. 8. Its creep rate is given by

$$\frac{\dot{\varepsilon}_s kT}{DGb} = 4.7 \times 10^8 \left(\sigma/G\right)^{5.7} \qquad (16)$$

Its correlated creep rate is not unlike that of the solid solution alloys shown in Fig. 8. Despite the nominal agreement, no generalization should

be inferred regarding climb-controlled creep of intermetallic compounds from this singular case.

H. Steady-State Creep of Dispersion-Strengthened Alloys.

High-temperature creep of dispersion-strengthened alloys is a complex phenomenon that is not well understood. The creep behavior is so sensitive to the type and nature of the dispersion that different processing histories often lead to creep by entirely different mechanisms even in the same alloy. For this reason it has proved difficult to systematically characterize all of the different types of creep behavior that have been reported for dispersion-strengthened alloys. However, two types have occured with sufficient frequency that some comments can be made.

The first type is characterized by a very high activation energy of creep (often several times greater than H_d) and a very high stress sensitivity ($n \simeq 40$ in one investigation). This behavior is frequently observed in metals in which a very fine dislocation substructure or fine grain structure is stabilized by the dispersed particles. Often such structures appear to have a fibrous structure. Examples of this type of behavior have been reported for Al - Al_2O_3 dispersion alloys (SAP)[107], Ni - Al_2O_3 alloys[108], TD nickel[109], and In - glass bead composites[110].

Guyot[111] has recently shown that the high-temperature creep of SAP appears to agree with predictions based on a mechanism involving the thermally activated breaking of attractive junctions. The high activation energy and stress sensitivity of creep which are observed in SAP can be semi-quantitatively accounted for by this mechanism. It seems possible that the very low creep rates which are observed in some dispersion-strengthened systems result from restraints that are imposed by a dispersed

TABLE X: Experimental Investigations of Creep in Dispersion-Strengthened Alloys. All Data Obtained From Constant Stress Creep Tests.

Metal	Ref.	Homologous Temperature Range of Creep Tests	n, Determined from Fig. 11	Average Inter-particle Spacing λ, in Å	Particle Radius r, in Å	$\frac{\lambda^2}{rb}$
Ni-1.00^{V}/o ThO_2 (a)	113	0.57 - 0.66	7.6	5290	214	52500
Ni-1.00^{V}/o ThO_2 (b)	113	0.56 - 0.73	8.0	2505	110	22900
Ni-2.66^{V}/o ThO_2	113	0.60 - 0.69	7.3	3670	263	20600
Ni-4.41^{V}/o ThO_2	113	0.68 - 0.72	~7	2990	275	13100
Ni-2.56^{V}/o ThO_2	113	0.57 - 0.75	7.5	1760	110	11400
Ni-0 % Cr - 1.00^{W}/o ThO_2 [Same as Ni-1.00^{V}/o ThO_2 (b)]	114	0.56 - 0.73	8.0	2505	110	22900
Ni-15.0 % Cr - 1.00^{V}/o ThO_2	114	0.64 - 0.83	6.3	2070	81	21200
Ni-24.8 % Cr - 1.00^{V}/o ThO_2	114	0.65 - 0.82	6.9	2165	78	24300
Ni-35.6 % Cr - 1.00^{V}/o ThO_2	114	0.65 - 0.83	6.2	2290	88	24100

phase on the climb recovery of attractive junctions.

The high-temperature creep of a second type of dispersion-strengthened metals seems to conform well with expectations based on the dislocation climb mechanism[77,112-114]. Creep is diffusion-controlled and the stress dependence of steady-state creep is given by a power law expression with n generally about 7. In TD nickel alloys this type of behavior is observed only after extruded material is "recrystallized" prior to testing to produce a less complex stabilized dislocation substructure[109,113].

The steady-state creep rates of two dispersion-strengthened systems of this second type are correlated with Eq. 4 in Fig. 11, and documented in Table X*. The members of one system have metal matrices while those of the other have alloy matrices. Both of the matrix materials are known to creep by the dislocation-climb mechanism when no dispersed phase is present. Cases where the alloy matrix alone creeps by the viscous-glide mechanism have not yet been investigated. In order to facilitate comparisons the $\dot{\varepsilon}_s kT/DGb$ versus σ/G curves for Ni, Ni - 10% Cu and Ni - 30% Cu are shown by broken lines. As shown in Fig. 11, dispersions invariably decrease the steady-state creep rate below that for the matrix alone and in some instances by over 4 orders of magnitude. In addition, the dispersion strengthened alloys exhibit a higher value of the stress

*The value of G used in all analyses was that of the matrix material alone. This was selected because during creep the significant dislocation reactions occur within the matrix.

exponent n of Eq. 4. The variation in n among the various types of dispersions, however, appears to be somewhat random suggesting that n might well be approximated by the average value of $n \simeq 7$. On this basis the steady-state creep rates of the dispersion strengthened systems might, over the available range of data, be approximated by

$$\frac{\dot{\varepsilon}_s bT}{DGb} = A_d \left(\sigma/G\right)^7 \qquad (17)$$

where A_d is now highly sensitive to the geometrical details of the dispersion.

The most popular theories for steady-state creep in dispersion-strengthened alloys are those presented by Ansell and Weertman[107]. More recently Ansell[115] discussed their possible validity in considerable detail. One analysis applies to cases where the stress can extrude dislocations past the dispersed particles by the Orowan process. The dislocation rings left about the particles are then eliminated by climb of dislocations, whereupon, new dislocations are emitted by fixed sources. As shown by Clauer and Wilcox[113], the dispersions in the systems documented in Fig. 11 are too fine to permit the operation of this model. In the alternate model dislocations cannot extrude between the particles, but the dislocations climb over the particles. Neglecting the questionable assumption regarding the operation of fixed dislocation sources, this model suggests that A_d increases linearly with λ^2/br, where λ is about the mean spacing between the particles on a slip plane and r is their mean radius. According to this model, $n \simeq 4.5$ in lieu of the above documented experimental value of about 7. Clauer and Wilcox[113] discussed a similar model. They suggested that an effective stress equal to the applied stress

minus an average back stress, be introduced in lieu of the stress σ. By judicious selection of such a back stress the value of n could be reduced to the theoretically expected value. Unfortunately, this concept is inappropriate for all climb-controlled mechanisms.

As shown by the data presented in Fig. 11, A_d seems to increase with λ^2/br. The data exhibit considerable scatter, however, and the observed increase is far from linear. A second major theoretical problem concerns accounting for the high values of n that are observed in dispersion-strengthened alloys.

I. Activation Energy for Diffusion-Controlled Creep

The previous analyses have shown that when creep is diffusion-controlled the creep rate can be represented by

$$\dot{\varepsilon} = A' \frac{DGb}{RT} \left(\frac{\sigma}{G}\right)^{\eta} \tag{18}$$

where A' is a parameter which is constant at steady state. For both Nabarro and climb-controlled creep D is given by Eq. 2a or 2b, while for viscous glide creep it is given by Eq. 11. Because of the inclusion of G and T in Eq. 18, the apparent activation energy for creep

$$Q_c = \left[\frac{\partial \ln \dot{\varepsilon}}{\partial\left(-\frac{1}{RT}\right)}\right]_{\substack{\sigma = \\ \text{constant}}} \simeq \left[\frac{\Delta \ln \dot{\varepsilon}}{\Delta\left(-\frac{1}{RT}\right)}\right]_{\substack{\sigma = \\ \text{constant}}} \tag{19a}$$

is always slightly different from the activation enthalpy of diffusion

$$H_d = \frac{\partial \ln D}{\partial\left(-\frac{1}{RT}\right)} \tag{19b}$$

It is convenient therefore to define an activation enthalpy for creep, H_c, which does not contain terms arising from either G or T:

$$H_c = Q_c - RT\left[(n-1)\frac{T}{G}\left(\frac{-\partial G}{\partial T}\right) - 1\right] \qquad (20)$$

When creep is exclusively diffusion-controlled it should be found that $H_c = H_d$.

For Nabarro creep, where n = 1, Eq. 21 reduces to simply $H_c = Q_c + RT$. An estimate of the bracketed term of Eq. 21 for cases where n > 1 can be deduced from the average variation of G with temperature. As shown in the Appendix, the shear modulus of most metals and solid solution alloys can be represented at high temperatures by

$$G = G_o\left(1 - \beta\frac{T}{T_m}\right) \qquad (21)$$

where G_o is the shear modulus of elasticity extrapolated to the absolute zero, T/T_m is the homologous temperature, and β is a material constant with a normal range of from 0.35 to 0.55. For such metals Eq. 21 reduces to

$$H_c = Q_c - RT\left[\frac{n\beta\left(\frac{T}{T_m}\right) - 1}{1 - \beta\left(\frac{T}{T_m}\right)}\right] \qquad (22)$$

For $\beta = 0.45$ and $n = 5$, H_c is equal to $Q_c - 0.16$ RT at $T/T_m = 0.5$ and equal to $Q_c - 2.27$ RT at $T/T_m = 1.0$. For a temperature of 1000°K, this corresponds to $Q_c - 0.3$ Kcal/mole and $Q_c - 4.5$ Kcal/mole respectively. The experimental error involved in most measurements of Q_c is usually at least ±5 Kcal/mole. Consequently for most metals and solid solution alloys undergoing creep by a climb or viscous drag mechanism, under most conditions $H_c \simeq Q_c$ to within the accuracy of the experimental data.

Throughout the preceding data analyses care was exercised to include

only data for which it could be shown that $H_c \simeq H_d$. The agreement between H_c and H_d that was observed for the pure metals has been documented previously[28]. Figs. 12-15 show that reasonably good agreement between H_c and H_d is obtained for climb-controlled creep of FCC alloys. For the intermetallic compound AgMg agreement between H_c and H_d to within 1 Kcal/mole is obtained. The correlation between Q_c and H_d that is observed in the Ni-ThO_2 and Ni-Cr-ThO_2 dispersion systems has been previously discussed by Clauer and Wilcox[113, 114]. The values of Q_c, H_c, and H_d that have been computed from their data are shown in Fig. 16.

Such comparisons are more difficult to make for alloys which creep by the viscous glide mechanism because of the scarcity of systems for which data is available on both H_c and H_d. In the case of glide-controlled creep H_d must be obtained from measurements of chemical inter-diffusivity or from the temperature dependence of the Darken expression for interdiffusivity, Eq. 11.

The activation energy for chemical diffusion in the Au-Ni system has been measured directly in early experimental work[116], but is known to be inaccurate, especially in the region of composition Au-80%Ni[117]. For this reason H_d for Au-Ni alloys was estimated indirectly from the value of $\tilde{D}$ at 860°C (the temperature of the creep investigations) using the assumed relation $D = \exp(-H_d/RT)$. Since the value of $\tilde{D}$ at this temperature is reasonably accurately established (see Appendix Fig. A3), this method might be expected to yield reasonable estimates for H_d. A comparison of H_c and H_d for alloys investigated in the Au-Ni system is shown in Fig. 17. Using this method somewhat better agreement is attained between H_c and H_d for this system than was previously thought to exist[33, 118].

Close agreement between H_c and H_d is found for creep of the β-CuZn

alloy in both the ordered and disordered state[98]. For this alloy H_d must be estimated from the temperature dependence of tracer diffusivity and chemical activity coefficient measurements, as chemical interdiffusivity data are unavailable. It follows from Eq. 11 that

$$H_d = \frac{N_B D_A^*(H_d^*)_A + N_A D_B^*(H_d^*)_B}{N_A D_B^* + N_B D_A^*} + \frac{\partial}{\partial(-\frac{1}{RT})} \ln\left[\frac{\partial \ln a_A}{\partial \ln N_A}\right] \qquad (23)$$

where H_d^* is evaluated from tracer diffusivity measurements[119] of each alloy species using Eq. 19b. The first term of Eq. 23 is, for convenience, called H^*, and the second term ΔH. Values of H^*, ΔH, H_d, and H_c for both ordered and disordered B-CuZn are given in Table XI for temperatures just above and below the critical ordering temperature (T_c = 741°K). The values of ΔH have been crudely estimated from available data[120] in Fig. A5 of the Appendix. As shown in Table XI close agreement is observed between H_c and H_d for CuZn in both the ordered and disordered state, although the values themselves change appreciably between the two states.

Table X: Activation Energy for Diffusion and Creep in β-CuZn

State of Order	Temperature (°K)	H^*	ΔH	H_d	H_c
		(Kcal/mole)			
Disordered	773-823	24.1	3.3	27.4	25
Ordered	653-713	39.7	4.7	44.4	41

V. CORRELATIONS BETWEEN STRUCTURE AND STEADY-STATE CREEP RATES

In the earlier sections of this report major emphasis was placed on the effects of the applied stress, shear modulus of elasticity, test temperature, diffusivity, and stacking-fault energies on the steady-state creep rates of some metals and alloys. Correlations between steady-state creep at high temperatures, crystal structure, grain size and substructure will now be discussed.

A. Crystal Structure

The mechanical behavior of most crystalline materials at low temperatures usually exhibits features which are unique to each type of crystal structure because of the differences which exist between the types and energetics of the dislocation reactions that are indigenous to each crystal structure. At sufficiently high temperatures, however, fluctuations in thermal energy become so violent that dislocations are rapidly activated past all short-range barriers to their glide even at quite low values of the applied stress. Thus, screw dislocations, even in metals containing quite low stacking-fault energies, seem to cross slip with relative ease at low stresses provided the temperature is sufficiently high. In contrast, however, dislocations containing edge components, which are confined to slip on their glide planes, can circumvent long range interactions only by dynamic recovery as a result of diffusion of vacancies under local chemical potential gradients so as to climb. These considerations suggest that high-temperature creep might be insensitive to differences in dislocation reactions in the several crystal structures. The previous analysis shows that in large measure this deduction is valid. Alloys which creep by the viscous-glide mechanism display nearly identical

creep rates over wide ranges of stress when correlated with Eq. 14, regardless of crystal structure. Metals and alloys which creep by the climb mechanism have creep rates which correlate into the same wide band when plotted as $\dot{\varepsilon}_s kT/DGb$ versus $(\sigma/G)^n$, regardless of crystal structure.

Despite such gross correlations, differences do appear. The rather consistent variation of n with Gb/Γ in the FCC metals strongly suggests that the separation of the partial dislocations by their attendant stacking fault is the major factor in accounting for the wide band of $\dot{\varepsilon}_s kT/DGb$ versus σ/G in this structure. The fact that the narrow band of $\dot{\varepsilon}_s kT/DGb$ versus σ/G for the BCC metals falls near that of Al, which has the lowest value of Gb/Γ for the FCC metals analyzed, seems to confirm the effect of stacking fault width on the climb mechanism. Solely on this basis, however, it is not evident as to why the creep rates of the HCP metals, which on the average have intermediate values of Gb/Γ, should cluster near those for FCC metals that have high values of Gb/Γ. Undoubtedly, other as yet unknown factors also play a role in high-temperature creep. This is further emphasized by the fact that the reported values of n for BCC metals vary from 4 to about 7. Different investigators often report quite different values of n for the same metal. Although such variations in n suggest that impurities in BCC metals might influence directly or indirectly their high-temperature creep rates; as yet their is no wholly conclusive evidence on this issue.

B. Effect of Grain Size.

The results of early investigations on effects of grain size on high-temperature creep have been reviewed by Conrad[121] and Garafalo[122]. The early reported data seemed to give rather inconclusive results.

Whereas some data suggested that the creep rates decreased with increasing grain size, others suggested that the opposite trend was valid. Garafalo[122] suggested that the reported trends inferred the existence of a minimum steady-state creep rate at some intermediate "optimum" grain size. Such a trend seems to have been obtained in monel[123].

The data that were documented in the earlier sections of this report, excluding, of course, that on Nabarro creep, refute the concept that the steady-state creep rate for either the dislocation climb or the viscous drag mechanism depends appreciably upon grain size. The values of $\dot{\varepsilon}_s kT/DGb$ versus σ/G for all metals or alloys of each class agree quite well with one another regardless of major variations in grain size. Moreover, the creep rates of single crystal Pb, Mo, AgMg, Ag_2Al, and β-CuZn correlate well with polycrystalline metals in their corresponding class. Even more convincing, however, is the observation that the steady-state creep rates for single crystals of Al (Fig. 3) and Al-Mg alloys, (Fig. 10) do not differ by more than a factor of 2 from those of polycrystalline test specimens when tested over a wide range of σ/G.

Recent data confirm the invariance of the steady-state creep rate with grain size above a critical value. The most conclusive investigation on this issue was reported on Cu by Barrett, Lytton and Sherby[124]. Additional evidence that steady-state creep rates are independent of grain size over the range of ASTM 8 to 1 in ferritic and austenitic steels has been summarized by Hopkin[125].

The evidence is equally firm that below a critical grain size the steady-state creep rate increases with decreasing grain size. The major evidence reported by Barrett, Lytton, and Sherby[124] for randomly

oriented Cu is shown in Fig. 19. Cube-textured Cu gave a similar result but developed a slightly lower steady-state creep rate which the authors ascribed to an orientation effect. Although Garafalo et al.[76] suggested that an optimum grain size for creep resistance is obtained in austenitic stainless steels, their data were also plotted in Fig. 19. Within the normal scatter band these data also suggest that as the grain size is decreased the steady-state creep rate remains constant until the grain size is reduced below a critical value, whereupon the creep rate increases with additional reduction in grain size. The fact that the critical grain size is about the same for Cu and austenitic stainless steel is undoubtedly a coincidence.

Although the rate of Nabarro creep increases with decreasing grain size it is easily demonstrated that it cannot be responsible for the above-mentioned grain-size effects. Its contribution to the total creep rate is negligible for the values of σ/G at which the above discussed grain-size effects are obtained. It will be shown later that the usual grain size effects are attributable to increased contributions of grain boundary sliding to the over all creep rate with decreasing grain size, particularly at the lower values of applied stress.

C. General Features of Creep Substructure.

The dislocation substructures which are developed during creep at high temperatures are, in many ways, similar to those that are formed during deformation at lower temperatures. This should not be surprising since all of the dislocation interactions which take place at low temperatures also take place at higher ones. The primary effect of a high temperature is to make thermally-activated recovery processes, such as

dislocation-climb and recyrstallization take place at a rapid enough rate so that they too contribute to the processes which determine the final disposition of dislocations. In the past there has been a tendency to emphasize the differences between substructures developed during creep and those developed at low temperatures where slip is accompanied by strain hardening and cross-slip but not climb. It is becoming increasingly apparent, however, that the dislocation substructures developed during creep have many features in common with those developed at lower temperatures. This is an important observation for it means that studies of low-temperature dislocation substructures can be used as a guide for future investigations of creep substructure. The discussion which follows will point out similarities and differences in high and low-temperature substructure.

The dislocation substructures which are produced during initial straining upon applying a stress at high temperatures are essentially the same as those produced during Stage III deformation below one-half of the melting point[126,127]. Climb recovery is negligible in such a short period of time. After stressing, however, climb recovery does begin and substructural changes take place which result in transient creep. These will be described later in this report and we will consider here only the substructure that is developed at steady-state creep.

The most prominent feature of any steady-state creep substructure is the non-homogeneity with which dislocations are arranged[126,128]. After creep deformation, just as after deformation at low temperatures[129], most dislocations are heavily concentrated in some regions of a crystal; far fewer are located in the regions in between. The regions of high dislocation density form a pattern of cells or subgrains which inclose

regions of lower density. The cell walls, which are developed during low temperature deformation, always encompass a measureable volume (often as much as 20% of a crystal), and they are composed of dense dislocation tangles[129]. In contrast, the subgrain walls which are developed during steady-state creep often encompass a volume which is too small to measure; they are better described as low-angle boundaries[126,128,130]. As a consequence the substructure which is developed during high-temperature creep is usually described as a collection of subgrains which are formed by tightly knit, two dimensional dislocation boundaries. Within the subgrains the density of dislocations is low[131].

In general, temperature seems to have less of an effect on the arrangement of dislocations within cells or subgrains than it does on their arrangement within the cell or subgrain walls. McLean[46,132] was the first to realize this and has emphasized that dislocations within subgrains are linked together to form a three dimensional Frank network[133-135], which is nearly identical to that which is found within cells during Stage III deformation at low temperatures. This observation is true for many low stacking-fault width FCC metals and BCC metals, although it may not apply to FCC metals with high stacking-fault width. Investigations of deformation substructures at low temperatures show that in higher stacking-fault width FCC metals, dislocation slip is mainly confined to the primary slip system, and that as a result, dislocations tend to be aligned along planes of the primary slip system[129]. It is not known whether this is observed in the same metals after high-temperature creep deformation, because to date no such metals have been fully investigated.

D. Formation of Subgrains.

Overwhelming evidence now makes it possible to conclude that well defined subgrains are formed during the creep of metals and solid solution alloys wherever the dislocation climb mechanism is rate-controlling. Subgrains are not formed during climb-controlled creep of most dispersion-strengthened metals, however. Isolated bits of evidence suggest that a fully developed subgrain structure does not develop when other high-temperature creep mechanisms are rate-controlling. The evidence for these conclusions will now be discussed.

The observation of a fully developed subgrain structure has been reported many times for low stacking-fault width FCC metals and BCC metals when creep is diffusion-controlled[136-144]. At one time it was suggested that subgrains might not form in high stacking-fault width FCC metals and alloys, but current evidence refutes this for climb-controlled creep. Careful investigations have revealed well-developed subgrain structures in Cu[126,143], and in high stacking-fault width Cu-16% Al alloys[130,145] ($Gb/\Gamma>500$) and austenitic stainless steels (8 wt.% Ni, $Gb/\Gamma>600$)[144]. Subgrain formation has also been reported by a number of observers for climb-controlled creep of several HCP metals: Mg[63,64,146-148], Cd[149], Sn[149], and Zn[150]. Subgrains have been observed to form in single crystals[126,128,130,143,145] as well as polycrystals. Thus, it seems well established that when climb is rate-controlling subgrain formation always accompanies creep in single phase metals. In the case of very fine grained polycrystalline metals, however, subgrains may not be observed if creep takes place at low stresses, for the steady-state subgrain size may approach or exceed that of the grains themselves. An example of this

that subgrains may develop in this alloy[8], but less extensively than in pure Al. This brief review shows that there are no firmly established systematic data regarding subgrain formation in alloys that creep by the viscous glide mechanism. Such evidence is needed because it might be significant in establishing the role of subgrains in high-temperature creep.

For obvious reasons subgrain formation is not observed when recrystallization occurs. Recrystallization has been observed in most polycrystalline FCC metals other than Al during creep at high stresses and rapid strain rates[11,33,36,37,160-167]. It has been reported to occur under the same conditions in only a few BCC metals[50,54]. It is not yet established whether recrystallization results from the migration of grain boundaries or from subgrain coalesence[164,168], but numerous observations suggest that recrystallization is often initiated near grain boundaries[164-168]. Whatever the mechanism of recrystallization it seems clear that it is initiated at regions of high local lattice strain. Thus, as first pointed out by Hardwick, Sellers, and Tegart[160], any process that lowers lattice strain energy also inhibits recrystallization. This is perhaps the explanation for the observation that recrystallization is observed more frequently in high stacking-fault width FCC metals than in Al or the BCC metals.

When recrystallization occurs, it is accompanied by a sudden acceleration of creep rate. This appears to result from transient creep in the recrystallized regions, and not from the actual process of recrystallization itself[164]. In the discussion which follows no further consideration will be given to this process.

Instead we shall consider in greater detail those substructural features which appear pertinent to steady-state creep. Because little information is available on the dislocation substructures which are produced during either viscous glide creep in alloys or during climb-controlled recovery in dispersion-strengthened materials, discussion will be limited to metals and alloys which creep by the dislocation-climb mechanism unless otherwise stated. For these metals the steady-state creep substructure can be characterized by:

a. The nature, arrangement and density of dislocations within the subgrains.

b. The subgrain size.

c. Types of subgrain boundaries and the misorientations across them.

E. Dislocations Within Subgrains.

As previously discussed, the arrangement of dislocations within subgrains after creep is similar in appearance to the arrangements that are observed in cells after low temperature deformation. An even greater similarity is found between the high and low temperature dislocation substructures when quantitative counts of dislocation densities are made. It has been well established that in many metals at low temperatures the density of dislocations, ρ, varies with the square of the flow stress according to the relation

$$\frac{\sigma}{2} = \alpha\, Gb\sqrt{\rho} \qquad (24)$$

where the shear modulus of elasticity is that which applies at the test temperature, and α is a constant equal to about 0.5[129]. Fig. 20 shows that this relation also exists for a wide variety of metals during high-temperature creep. The figure contains all known measurements of

dislocation densities that have been made within subgrains after steady-state creep[46,73,83,99,113,126,128,153,169-171]. Discounting the etch pit data, which are know to be unreliable in Fe at higher values of ρ^*, it appears that the average value of $\sqrt{\rho}\, b$ at the steady state for metals and alloys that creep by the dislocation climb mechanism is only slightly lower at the same values of σ/G than those measured following low-temperature deformation. The mean value of $\alpha \simeq 0.6$ applies to steady-state creep by climb in the reported cases. It is significant that the W-Re alloy, which creeps by the viscous glide mechanism, also obeys the same relation. It has dislocation densities which are identical in value to those measured in pure W, which creeps by climb. The dispersion strengthened Ni-ThO_2 metal is the only major exception to this relation. The reason for this is not known.

The similarities which are found between dislocation substructures after high and low temperature deformation within subgrain or cell interiors suggest that dislocation substructures achieve a mechanical equilibrium as a result of dislocation interactions whenever plastic deformation occurs. This has long been recognized in the strain hardening theories at low temperatures, but has not always been included in theories

---

*Etch pitting in many metals and alloys is sensitive to impurity and alloy content, and often there is not a one to one correspondence between etch pits and dislocations. Etch pitting can underestimate the number of dislocations in a crystal[73,83,99,140], as data on Fe-3w/o Si in Fig. 20 show, since several dislocations may correspond to a single etch pit. This problem is more acute for substructures that are produced at high σ/G levels than at low, for in the former dislocations are more closely spaced. For this reason etch pitting studies sometimes underestimate the stress dependence of dislocation density[99].

of dislocation climb-controlled creep.

The observations which are presently available show that two of the assumptions made in early climb theories about the dislocation substructure during creep are not justified. Piled-up arrays of edge dislocations from sources on adjacent slip planes are never observed. Recent theoretical calculations show the reason--such arrays are actually unstable; the lead dislocations of the arrays by-pass one another, eventually forming a series of edge dipoles. Observations also show no experimental justification for the prevalent theoretical assumption that dislocations are generated at fixed sources. Instead, they suggest that there are many possible sources for dislocations, both during creep and low-temperature deformation. Dislocations in the interior of subgrains undoubtably act as sources of additional dislocation segments as they cross slip and climb[175,176]. Subgrain[175,176] and grain boundaries[131] also act as sources for some dislocations, although they probably act more effectively as sinks for dislocations than as sources. McLean[134] has emphasized that dislocations collect at grain boundaries during deformation[177], and that these may be, in large measure, responsible for the higher rates of strain that are found near grain boundaries during creep.

Up to this point there has been no mention of the character of dislocations which was observed within subgrains during creep. The recent investigations by Clauer, Wilcox and Hirth[53,128] on BCC Mo show that a majority of the dislocations which they observed were in edge orientation, a fact which provides stong evidence for the dislocation climb recovery mechanism of creep in preference to the jogged-screw dislocation glide mechanism[73]. The only other extensive investigation that has been made

of dislocation character after creep is that of Dingley and Hale[178] on Fe and dilute Fe alloys. After deforming specimens over the temperature range -117 to 600°C, they report finding dislocations within a three dimensional network which have Burgers vectors of a<100> and a<110> as well as the expected 1/2a<111> type. The proportion of each type is roughly 20%, 20%, and 60%. and it is unaffected by temperature of deformation, alloy content, strain, dislocation density, or rate of straining. They also report that there is no tendency for any of these dislocations towards either edge or screw character. These findings are not in disagreement with those of Clauer et al[128]. Numerous a<100> dislocations were observed within dislocation subboundaries in Mo. Both investigations agree that screw dislocations do not dominate within subgrains as would be required if the jogged-screw dislocation mechanism controlled high-temperature creep.

F. Subgrain Size.

The subgrain structure which is observed to develop over the transient stage of climb-controlled creep has been sufficiently studied in polycrystalline metals to make several generalizations now possible. During steady-state creep the subgrain structure remains at steady state, although there is no doubt that individual subgrains are in a constant state of change thoughout the duration of creep. In polycrystalline metals, subgrains are always observed to be roughly equiaxed and constant in size throughout steady-state creep even when high strains are attained. In fact, Wong, McQueen and Jonas[175,179,180] have shown that subgrains remain equiaxed (and constant in size) to strains of 3.7, while grains themselves become elongated. The observations were made in Al after hot

extrusion tests at strain rates very much higher than those encountered in creep, but they reinforce the findings of creep investigations which cannot be carried out to such high total strains. These findings mean that subgrain formation is a dynamic process which continues to take place throughout the course of climb-controlled creep.

Subgrains which are formed in polycrystalline metals are not uniform in size throughout the metal, but they cluster around a mean value which is reproducible at a given stress level regardless of the previous stress history or of the original substructure[181-185]. It has been firmly established that the mean subgrain size, δ, is independent of temperature[181,186-188], strain[181,187,188] and usually of grain size[76,140,189,190], but varies strongly with stress, σ/G[186,189] or equivalently with $\dot{\varepsilon}_s kT/DGb$. The dependence of the mean subgrain size upon stress is shown in Fig. 21 for those polycrystalline metals and alloys in which it has been systematically investigated*.

These data reveal that subgrain size decreases about linearly with the reciprocal of σ/G. The effect of stacking fault width on the steady-state creep rate for the climb mechanism suggests that the subgrain size might also be influenced by this parameter. Additional support for this speculation is provided by the well-known effect of stacking fault width on the cell size that is developed during low temperature deformation.

---

*Measurements on subgrain size for W[99,191] and type 304 austenitic stainless steel[192], were not available at the time this figure was compiled.

However, the evidence presented in Fig. 21 does not confirm this concept. Data by Warrington[144] on austenitic stainless steel show, for example, that subgrains of identical size are obtained in alloys in which Gb/Γ doubles from a value of somewhere near 350 to about 700.

The subgrain size of Al appears to be significantly greater than those of other metals, but it is not clear whether this observation is reliable. Measurements of subgrain size in Al were taken from early substructural investigations which used polarized-light optical microscopy on specimens that were first anodized by electrolytic etching to reveal subgrains. The technique is based on the assumption that the orientation of the corrugated oxide film which forms is uniquely related to the subgrains beneath the film. Recent investigations[175,176], using both this technique and transmission electron microscopy, however, have shown that this assumption is not justified when subgrains are smaller than 10 μ ($\frac{d}{b} = 4 \times 10^4$), because optically observed subgrains cover an area which typically corresponds to 5 - 20 actual subgrains. It is not known by how much this technique overestimates subgrain size in Al when the subgrains are larger than 10 μ, as they undoubtably are after creep at low stresses. However, subgrain misorientation angles, revealed on crept specimens by this technique[137, 185,187,189,193,194], are several times higher than those measured by electron microscopy[128,191,195], suggesting that optically observed subgrains do not correspond well to the real subgrain structures.

Discounting the Al data in Fig. 21, the mean subgrain size for all of the polycrystalline metals investigated is given by

$$\frac{\delta}{b} = 20 \left(\frac{\sigma}{G}\right)^{-1} \qquad (25)$$

to within a factor of 4 times. Many more detailed investigations will be required to establish the accuracy and validity of this equation for other metals and alloys and for wider ranges of σ/G.

In some investigations of polycrystalline metals it is noted that a significantly smaller subgrain size is found along certain grain boundaries[150,169,196]. This observation suggests that higher stresses may exist in local regions due to stress relaxations elsewhere along the boundaries.

A number of recent investigations have shown that a banded subgrain structure is often produced in polycrystalline grains[140,169] or in single crystals[128,130,145,197] when slip occurs predominately on one or two slip systems. The banded appearance of the substructure is due to the presence of long planar subboundaries which extend completely across entire grains in polycrystalline Fe-3wt.%Si[169]; extend for long distances in Cu[197] and Cu-16% Al single crystals[130,145], and extend across the entire crystal in single crystal Mo[128]. These planar boundaries have been shown to parallel traces of the primary slip systems and to have the same spacing as slip bands which are observed on crystal surfaces. In single crystals of Cu-16% Al they are observed after tests of $\sigma/G \gtrsim 10^{-4}$, but not after tests at lower stress; heavy slip band traces are generally observed on single crystal specimens of most metals after creep testing at higher stresses, but not at lower stresses where fine slip predominates. All of the available evidence points to the conclusion that these bands of long planar boundaries are simply highly magnified views of the slip bands which are often observable macroscopically.

The detailed studies of Clauer, Wilcox and Hirth[128] show that,

while these banded substructures often appear quite different from the equiaxed subgrain structures that are usually found in polycrystals, they are likewise composed of subgrains. The difference in appearance arises because the subgrain structure which develops within slip bands is much finer in scale than that which develops between the bands. Fig. 22, reproduced from the studies on Mo by Clauer et al., shows that the subgrains which form in slip bands are narrow, highly elongated, and much smaller than the equiaxed subgrains which comprise the space between bands.

The factors responsible for formation of these two scales of creep substructure are not yet known. It seems clear, though, that the climb recovery is not the primary factor that is involved, for the pattern of Fig. 22 is established in Mo single crystals upon initial straining. At $\varepsilon = 0.01$ the pattern is clearly defined by a fairly regular cell structure which is somewhat finer in scale than the subgrain structure which later evolves. Over the transient strain interval of $\varepsilon = 0.02$ to 0.42 the pattern changes only in scale and in the perfection of its subgrain walls. This shows clearly that climb recovery modifies the substructure that is produced during creep deformation, but is not directly responsible for originating the cellular pattern in the first place. Both this observation and the one previously made on dislocation densities suggests that slip processes are primarily responsible for determining the arrangement of dislocations during plastic deformation, and that climb recovery only modifies this fundamental pattern.

This leads one to think that perhaps subgrain size and dislocation densities (within subgrains) are related. Indeed such a relation appears to exist. If the average distance between dislocations within subgrains,

$\bar{d}$, is defined as $1/\sqrt{\rho}$, then from Eqs. 24 and 25 it follows that

$$\delta \simeq \frac{10}{\alpha} \bar{d} \simeq 20 \bar{d} \qquad (26)$$

Subgrain size is directly proportional to average dislocation spacing. This relation seems to have general qualitative validity. The investigations of Clauer, Wilcox and Hirth[53,128] show that between slip bands, where the dislocation density is low, subgrain size is large. Within slip bands, where the total dislocation density is much higher and where slip is much more intense, subgrain size is much smaller. A higher dislocation density is often observed near some grain boundaries in polycrystalline metals than in interior regions. Likewise, smaller subgrain sizes are observed adjacent to some grain boundaries. The reason for this relation between subgrain size (or equivalently cell size) and dislocation density undoubtabley is hidden in the complex processes which are responsible for cell formation during plastic deformation.

G. Subgrain Boundaries.

The subboundaries that are observed in crept polycrystalline metals are generally observed to consist of well-formed tilt boundaries, regular hexagonal dislocation networks, and irregular networks which have a mixed edge-screw dislocation character[46,75,99,131,143,191,195,198,199]. Boundaries composed of complex dislocation tangles have frequently been reported[75,99,131,143], but most of these observations appear to have been made upon specimens which were still in the primary stage of creep or on specimens which were tested at too high a value of $\dot{\varepsilon}_s kT/DGb$ for dislocation climb to be the rate-controlling creep mechanism.

It might be expected that subboundaries which are developed during the creep of oriented single crystals might be considerably simpler,

because few slip systems contribute dislocations to the subboundaries. The work of Clauer, Wilcox and Hirth[128], which is the only thorough work of this kind, seems to justify this view. Almost all of the subboundaries which they observed with transmission electron microscopy were found to be simple tilt boundaries. These consisted primarily of two types of planar {111} tilt boundaries plus numerous segments of {100} tilt walls which were shown to have been produced through reaction of the {111} walls. The tilt walls were mobile during creep and captured dislocations as they swept through regions between other subboundary segments. Although these observations were made late in the transient stage of creep, it seems that they might also apply to the steady state.

From these observations it is obvious that the early concept of subgrain formation through polygonization of edge dislocations under stress is not wholly tenable. Some subgrain boundaries develop through the climb recovery of dislocation tangles which form upon initial straining of a metal. Others develop during the course of creep by coalescence of other subgrain boundaries, as Clauer et al. have shown. Yet the process ultimately responsible for subgrain formation is still unexplained.

Another unresolved issue, which is perhaps of greater importance to theories of climb-controlled creep, is the role of subgrain boundaries in the creep process. A basic concept of all theories of steady-state creep is that each element of the dislocation substructure which is involved in the rate-controlling creep mechanism must achieve a steady state whenever the creep rate is constant. As has been demonstrated already, both the mean size of subgrains and the denisty of dislocations within subgrains achieve a steady state when the creep rate does. On this basis it might

be anticipated that the misorientation of the subgrains should achieve the same steady-state value for a given value of σ/G regardless of the extent of strain or time in the steady state. Certainly this must be the case if subgrain boundaries enter in any way into the rate-controlling mechanism of creep. The evidence that is currently available on this issue is inconclusive.

Early investigations by McLean[187,189,194] and McLean and Farmer[193] showed that the average misorientation angle between adjacent subgrains, when measured by polarized light optical microscopy on Al or some of its dilute alloys, increases continuously with creep strain both during transient and steady-state creep. The measured angles of subgrain misorientation cover an appreciable range of values at any given strain, ε, but the mean of hundreds of measurements, θ (expressed in radians), follows the relation $\varepsilon = \theta$ with a reasonable degree of accuracy. These findings were substantiated in large measure by the subsequent investigations of Kelly and Gifkins[185] and Busboom[137], which used the same technique to measure subgrain misorientation. However, recent electron-microscopy work[175,176] shows that these investigations were not measuring misorientation angles between adjacent subgrains, but were instead measuring angles between groups of subgrains. The anodized film which forms on Al is not sensitive to subgrain misorientation angles of $1/2^\circ$ to 1°[185,194], and unfortunately many subgrain boundaries fall into this range[128,191,195]. Thus, the findings of these investigations are incorrect quantitatively, and perhaps also qualitatively. They cannot be used as conclusive evidence for progressive subgrain misorientation during creep.

X-ray microbeam back reflection techniques have been used to

investigate subgrain misorientation during creep but the results of these investigations are not subject to unambiguous interpretation. When a polycrystalline metal is examined with a monochromatic x-ray microbeam, reflections from a few properly oriented grains are visible. Prior to creep testing of an annealed metal these reflections are sharp, but upon initial straining they become diffuse showing that considerable lattice distortion is introduced into the grains. Over the course of transient creep, however, an arc of fine spots develops within the diffuse pattern, and by the onset of steady-state creep all that remains is a series of fine spots which spead over an angle of a degree or so about the orientation of the original grain. These correspond to reflections from individual subgrains which develop within the grain. The angular spread of the arcs that originate from different grains within a polycrystal often covers a comparitively wide range of values at a given strain. But several investigations show that the mean angular spread of arcs from different grains steadily increases over both the transient and steady-state stages of creep[181,193,195]. If one assumes that most adjacent spots within an arc originate from adjacent subgrains, then it would appear that the mean subgrain misorientation increases continuously with strain. However, there is no experimental evidence to warrant such an assumption. Without it, little can be concluded about the angles of misorientation that are produced by individual subgrain boundaries within a grain.

Electron microscopy investigations do not have this disadvantage, for misorientation angles between adjacent subgrains can be directly measured. No systematic investigations of subgrain misorientation during creep have

been made using this technique. However, measurements from a few creep studies show that misorientation angles generally range from 0.3 to 1 degree with almost no angles exceeding 2°[128,191,194].

Similar investigations on Al[175,179] show that after hot extrusion to a strain of 3.7 subgrain misorientation angles seldom exceed 2°*. More systematic observations on hot compressed Armco iron and silicon steel show that misorientation angles range from less than 1° to about 7°, but do not vary systematically with strain, strain rate, or temperature[200]. All of these hot working studies were conducted at higher stress levels than are encountered during creep, but they suggest the existence of a limiting subgrain misorientation for plastic deformation at high temperatures. The average subgrain misorientation angles that have been reported for hot worked metals after very large strains are generally larger than those reported from creep investigations. Thus, these observations do not necessarily imply that a limiting subgrain misorientation is reached during steady-state creep. The observations of Hammad and Nix[131] which attempt to show this directly, are far too limited to prove the point.

Obviously the evidence on changes in subgrain misorientation during steady-state creep are currently inconclusive. The subject is one that should command some attention in future experiments.

H. Reflections on Substructure.

A complete theory for steady-state creep should be able not only to account for the observed steady-state creep rate in terms of the variables

---

*McLean's formula, $\varepsilon=\theta$, implies that misorientation angles of 210° should have been observed.

of σ, G, D, T, Gb/Γ, etc., but should equally be able to predict the pertinent steady-state substructures. Obviously, such substructures form an integral part of a realistic model for steady-state creep. On the other hand, it appears as if this task is so formidable in view of the versatility of dislocation reactions that it will not be possible even over a considerable period of time to predict the steady-state substructure from first principles. Over this time interval the less pretentious objective of predicting the effects of σ, G, D, T, Gb/Γ on $\dot{\varepsilon}_s$ based on experimentally established substructural knowledge may be fruitful. Major attempts to do this have recently been summarized by Weertman.[70] This also was the viewpoint adopted here in arriving at the theoretical expression for high-temperature creep by the viscous drag mechanism given by Eq. 15.

A major question in development of theories concerns the experimental identification of the structural and of the substructural details that might affect the steady-state creep rate. This is seldom an easy task even when extensive experimental correlations have been established. For example, no serious theory for steady-state creep has yet considered the possible influence of subgrain size. Furthermore, no definitive experimental checks on this possibility are easily visualized. By inference, therefore, it might be thought that subgrain size plays no special role in steady-state creep.

It appears inevitable, however, that the principle of kinetic reciprocity must be operative during steady-state creep. On this basis the externally controlled variables of σ and T induce a steady-state creep rate when the internal variables of substructure also achieve a steady-state. The steady-state represents one of intimate kinetic balance among

all significant variables. If any one of the internal variables were, if possible, to be independently altered, the creep rate would also be altered. On this basis all creep-induced steady-state substructural features are believed to be significant to the observed creep rate. Of course, variations in some of the steady-state substructural features may produce larger changes in the creep rate than others and may, therefore, appear to be of greater importance. The above remarks include variations in substructure due to alloying dispersion strengthening etc.

I. Grain-Boundary Sliding.

One of the most controversial topics in the field of high-temperature deformation of metals is grain-boundary sliding. Grain-boundary sliding is important because it results in increased creep rates and because it promotes cavitation in grain boundaries which then leads to rupture. The last two phenomenon will not be discussed in this report and attention will be directed exclusively toward effect of grain-boundary sliding on the creep rate.

Numerous difficulties have been encountered in devising accurate procedures for determining quantitatively the contributions of grain-boundary sliding to creep strain. In the past analyses and methodology have not always been accurate, however, substantial improvements have been made recently. Since these issued have been recently reviewed[201-202], they will not be discussed again here. Another difficulty arises from the highly statistical nature of grain-boundary sliding. Other auxiliary factors lead to problems in measurement: grain-boundary reorientation at surfaces due to surface tension effects, grain-boundary migration, and grain growth. All require special consideration dependent on the experimental technique

that is employed. Despite questions concerning quantitative accuracy, particularly in the earlier investigations on grain-boundary sliding, many of the observed trends, nonetheless, have qualitative significance.

Observations have established that three distinctly different types of grain boundary sliding occur. When sliding is limited to submicroscopic regions of a boundary, as in damping capacity experiments, one type of behavior is observed. When sliding occurs over a relatively long length of boundary but is unconstrained by adjacent grains, as in bicrystals, another type of behavior results. Yet a third type is obtained when sliding occurs in polycrystalline aggregates, where continuity conditions exert considerable control over the sliding process.

Damping capacity experiments show that local microscopic grain-boundary sliding obeys a Newtonian viscosity law

$$\dot{v}_k = A_k \sigma \exp\left(-\frac{Q_k}{RT}\right) \qquad (27)$$

such that v_k increases linearly with σ and has an activation energy Q_k which equals that for volume diffusion. These results indicate that grain boundaries consist of islands of "good" and "poor" atomic fit, and that the number of such islands depends on boundary orientation as well as on the misorientation between adjacent grains. Under the action of a shear stress which parallels the boundary, the atoms of "poor" atomic fit move over atomic distances leading to very high rates of grain-boundary sliding, but very small average shear displacements across the boundary.

In contrast grain-boundary and boundary-zone sliding in bicrystals give macroscopically measureable shear displacements. The processes by which this takes place are complicated and not yet well understood. As a result of stress concentrations on the islands of "good" fit and at

grain-boundary ledges etc., macroscopic sliding takes place across the boundary. For such sliding it is expected that

$$v_b = A_b \sigma^2 e^{\frac{-Q_b}{RT}} \tag{28}$$

where the stress squared term arises from stress concentrations and Q_b is the activation energy for grain-boundary diffusion.

The simple model described above, however, is seldom operative because grain boundaries are seldom atomically flat. Boundary roughness undoubtedly accounts for the phenomenon of zone-boundary sliding, which is characterized by crystal deformation in a zone on either side of the grain boundary, recovery and polygonization in the grain boundary zone, and grain-boundary migration. Shear displacements vary from point to point along the boundary and the rate of displacement at any one point varies appreciably and cyclically with time. It has not yet been clearly established as to whether crystallographic slip, polygonization, or grain-boundary migration determine the average grain-boundary velocity of shearing. In any event the average velocity of displacement across the grain-boundary zone might be represented by the non-Newtonian expression

$$v_z = A_z f_z\{\sigma\} e^{\frac{-Q_z}{RT}} \tag{29}$$

Only a few data are available on the effect of stress on the grain-boundary displacement velocity. As shown by Stevens[201] these suggest that $f_z\{\sigma\}$ seems to vary as σ^1 to $\sigma^{2.8}$ and $\exp(-\sigma_o/\sigma)$ for individual cases. As shown in Table XII, the reported activation energies, Q_z, often agree reasonably well with those for self-diffusion. In a few cases, however, they appear to be somewhat higher[203] and lower[204] than those for self diffusion.

TABLE XII: Activation Energies for Bicrystal Sliding.

Metal	Q_z, Kcal/mole Bicrystal Sliding	Q_d, Kcal/mole Self-Diffusion	Ref.
Cu	40.0	47.0	205
Sn	19.2	23.0	206
Al	29.2 - 39.4 (high angle boundary)	34.0	207
Zn	25.0	24.3	208

The velocity for macroscopic grain-boundary sliding in bicrystals is known in a number of cases to be 10^{-2} to 10^{-8} that for microscopic grain-boundary sliding as deduced from damping capacity measurements. Obviously, the islands of "poor" fit are somewhat relaxed in the macroscopic grain-boundary sliding experiments in bicrystals.

The velocities of shear displacements across grain-boundaries in polycrystalline aggregates are yet orders of magnitude lower than across grain-boundaries in bicrystals. Obviously, additional constraints to grain-boundary sliding are encountered in the polycrystalline aggregates. These arise principally from the need to maintain continuity over boundary rough spots and at triple points. In view of the more rapid rate of grain-boundary sliding in bicrystals than in polycrystals, it appears that the shear stress across most grain boundaries in polycrystals relax very rapidly after the application of a stress. But this results in only small shear displacements of boundaries at this time because restraints from adjacent grains hinder extensive sliding. In order to obtain macroscopically measurable shear displacements across the grain-boundaries, the stress concentrations in the vicinity of the triple points must induce crystallographic mechanisms of deformation or mass transfer by diffusion. As shown in the earlier sections of this report crystallographic mechanisms such as dislocation climb are expected to dominate at high stresses where the diffusional mechanisms, (vide e.g. Nabarro creep) are much slower. At very low values of the applied stress, however, vacancy type of diffusion-controlled mass transfer should dominate. In the case of grain-boundary sliding, it is expected that grain-boundary rather than volume diffusion will be more rapid.

Most grain-boundary shearing results have been reported in terms of χ where χ is given by $\varepsilon_{gb}/\varepsilon_t$, the ratio of the contribution of strains due to grain-boundary shearing to the total strain. Although, as previously mentioned, the absolute values of this ratio may sometime be in error, especially for the earlier data that have been reported, the qualitative trends are nevertheless usually correct.

Extensive data[201], particularly for higher values of σ/G, suggest that χ has the same value over both the transient and steady-state stages of creep. The quantitative similarity between curves of ε_{gb} versus time and ε_t versus time (creep curves) suggests that grain-boundary sliding is probably controlled by the same mechanisms that are operative in the crystallographic creep of the grains themselves. This concept is further supported by the observation[203,209] that the apparent activation energy for grain-boundary sliding agrees quite well with that for crystallographic creep and that for diffusion.

Observations[210] show that upon ordering in beta brass, $\dot{\varepsilon}_g$ decreases by the same ratio as does creep rate; so that χ remains constant. This is strong evidence for the concept that grain-boundary shearing depends on crystallographic mechanisms of creep. Similar observations[149], that χ remains constant during certain precipitation reactions whereas ε_t changes substantially, also provide strong support for this thesis.

Three exceptions to the general trends on the constancy of χ over the full creep range have been reported. One[211] is at variance with the data of several other authors on grain-boundary shearing in Al[156,194]. The remaining two examples[212,213] refer to alloys in which the observations indicate that χ remains fairly constant during much of the

transient creep stage but then decreases as deformation continues. Several different "reasons" might be offered to account for such exceptions to the usual trend. On the other hand, none have yet been given experimental confirmation.

Most observations reveal that χ increases with decreasing grain size. The data in Fig. 19 on the effect of grain size on the steady-state creep rates further support this concept. One set of data[123] at variance to these trends appears to be obviously questionable.

Most existing data reveal that χ increases as σ/G is decreased. This trend is not necessarily at variance with the concept that grain-boundary shearing might be controlled by accomodations at grain boundary projections and triple points etc. by crystallographic creep mechanisms. Relaxation of the stress across islands of the grain-boundary by diffusional mechanisms is expected to be more complete at the lower levels of the stress. Higher local stress concentrations are therefore expected at the lower stress levels causing higher relative contributions of grain-boundary shearing to the total creep strain. Thus, higher values of χ are expected at the lower stress levels due to higher stress concentrations at the periphery of partially relaxed islands in the boundary. Two examples of the variation in χ with σ/G are given in Fig. 23, for Al[156] and stainless steel[152]. Although the absolute values of χ might be somewhat in error, the trends reveal that χ decreases with increase in σ/G.

An extension of these concepts to grain-boundary sliding at lower levels of σ/G where the sliding is grain-boundary diffusion-controlled leads to superplasticity.

J. Superplasticity.

Superplasticity is the subject of considerable research at present[214-216]. A study of the various alloy systems that have been investigated reveals that there are two prerequisites for the operation of superplastic behavior: a temperature greater than about one-half of the melting point (0.5 T_m), and a fine and stable grain size that does not undergo significant grain growth or recrystallization during elevated temperature deformation. Earlier suggestions that a eutectic type or a precipitation type of reaction is necessary for superplasticity have not been borne out by later investigations. For example, Gifkins[217] noted superplastic behavior in Pb-Tl alloys which are composed of just a single phase. In a typical superplastic eutectic alloy the second condition is often satisfied because both recrystallization and grain growth tend to be restricted by the presence of the small separate grains of the two phases.

Metallographic observation on typical superplastic alloys after deformation, reveals that:

1) The grain size does not change significantly during superplastic deformation.
2) Grains remain essentially equiaxed.
3) There are large relative rotations of adjacent grains.
4) Voids are not commonly observed at the grain boundaries of alloys when they are deformed in the superplastic range.
5) Previously inscribed straight scratches across grains become curved suggesting that some grain deformation also occurs.
6) Usually very few dislocations are noticed within the grains in the low strain rate range of the superplastic behavior, but there

is a progressive increase in dislocation density as the rate of straining increases. Ultimately at the high stress range of the superplastic region, the substructure is similar to that developed during typical high-temperature creep deformation at the same stress.

Mechanical data on superplasticity typically reveal[218-220] that the deformation rate has a n = 2 power stress dependence. The two power stress dependence often extends over four orders of magnitude of strain rates. This means that superplasticity cannot be envisioned as a region of transition between two mechanisms which have a high (n=4-5) and a low (n = 1) stress dependence. It is expected, however, that at sufficiently low values of σ/G, Coble or Nabarro creep might dominate and the strain rate become linear with stress. Some data in the literature suggest powers of the stress that approach unity[216].

The effect of grain size on the strain rate, as investigated by several workers[216,221], reveal that strain rate increases with a decrease in grain size. The analyses presented in the literature include d^{-2} and d^{-3} dependences where d is the grain size. Although Packer and Sherby[220] have analyzed the data on a Pb-Sn alloy on the basis of a d^{-3} dependence, it seems more likely that the majority of superplastic alloys follow a d^{-2} dependence of strain rate.

The activation energy of deformation in the superplastic region has not been extensively investigated. Ball and Hutchinson[219] observed that in an Al-Zn eutectoid alloy the activation energy for superplasticity falls between the activation energies for grain boundary diffusion of Zn and Al. Evans[222] observed that the strain rate of fine-grained Cu,

monel, and one austenitic alloy can be correlated satisfactorily with the activation energy for grain boundary diffusion. Hayden et al.[221], on the other hand, suggested that in a complex Ni-Fe-Cr-Ti-Al alloy the activation energy for superplastic deformation is that for volume diffusion, similar to that for pure Ni.

None of the suggested theories can explain all the details of currently available data on superplasticity. Avery and Backofen[216] have suggested the possibility of Nabarro creep in a Pb-Sn alloy. But strong evidence from recent experimental work refutes the n = 1 stress dependence that is required. Packer and Sherby[220] have analyzed the low strain rate data of Avery and Backofen using an empirical relationship of the form

$$\frac{\dot{\varepsilon}_s kT}{DGb} = \text{constant } \left(\frac{\sigma}{G}\right)^2 (b/d)^3 \qquad (30)$$

and obtained improved agreement. Gifkins and co-workers[217,223] have analyzed their data on Pb-Tl alloys using the semi-theoretical relationship:

$$\frac{\dot{\varepsilon}_s kT}{D_b Gb} = \text{constant } \left(\frac{\sigma}{G}\right) (b/d)^2 \qquad (31)$$

where D_b is the grain boundary diffusivity. The estimated rates were too slow to account for the superplastic strain rates for their Pb-Tl alloy. A studied review of available data indicates that the strain rate can be more satisfactorily correlated with σ^2 and d^{-2}. Such a correlation suggests that either:

$$\frac{\dot{\varepsilon}_s kT}{DGb} = K (\sigma/G)^2 (b/d)^2 \qquad (32)$$

or

$$\frac{\dot{\varepsilon}_s kT}{D_b Gb} = K' (\sigma/G)^2 (b/d)^2 \qquad (33)$$

depending on whether the activation energy is that for self diffusion or grain boundary diffusion. A reanalysis of the data on Pb-Sn[216] and Al-Zn[219] reveals that the constant K in Eq. 32 varies by four orders of magnitude. Equation 33 on the other hand, gives a correlation that is consistent with the trend of experimental observations. Equation 33 is essentially the same as that given by Ball and Hutchison[219].

It is instructive to outline the basis for Eq. 33 before describing any experimental correlations. Ball et al. assume that during deformation groups of grains whose boundaries are suitably aligned tend to slide as units. Certain grains that obstruct the relatively easy motion of grain units by grain boundary sliding yield under the resulting stress concentration. In the superplastic condition dislocations traverse such yielded grains and pile up at the opposite grain boundary until their back stresses prevent further grain-boundary sliding. The stress concentration at the head of the pile up causes accelerated diffusion and dislocations escape by climb into and along grain boundaries. The continued operation of this mechanism permits further boundary sliding. Following Friedel[224], the velocity of climb is presumed to be controlled by the rate of diffusion of vacancies in the grain boundary. When a is the unit of sliding, R is the ratio of the numbers of easy sliding to obstructing grains, and the distance of climb to the annihilation site is some fraction d/x of the grain diameter, theory predicts for the steady-state strain rate

$$\dot{\varepsilon}_s = \frac{2\, a\, x^2\, b^2\, R^2\, \sigma^2}{4\, d^2\, G\, k\, T}\, D_b \qquad (34)$$

which can be rewritten as Eq. 33, where the constant K' is given by

$$K' = \frac{a\, x^2\, R^2}{2b} \simeq 50 \text{ to } 100 \qquad (35)$$

The paucity of data on grain boundary diffusion in the literature makes accurate correlation difficult. The difficulty is compounded by the fact that most of the superplastic alloys have extremely fine grain sizes. In the absence of any positive reference in the literature on grain-boundary diffusion in the phases under consideration, the activation energy of grain boundary diffusion is taken to be one-half that of lattice diffusion. The lattice diffusion in a two phase binary alloy is approximated according to Eq. 2b: $D_{alloy} = (D_A^* D_B^*)/(N_B D_A^* + N_A D_B^*)$ where N_A and N_B are the atomic fractions respectively. This assumes that most of the grain boundaries are located between A and B phases as opposed to A-A and B-B boundaries. Metallographic examination of Al-Zn[219] and Pb-Sn system[216] suggests that the majority of grain boundaries are between dissimilar phases. Consequently, the correlation suffers from the crude approximation used to estimate diffusivities. But in the absence of a better estimate it suffices to indicate how the correlation follows the trend of experimental results. The correlation is shown in Fig. 24 for an Al-Zn[219] eutectoid alloy and in Fig. 25 for a Pb-Sn[216] eutectic. The solid or broken curves are theoretical correlations and the datum points are from experimental results. Fig. 24 shows that the datum points follow Eq. 33 for superplasticity up to $\sigma G = 10^{-3}$. At higher stresses the data agree well with the theoretical curve for dislocation climb

($n = 4.3$)*. The strain rate predicted by Coble[225] grain-boundary diffusion creep (which will be discussed in the next section) is too slow to contribute effectively to the strain rate above $\sigma/G = 10^{-4}$. Two data points suggest that Coble creep may become significant at lower stresses.

For the Pb-Sn alloy (Fig. 25) little error is introduced by the assumption of only Pb-Sn boundaries because the activation energy for lattice diffusion, and accordingly the energy for grain-boundary diffusion, in Pb and Sn is nearly the same. Thus it seems to be a reasonable estimate for the diffusivity in a Pb-Sn phase boundary. Again the correlation between the data for different grain sizes and the estimated relationship from superplasticity is acceptable. At higher values of σ/G, the data agrees well with that for creep of pure Sn[226] by climb of edge dislocations ($n = 5.1$). It might be noted that the rates predicted by Coble creep do not make any significant contribution to the superplastic strain rates in the stress range that was investigated. The value of the constant in Eq. 33 is estimated to be 53 for Al-Zn alloy and 115 for Pb-Sn alloy, which compares well to the value of approximately 50-100 predicted from the theory of Ball and Hutchison[219].

Because of the rather gross assumptions that must be made to check correlations of superplastic deformation rates, no definitive conclusions can be reached. However, the agreement that is obtained between Eq. 33

---

* This analysis is based upon the assumption that $D/D_b = \exp(-H_d/2RT)$ for Sn.

and experiment is encouraging. More data are needed at low values of σ/G and more accurate values of grain-boundary diffusivities must be obtained before a more accurate correlation for the mechanism of deformation in superplasticity can be offered.

VI. CORRELATIONS OF CREEP MECHANISMS

In the preceeding sections of this report various identifiable diffusion-controlled creep mechanisms were isolated for individual examination relative to the various factors that affect their steady-state creep rates. In the present section a comparison will be made of these mechanisms in order to reveal the ranges of conditions over which each mechanism predominates and how the various mechanisms are related one to another. This will be done in such a way as to provide a unified semi-quantitative picture of the creep resistance of metals and alloys when diffusion-controlled creep mechanisms are operative. Although major emphasis will be given to those creep mechanisms that have now been firmly established as operable, additional possible mechanisms will also be described.

The steady-state creep rates, as given by $\dot{\varepsilon}_s kT/DGb$ versus σ/G, for a number of mechanisms which are volume-diffusion controlled are shown in Fig. 26. With the exception of the low stress data for Al, shown by datum points, the various curves are representative of types of mechanisms and are discussed in more specific terms of alloys solely for purposes of identification.

For metals and alloys in which dislocations glide rapidly, the mechanism is climb-controlled as typified by the Ni curve. When solid-solution alloying results in a viscous glide, the viscous creep mechanism controls as typified by the Ni - 50% Au curve. Consequently, the creep rate for viscous glide is invariably below that for the climb-controlled mechanism when the differences in the two operative diffusivities are taken into consideration. As previously described, however, climb always occurs

in alloys where the creep rate is viscous glide-controlled. The value of $\dot{\varepsilon}_s kT/DGb$ for the climb mechanism, however, falls below that for the viscous glide mechanism for $\sigma/G \lesssim 10^{-4}$. Since the climb-controlled and the viscous glide-controlled mechanisms are mutually exclusive, only the slower can control the creep rate. Consequently it is anticipated that alloys which exhibit viscous glide mechanisms at high values of σ/G will revert to climb-controlled mechanisms when σ/G is decreased somewhat below about 10^{-4}. At present there are no data on creep of alloys that span a sufficiently wide range of σ/G to verify this prediction.

The improvement in creep resistance due to dispersion strengthening can be seen by comparing the creep data in Fig. 26 for Ni - 4.4 v/o ThO_2 with that for Ni. The improvement in creep resistance of the dispersion strengthened alloy increases as the stress is decreased so long as no other mechanism intervenes, since n is greater for this alloy than for pure Ni.

Typical curves illustrating the correlations with Nabarro creep for three different grain sizes are also shown in Fig. 26. Since it provides an independent mechanism, the total creep rates that are operative during the climb, viscous glide, or dispersion-strengthened mechanisms must include the contribution from Nabarro creep. As seen from the curves of Fig. 26, this contribution is small for high values of σ/G. At very low values of σ/G, however, dependent on grain size, the contributions of creep controlled by the climb, viscous glide, or dispersion-strengthened mechanisms are small and Nabarro creep predominates. As shown by the several broken curves, the transition from predominantly climb or dispersion-strengthened creep to predominantly Nabarro creep, occurs over less than one order of

magnitude change in σ/G.

Friedel originally suggested that subgrains, as well as grains, might also undertake Nabarro creep. The conditions under which this might be possible were studied in detail by Weertman[70]. Assuming that the subgrain diameter varies with σ/G as given by Eq. 25, Nabarro creep across the subgrains becomes

$$\frac{\dot{\varepsilon}_s kT}{DGb} = 10^{-2} \left(\sigma/_G\right)^3 \qquad (36)$$

This relationship is given by the solid curve marked "Nabarro subgrain" in Fig. 26. As shown, it cannot effectively increase the creep rates obtained for the predominantly climb-controlled mechansim at high values of σ/G. The subgrains are so large at lower values of σ/G that it appears to be unimportant here as well.

Recently Nabarro[227] proposed a theory for high-temperature creep based on the climb of dislocations from Bardeen-Herring sources. Unlike the Weertman dislocation-climb model, it does not require glide of dislocations to provide the strain; in N-B-H creep the strain arises from mass transport of atoms to and from climbing Bardeen-Herring sources by a vacancy diffusion mechanism. More recently Weertman[70] discussed the theoretical basis for this mechanism. The creep rate for this mechanism is given by

$$\frac{\dot{\varepsilon}_s kT}{DGb} \simeq \frac{1}{12 \ln\left(\frac{8G}{\pi\sigma}\right)} (\sigma/G)^3 \qquad (37)$$

The expected trend for this mechanism, as shown by the dotted and dashed line labeled N-B-H in Fig. 26, falls below the line "Viscous" for viscous

creep of Ni - 50 % Au alloy. It seems to the authors that the special requirements for the operation of the N-B-H, e.g., the regularity and size of the Frank network, are not easily satisfied so that glide plus climb-controlled creep or viscous glide-creep should prevail, since glide of dislocations disqualifies the N-B-H model in most cases of interest.

Despite the fact that current knowledge on volume-diffusion controlled high-temperature creep appears to be very complete, it is nevertheless admitted that new and presently unknown mechanisms might yet be uncovered. Data on creep of polycrystalline Al by Harper, Shepard and Dorn[156] is illustrative of this possibility. Their data are shown by the datum points on the curve for Al in Fig. 26. Above $\sigma/G \simeq 10^{-5}$, the data agree well with that for climb-controlled creep where $n = 4.4$. Below $\sigma/G \simeq 10^{-5}$, however, the creep data give the stress exponent $n = 1$ suggestive of Nabarro creep. The Nabarro creep curve for the grain size that was employed, namely $b/d = 7.7 \times 10^{-8}$, is shown in Fig. 26 as "Nabarro No. 1". Since it falls about three orders of magnitude below that obtained experimentally, the observed creep could not have occured by the Nabarro mechanism. This was also confirmed by the fact that the strains were about the same within the grains as across the grain boundaries. Furthermore, a single crystal test gave almost the same creep rate as did the polycrystalline aggregate. Obviously, some as yet unidentified volume-diffusion mechanism is operative.

Coble[225] has shown that stress-directed diffusion of vacancies can take place by grain-boundary diffusion as well as by Nabarro volume diffusion. The creep rate by this mechanism increases with the reciprocal

of the cube of the grain diameter according to*

$$\frac{\dot{\varepsilon}_s kT}{D_b Gb} \simeq 48 \left(\frac{b}{d}\right)^3 (\sigma/G) \qquad (38)$$

where the thickness of the grain boundary is taken as about 2b and D_b is the grain boundary diffusivity. This grain-boundary diffusion mechanism should predominate over the volume diffusion Nabarro mechanism when

$$48 \left(\frac{b}{d}\right) \frac{D_b}{D} > 7 \qquad (39)$$

If vacancy generation and absorption is highly efficient the total creep rate is given by

$$\frac{\dot{\varepsilon}_s kT}{DGb} = \left\{ 7\left(\frac{b}{d}\right)^2 + 48 \frac{D_b}{D} \left(\frac{b}{d}\right)^3 \right\} \sigma/G \qquad (40)$$

which is the sum of that arising from Nabarro and Coble creep. Although there has been no definitive experimental confirmation of Coble creep in metals and alloys up to the present, it nevertheless must be given serious consideration in view of its firm theoretical justification. Predicted creep rates based on Coble's model are shown for three grain sizes in Fig. 27 in terms of $\dot{\varepsilon}_s kT/D_b Gb$ versus σ/G curves where D_b is the grain-boundary diffusivity.

As previously discussed, one of the least known high-temperature mechanisms of creep is that which leads to superplasticity. The

---

*An analysis of Coble's theory by the present authors revealed that the constant in Eq. 38 should be 48 as given above for relaxed grain boundaries in lieu of the value 148 determined by Coble.

correlation between this mechanism and Coble creep might be based on the assumption of the nominal validity of the model for superplasticity proposed by Ball and Hutchison. Such predicted curves for superplasticity are also shown in Fig. 27. To permit ready comparison, the creep curves for the dislocation climb mechanism can be rewritten as

$$\frac{\dot{\varepsilon}_s kT}{D_b Gb} = 2.5 \times 10^6 (\sigma/G)^n (D/D_b) \qquad (41)$$

Assuming that the activation energy for grain boundary diffusion H_b, is equal to one-half of that for lattice diffusion H_d, $D/D_b = e^{-H_b/RT}$. The three curves for climb of Al ($n = 4.4$), as shown in Fig. 27, correspond to three temperatures: 900°K, $D/D_b = 8.2 \times 10^{-5}$, $H_b/RT = 9.4$; 700°K, $D/D_b = 5.5 \times 10^{-6}$, $H_b/RT = 2.1$; and 500°K $D/D_b = 4.13 \times 10^{-8}$, $H_b/RT = 17$. The creep due to superplasticity is additive to that due to climb. Hence about one-half order of magnitude below the point of intersection of the curves for climb and superplasticity, climb-controlled creep no longer significantly affects the total creep rate. Similarly, at one-half order of magnitude of stress level above the point of intersection, creep due to superplasticity is negligible. The resultant creep rate between these limits are shown by the fine dashed lines in Fig. 27 which fare from creep due to climb for a particular temperature (or H_b/RT) into that for superplasticity for a particular value of b/d. It is seen that for a given grain size the transition from superplasticity to creep by climb occurs at increasing values of σ/G as the temperature for creep by climb decreases.

Most experimental observations on superplasticity conform to the suggested trend of decreasing values of n from that appropriate for climb

to that of n = 2 which applies in the superplastic range. As shown, the superplastic range is expected to cover a wide range of $\dot{\varepsilon}_s kT/D_b Gb$ when the grain size is small. Although the concepts presented here suggest that Coble creep should predominate at low values of σ/G, experimental confirmation for this transition is lacking perhaps due to limitations in the range of σ/G that were investigated. Furthermore, other types of mechanisms and perhaps Nabarro creep could also intervene to complicate the simple trends suggested in Fig. 27. Much more detailed and thorough investigations are needed to clarify the creep of fine-grained metals and alloys at low values of σ/G.

VII. TRANSIENT CREEP

Early investigations[228] showed that

$$\varepsilon \equiv \varepsilon \{ t\, e^{\frac{-Q_c}{RT}} \} \qquad \text{for } \sigma = \text{const.} \qquad (42)$$

over both the transient and the steady-state stages of creep at high temperatures. In this formulation ε is the total strain, which is the sum of the initial strain ε_o upon stressing at t = o and the creep strain up to time t. The apparent activation energy, Q_c, for creep was shown to be insensitive to the stress, strain, grain size, temperature etc.; it agreed well with the activation energy for diffusion. Except for extensive reconfirmation of Eq. 42, little additional progress was made over much of intervening time interval in further advancing an understanding of the transient stage of creep. During the past two years, however, several important observations have been made that have led to a more complete analysis of transient creep.

A studied review of all pertinent data reveals that only those metals and alloys that undergo initial straining upon stressing exhibit the usual normal transient (NT) stage of creep. This group includes all metals and almost all alloys for which $n \simeq 5$, and perhaps a few alloys for which $n \simeq 3.3$. Those alloys which do not undertake significant initial straining at t = o upon application of the stress do not exhibit the usual normal transient stage (NT) of creep. They instead display one of three different types of transient behavior. The few $n \simeq 5$ alloys of this type show an almost negligible initial strain and an extremely brief normal transient (BNT). Alloys of the $n \simeq 3.3$ class which undergo no initial

strain show either a brief inverted transient (BIT) over which the creep rate increases towards the steady state or no transient behavior at all (NoT). A few $n \simeq 3.3$ alloys show BNT behavior. Such BNT and BIT seldom extend beyond the first ten minutes of the test. It is not yet understood why some alloys show initial straining and others do not. Known examples of alloys which display BNT, BIT and NoT behavior are documented in Table XIII and illustrated in Fig. 1.

The decreasing creep rates over the normal transient stage of creep, under constant values of the independent variables of stress and temperature, must be ascribed to the development of more creep resistant substructures over primary creep. Since normal transient creep is contingent upon the occurrence of initial straining, normal transient creep rates are the result of changes in the substructure from that which is produced immediately upon stressing to that which pertains to the steady state.

The substructures which are formed upon initial straining at creep temperatures closely resemble those which are developed during Stage III deformation at lower temperatures[126, 127, 131]. Most dislocations are arranged in a rough cellular pattern which is composed of dislocation entanglements as previously described. Each pitting studies[126, 128, 130] show that during the early portions of transient creep the cellular structure remains observable, but in many localized areas dislocations rearrange to become either randomly distributed or to develop partially formed subboundaries. Electron transmission microscopy[75, 128, 131] shows that at this time loosely-knit subgrain boundaries are being developed through dislocation untangling and redistribution of dislocations. No abrupt changes in the dislocation substructure occur during the transient stage.

Table XIII: ALLOYS THAT DISPLAY BRIEF NORMAL TRANSIENTS (BNT), BRIEF INVERTED TRANSIENTS (BIT), AND NO TRANSIENTS DURING DIFFUSION-CONTROLLED CREEP.

Alloy	n	ε_o	Type of Transient	Creep Curve Type - Fig. 1	Reference
Mg - 12% Li	4.8	0	BNT	B_1	86,87
AgMg	5.7	<0.001	BNT	B_1	3
Fe - 3.9% Mo	>4*	0	BIT	B_3	80
Au - 10 to 87% Au	3-3.4	?	BNT	B_1	33
W - 25 to 30 wt. % Re	3.8	0	NoT	B_2	99
β - CuZn	3-3.4	<0.0004	NoT	B_2	98
Al - 3.1% Mg	3.5	0	NoT	B_2	5
Al - 2.1% Mg (low stresses)	3.5	0	BIT	B_3	8
Al - 2.1% Mg (higher stresses)	3.5	>0	BNT	B_1	8
Ag_2Al	3.6	0	BIT	B_3	6

*Reported for alloy of similar composition (ref. 83).

Rather, as strain increases, larger numbers of roughly-formed subgrain boundaries develop, cells become diffuse as dislocations climb and glide away, and those subboundaries which are already formed become better defined and more tightly knit. A subgrain structure emerges gradually and is perfected over the latter stages of the transient creep. Electron micrographs on Mo[128] show that subgrain boundaries which are reasonably perfect can migrate through glide and climb to aid the development of the subgrain structure. Finally at the secondary stage of creep a subgrain structure is developed which is characteristic of the steady-state. In two investigations the mean subgrain size that was developed was at least twice as large as the cells originally present[126, 128]. This means that on the average eight or more cells dispersed in order to form each subgrain, which shows the high degree of mobility of dislocations within the cellular structure during the transient stage of creep.

As outlined above the substructural changes that attend normal transient creep are extremely complex. This complexity is clearly revealed by the detailed investigations of Clauer, Wilcox and Hirth[128]. Undoubtedly these substructural changes are significant to the transient creep rate. Such changes in the different substructural details over the transient stage are undoubtedly interrelated. For example, the dispersal of the entanglements, the build-up of low angle boundaries, the changes in density of dislocations, and the alterations in misorientations across low angle boundaries, etc., are not mutually independent. Among these various details, only the dislocation density has been placed on a quantitative basis.

Several investigators have attempted to follow the change in disloca-

tion density with strain over the transient stage of creep[126, 128, 140, 195]. Admittedly, to accomplish this with satisfactory accuracy is extremely difficult, particularly in view of the major changes that take place in the geometrical distribution of dislocations.

Furthermore it is not immediately apparent how the density of dislocations should be partitioned among those entangled in the disappearing cell walls, those adding to the growing low angle boundaries, and those that are meandering about more or less randomly. Early in the transient stage it is customary to count all dislocations including those in the entangled cell walls and those in the body of the cells despite the fact that each group might contribute differently to the transient creep rate. As the transient creep rate approaches that for the steady state, it is customary to count only those dislocations that are within the subgrains. But, as discussed earlier, the subgrain boundaries are undoubtedly moving and consequently the dislocations in the subboundaries also warrant special attention.

Results on the variations in dislocation density within the subgrains with creep strain are recorded in Fig. 28 where $\dot{\varepsilon}/(\dot{\varepsilon}_s \rho b^2)$ is plotted as a function of ε for Cu single crystals and polycrystalline Fe - 3.1 wt.% Si, and as a function of $(\varepsilon - \varepsilon_o - \dot{\varepsilon}_s t)/\dot{\varepsilon}_T$ for Mo single crystals, where ε_o is the initial strain and ε_T is the total transient strain. This method of plotting was selected because several investigators suggested that $\dot{\varepsilon}$ might be linearly related to ρ. As shown the figure, however, $\dot{\varepsilon}/(\dot{\varepsilon}_s \rho b^2)$ seems to decrease over the primary stage revealing that the expected linear correlation of $\dot{\varepsilon}$ with ρ is not valid. If creep were controlled by the motion of jogged screw dislocations, it might be expected that $\dot{\varepsilon}$

would increase linearly with ρ. The effect of dislocation density on climb-controlled creep, however, need not be linear because with higher densities of dislocations the climb time would be shorter but the area swept out by the dislocations would also be smaller. The effect of these counteracting influences on $\dot{\varepsilon}$ has not yet been formulated.

The etch pit studies which were used to compile Fig. 28 show that during transient creep the density of dislocations within the subgrains seems to decrease by a factor of about 2 for Fe-3.1 wt.% Si by about 5 for Mo. This reveals that α of Eq. 24 increases slightly during transient creep, whereas, the data recorded in Fig. 20 suggests that α is "about" the same for dislocations within the subgrains at the steady state as it is at atmospheric temperatures during formation of entanglements. Both statements appear to be valid within the accuracy of estimating ρ by etch pit techniques over the transient stage of creep.

Detailed electron microscopic investigations by Clauer, Wilcox and Hirth[128] have shown that tilt boundaries form a significant part of the substructure during transient creep of single crystals of Mo. The evidence strongly suggests that such tilt boundaries migrate. No estimate has yet been made on the contribution of tilt-boundary migration to the transient strain rate.

Accepting the present, admittedly unsatisfactory, state of knowledge concerning substructure, it nevertheless appears that dislocation densities decrease only slightly during transient creep. In contrast, major changes occur in the geometrical arrangements of dislocations from initial conditions of entanglements at cell boundaries to their dispersal during transient creep, and finally to well-defined subgrains separated by low-

angle boundaries when the steady-state rate is achieved. In the absence of entanglements, which is coincident with no initial straining upon stressing, little or no transient creep takes place. In these cases the steady-state dislocation density is established after 5 to 10 minutes of creep as reflected in the brief, normal, or inverse transients that are often obtained. Such adjustments in dislocation density occur with only minor changes in the creep rates.

In view of the proceeding discussion we now postulate, as suggested by Gupta and Strutt[126], that transient creep, with attendent high strain rates, arises principally as a result of the dispersal of entanglements by the climb mechanism. This dispersal is expected to follow unimolecular reaction kinetics with a rate constant that depends on the creep mechanism. As shown by Webster, Cox and Dorn[229] such kinetics can be formulated as

$$\frac{d(\dot{\varepsilon} - \dot{\varepsilon}_s)}{dt} = -k\dot{\varepsilon}_s(\dot{\varepsilon} - \dot{\varepsilon}_s) \tag{43}$$

where the rate constant is $k\dot{\varepsilon}_s$, assuming $\dot{\varepsilon}_s$ results exclusively from climb kinetics. Integrating once gives

$$\dot{\varepsilon} - \dot{\varepsilon}_s = (\dot{\varepsilon}_i - \dot{\varepsilon}_s)\, e^{-k\varepsilon_s t} \tag{44}$$

where $\dot{\varepsilon}_i$ is the initial creep rate at $t = 0$. A second integration yields

$$\varepsilon = \varepsilon_o = \dot{\varepsilon}_s t + \frac{\dot{\varepsilon}_i - \varepsilon_s}{k\dot{\varepsilon}_s}\,(1 - e^{-k\dot{\varepsilon}_s t}) \tag{45}$$

where ε_o is the initial strain upon stressing and

$$\frac{\dot{\varepsilon}_i - \dot{\varepsilon}_s}{k\dot{\varepsilon}_s} = \varepsilon_T \tag{46}$$

where ε_T is the transient strain. Since the kinetics of reaction are

known to be the same over the transient and steady-state conditions it necessarily follows that $\dot{\varepsilon}_i = K\dot{\varepsilon}_s$ where K is a constant greater than unity. Therefore

$$\frac{\dot{\varepsilon}_i - \dot{\varepsilon}_s}{k\dot{\varepsilon}_s} = \frac{K - 1}{k} = \varepsilon_T \qquad (47)$$

where K, k and ε_T are constants independent of stress and temperature.

Equation 45 was first suggested on a purely empirical basis by McVetty[230] for correlating the transient and steady-state creep rates. Recently it has been applied with success by Garafalo, Conway and Mulliken[231], and Wilshire and Evans[232]. More often, however, Andrade's empirical equation[233], namely

$$\varepsilon - \varepsilon_o = \dot{\varepsilon}_s t + Bt^{1/3} \qquad (48)$$

is employed for this purpose. It too is often in fair agreement with high temperature creep data. However, if Andrade's equation is to account reasonably well for the effects of stress and temperature on the creep rate, it is necessary to further assume that B is proportional to $\dot{\varepsilon}_s^{1/3}$. The major objection to the application of Andrade's equation to high-temperature creep, though, concerns its prediction of infinite initial creep rates; whereas, carefully conducted investigations reveal that they are actually finite.

If transient creep follows first order kinetics so that it can be described by Eq. 45, the following must apply:

1. The initial strain upon stressing, ε_o, depends on the original state of the metal or alloy and the value of σ/G.

2. The initial creep rate $\dot{\varepsilon}_i$, for a given metal or alloy is a constant multiple, K, of the steady-state creep rate $\dot{\varepsilon}_s$, regardless of stress

and temperature. It is independent of the initial strain, ε_o.

3. The rate of dispersal of the entanglements depends on the same function of stress and temperature as does the secondary creep rate.

4. As the entanglements disperse the creep rate decreases in a manner which seems to suggest that strain hardening is occuring. Strain hardening, however, usually has the implication of increased density of dislocations, whereas, during the dispersal of the entanglements the density of dislocations decreases slightly. In order to avoid false implications it appears that the term recovery strengthening due to entanglement dispersal by climb is preferable. The significant issue is that the rate of such recovery strengthening depends on stress and temperature in the same way as does the secondary creep rate.

5. For any given metal or alloy the transient strain ε_T is constant independent of stress or temperature.

6. For a given metal or alloy there exists a universal high-temperature transient and steady-state creep curve of the form

$$\varepsilon - \varepsilon_o = f\{\dot{\varepsilon}_s t\} = \phi\{(\frac{\sigma}{G})^n \frac{DGb}{kT} t\} \qquad (49)$$

where the function f is derived from Eq. 4. This relationship is an extension of Eq. 42, which now incorporates the effects of stress as well as temperature on the shape of transient creep curve.

With minor exceptions, which will be discussed later, above items 1, 2 and 5 have been confirmed for a few metals and alloys by a number of investigators[75, 229, 232]. Rather than review each case in detail a summary will be given on all pertinent published data on transient creep

curves.*

Fig. 29 shows the initial strains, ε_o as functions of σ/G for the accessible examples. These data refer to the modulus-adjusted athermal stress-strain curves at high temperatures. In general, such data exhibits considerable scatter as a result of difficulties in technique of measuring the initial strains immediately following stressing. The secondary creep rates $\dot{\varepsilon}_s$, for the metals and alloys in question are shown in Fig. 30, where log $\dot{\varepsilon}_s kT/DGb$ is plotted as a function of the log σ/G. All examples clearly fall into the category of creep by the dislocation-climb mechanism. As a typical example of the universal creep curve the case of polycrystalline Ni[234] is shown by the datum points in Fig. 31. Regardless of stress or temperature all data fall well on a single curve. The remaining cases that were examined were equally consistent. The value of ε_T can be deduced directly from Fig. 31. Equally, the rate constant k is also determinable from these data. The solid line refers to the theoretical expression given by Eq. 49; it illustrates the good agreement of the theory with the experimental results. Fig. 32 illustrates that the initial creep rates, $\dot{\varepsilon}_i$, for a series of stresses and temperatures are greater than the secondary creep rates,

---

* The authors express their appreciation to Mr. Kamal Amin for making this summary available to them.

TABLE XIV: A SUMMARY OF ANALYZED TRANSIENT CREEP DATA

Metal	Crystal Structure	Grain Size (mm)	$\frac{Gb}{\Gamma}$	ε_T	k	K	Data from Reference
Mo [S]	BCC	-	-	0.052	173	10.0	235
Nb	BCC	0.17-0.36	-	0.032	116	4.70	236
Fe-0.23 wt. % C Steel	BCC	Austenitic Grain Size 0.021 - 0.104	-	0.024	116	3.77	237
Ag	FCC	0.017	333	0.013	99	2.28	43
AL	FCC	0.21	49	0.105	82	9.56	8
Cu	FCC	0.03	188	0.0085	277	3.35	37
Ni	FCC	-	93	0.042	346	12.9	234

$\dot{\varepsilon}_s$, by the constant factor K regardless of stress or temperature. A summary for all examples that have been analyzed is given in Table XIV.

Whereas the transient strain, ε_T, exhibits rather pronounced variations from case to case, the rate constant k seems to be somewhat less variable. Undoubtedly, both depend on significant substructural details. Up to the present, however, no consistent trends invariations of k or K have been uncovered relative to grain size, stacking-fault energies, or any other pertinent structural details.

Evans and Wilshire[232] noted that Eq. 45 becomes inaccurate for creep of Fe at low stresses. Similar discrepancies which arise in the creep of austenitic stainless steels have been shown by Webster, Cox, and Dorn[229] to arise from the increased contribution of grain-boundary sliding to the total creep rate at the low applied stresses. When grain-boundary sliding prevails, $\dot{\varepsilon}_s$ no longer represents the secondary creep rate resulting from climb alone, and therefore, $k\dot{\varepsilon}_s$ is no longer the pertinent rate constant for dispersal of entanglements. Once grain-boundary sliding is better understood quantitatively, this factor can also be taken into consideration so as to account for transient creep at low stresses in polycrystals.

VIII. STRAIN HARDENING, RECOVERY AND CREEP.

As early as 1926 Bailey[238] proposed that creep resulted from recovery of the strain-hardened state. Orowan[239] twenty years later applied this concept in his discussions on the origin and nature of creep. Although the recovery concept of creep seems to have been widely held over the intervening years, no serious experimental confirmation of this assumption was attempted until stimulated by the recent investigations of Mitra and McLean[141,240]. Interest in this phenomenological concept of creep stems from the fact that is is not subject to the limitations of any specific creep or recovery model, and so might be widely applicable.

Orowan expressed the significant relationship in terms of the flow stress, σ, as

$$d\sigma = \left(\frac{\partial\sigma}{\partial t}\right)_{\varepsilon} dt + \left(\frac{\partial\sigma}{\partial\varepsilon}\right)_{t} d\varepsilon \qquad (50)$$

which assumes the existence of a mechanical equation of state. For creep under a constant stress therefore,

$$\dot{\varepsilon} = \left(\frac{\partial\varepsilon}{\partial t}\right)_{\sigma} = \frac{-\left(\partial\sigma/\partial t\right)_{\varepsilon}}{\left(\partial\sigma/\partial\varepsilon\right)_{t}} = \frac{r}{h} \qquad (51)$$

where r is the rate of recovery and h refers to the rate of strain hardening. If independent experimental determinations of $\dot{\varepsilon}$, r, and h verify Eq. 51, the validity of the recovery model will have been established.

The most recent attempt to check the validity of Eq. 51 by Watanabe and Karashima[52] involved straining the specimen in a tensile testing machine especially instrumented to permit this to be done under constant stress from which $\dot{\varepsilon}$ could be obtained. At various stages the cross-head

motion was arrested and the value $r = -(\partial\sigma/\partial t)$ was determined for the instant of arrest. Shortly thereafter, h was also evaluated during creep, by increasing ε rapidly by an amount $\Delta\varepsilon$ and determining $\Delta\sigma$. It was found that r increased with the stress and temperature in a manner coincident with that for the steady-state creep rate, while $h \simeq (\Delta\sigma/\Delta\varepsilon)_t$ was independent of the stress level. The good agreement that was obtained between $\dot{\varepsilon}$ and r/h, as so evaluated, was thought to confirm the validity of the recovery model.

Actually, this agreement was inevitable regardless of type of creep mechanism or any other detail. When the cross-head motion was held constant the strain rate was

$$\dot{\varepsilon} + \dot{\varepsilon}_{E'} = \dot{\varepsilon} + \frac{1}{E'}\left(\frac{\partial\sigma}{\partial t}\right) = 0 \qquad (52)$$

where $\dot{\varepsilon}$ was the creep strain rate during stress relaxation and $\dot{\varepsilon}_{E'}$ the elastic response of the specimen and the machine. E' refers to the apparent machine and specimen modulus. At the start of the stress relaxation experiments, $r = -(\partial\sigma/\partial t)_{t=o} = E'(\dot{\varepsilon})_{t=o}$.

Such stress relaxation tests measure only the creep rate, since $(\dot{\varepsilon})_{t=o}$ is itself the creep rate. The agreement that was found between creep rate and r/h follows directly from the method used to measure h: $h = \Delta\sigma/\Delta\varepsilon = 1/E'$. The hardening rate was observed to be independent of stress as it obviously must be when measured in this way. This kind of a test merely proves that the same $\dot{\varepsilon}$ for creep is obtained from a creep test and a stress relaxation test and nothing more, regardless of the mechanism.

The technique introduced earlier by Mitra and McLean[141] differed slightly from that employed by Watanabe and Karashima. They decreased

the stress by $\Delta\sigma$ after steady-state creep was established. After a time Δt, the specimen seemed to give a steady-state creep rate for the reduced stress, from which $\Delta\sigma/\Delta t$ was determined for the limit of $\Delta\sigma \to 0$. This was done for a series of stresses, from which $(\partial\sigma/\partial t)_\varepsilon$, was evaluated. The rate of strain hardening was established by room temperature tensile testing of the structure that had been produced by steady-state creep. This was converted to the slope $d\sigma/d\varepsilon$ at the test temperature by introducing the effect of temperature on the modulus of elasticity. Whereas h decreased somewhat as the stress for steady-state creep was increased, r increased rapidly with the creep stress. The relationship given by Eq. 51 for $\dot{\varepsilon}$ was crudely obeyed.

The basis of the Mitra-McLean approach seems to be somewhat more acceptable than the stress relaxation approach of Watanabe and Karashima. But, as shown by Mitra and McLean[141] and Ishida and McLean[171], their measurement of Δt for recovery might be seriously in error. The recovery curve following a reduction in stress has previously been investigated by Bayce, Ludemann, Shepard and Dorn[241], Ludeman, Shepard and Dorn[242], and Raymond and Dorn[244]. Bayce et al.[241], in particular, showed that in Al the microstrains attending a decrease in stress always involve a rapid time-dependent anelastic creep recovery in addition to immediate elastic recovery. Contrary to the assumptions[239,240] made in strain hardening and recovery theories for creep, the creep rate does not vanish upon reduction of the stress. Rather, in conjunction with the minor amount of creep recovery just mentioned, a finite creep rate, $\dot{\varepsilon}_1$, is obtained following the anelastic creep recovery. With continued straining the creep rate decreases from $\dot{\varepsilon}_1$ to a lower value $\dot{\varepsilon}_2$. Following this, the

creep rate increases from $\dot{\varepsilon}_2$ to the steady-state value, $\dot{\varepsilon}_s$, appropriate for the new stress. The recovery curve following a stress reduction is distinctly more complicated than assumed by Mitra and McLean. This questions the validity of their approach and suggests that the substructural changes which follow a reduction in stress are extremely complicated.

The shape of the creep curve that is obtained upon a sudden reduction in stress is different for metals and alloys which creep by the mechanism of dislocation climb ($n \simeq 5$) than for alloys which creep by viscous glide ($n \simeq 3$). As shown in Fig. 33 and 34, a sudden reduction in stress is always accompanied by an abrupt drop in creep rate. Following this sudden drop, the creep rate either increases ($n \simeq 5$, Fig. 33) or decreases ($n \simeq 3$, Fig. 34) with time until the steady-state creep rate appropriate to the lower stress level is obtained. Immediately after the drop in stress the dislocation density, in the $n \simeq 3$ alloy, although lower than that prior to stress reduction, is still higher than the steady-state value for the lower stress level. For viscous-glide creep, strain rate is proportional to dislocation density. Hence, the initial creep rate immediately after stress reduction is higher than the steady-state value for that stress. During the recovery period, as the dislocation density decreases toward the steady-state density, the instantaneous creep rate approaches the new steady-state creep rate.

In the $n \simeq 5$ case (Al, Fig. 33) immediately after the reduction in stress, although minor adjustment in the dislocation density does take place, both the density and the subgrain size correspond more closely to that which were present in the substructure before the stress was dropped. During the subsequent period of recovery, the dislocation density decreases

and the subgrain size increases to values appropriate to the steady-state substructure for the lower stress level. Metallographic observations[242,243] reveal that the increase in creep rate is parallelled by a simultaneous migration of subboundaries and readjustment of the substructure of the specimen. The subboundaries slowly sweep out volumes leaving a "recovered" structure in their wake. The increased creep rate with time during recovery, in this case, seems attributable to subboundary migration. If creep rate were proportional to the dislocations in the body of subgrains, it should have decreased instead of increased during the recovery period. Finally, however, the swept-out regions and the regions which recovered by climb achieve the steady-state density of dislocations and subgrain size corresponding to the reduced stress level. Thus the substructural changes that take place during the recovery period which follows an abrupt decrease in stress are very different from those which take place during transient creep.

Figure 35 shows the results of Raymond and Dorn[243] in which the drop-in-stress technique was used to determine the initial creep rate upon stress reduction, $\dot{\varepsilon}_{ir}$, as a function of stress level. The $\dot{\varepsilon}_i$ and $\dot{\varepsilon}_s$ curves in the same figure correspond to initial and steady-state creep rate respectively in the absence of any stress-reduction. Attempts were made to approximate the effect of σ/G on the creep rate per se, by so adjusting σ/G as to maintain, at least instantaneously, the same substructure. Al specimens were crept at a constant value σ_o/G from A to the steady-state at B. After the steady-state was reached, σ/G was reduced by different amounts, $\Delta\sigma$, to σ_r/G in a series of independent similar tests. Immediately following a very brief interval of anelastic

creep recovery, the initial creep rate $\dot{\varepsilon}_{ir}$ was determined for the various values of σ_r/G. Since the amount of anelastic recovery, although quite small, increased as lower values of σ_r/G were used, the various initial creep rates at the reduced stress levels do not correspond to exactly the same substructure. However, it seems reasonable to believe that no major changes in substructure took place from that which was obtained at the previous steady-state value for σ_o/G. Thus the curve designated $\dot{\varepsilon}_{ir}$ refers to the creep rate as a function of σ_r/G for about the same substructure. During continued creep the creep rate increased and finally achieved the steady-state values appropriate to the reduced stresses. The curve connecting the datum points $\dot{\varepsilon}_{ir}$ can be represented by

$$\dot{\varepsilon}_{ir} = \dot{\varepsilon}_{so} \exp\left[\beta \frac{(\sigma_o - \sigma_r)}{G}\right] \tag{53}$$

as shown by the curve through the datum points, where $\dot{\varepsilon}_{so}$ and σ_o are the secondary creep rate and the original stress before the drop in stress. These results agree well with earlier data by Sherby, Frenkel, Nadeau and Dorn[244] obtained in a somewhat similar fashion, in that β is independent of the temperature. They reveal that the creep rate increases more rapidly with σ/G for approximately constant substructure than it does for the various steady-state substructures. Obviously, any realistic theory of creep must take the substructure into serious consideration.

IX. SUMMARY

Over the past 15 years much progress has been made in rationalizing the creep behavior of metals and alloys at temperatures above about one-half of their melting temperature. In general, metals, solid-solution alloys, many dispersion-strengthened alloys, and some ordered alloys creep by one or more of several diffusion-controlled mechanisms. Some special dispersion-strengthened alloys, however, appear to creep in accord with Guyot's[111] mechanism of thermally activated breaking of attractive junctions. The steady-state creep rates from all diffusion-controlled mechanisms can be correlated by the expression $\dot{\varepsilon}_s kT/DGb = A(\sigma/G)^n$. The various diffusion-controlled mechanisms differ from one another only with regard to (1) the diffusivity D that is involved; (2) the value of A and the structural factors that are incorporated in it, and (3) the value of n. This is summarized in Table XV. Not included in this table are the mechanisms of Nabarro-Herring-Bardeen climb creep of Frank-Read sources, Nabarro creep in subgrains, and Coble creep in subgrains. These mechanisms have not been confirmed experimentally; further, it is questionable on theoretical grounds whether they can ever take precedence over other mechanisms.

Despite the advances that have been made towards an understanding of high temperature creep, many important issues remain unsolved. For the usual ranges of σ/G they concern: (1) the origin of the variance of n that is observed in BCC metals undertaking the climb mechanism. (2) The reason for the high values of n in dispersion-strengthened alloys. (3) The reason why viscous glide mechanisms are rate-controlling in some solid solution alloys but not in others.

TABLE XV: Creep Mechanisms

Mechanism	Diffusivity, D	A	n
Nabarro	Volume by Vacancy Exchange	$7(b/d)^2$	1
Coble	Grain Boundary by Vacancy Exchange	$50(b/d)^3$	1
Weertman Climb (FCC)	Volume by Vacancy Exchange	2.5×10^6	4.2 - 5.5 increasing with Gb/Γ
Weertman Climb (BCC)	"	$\sim 2.5 \times 10^6$ variable	~4.5 but variable $4.0 \leq n \leq 7$
Weertman Climb (HCP)	"	$\sim 2.5 \times 10^6$	$3.0 \leq n \leq 5.5$
Weertman Viscous Glide in Solid Solution Alloy	Chemical Interdiffusivity	3	$3.0 \leq n \leq 3.5$
Dispersion-Strengthened Alloys	Volume by Vacancy Exchange	Less than 2.5×10^6 Decreasing With Interparticle Spacing and With Increasing Particle Height	$6.0 \leq n \leq 8.0$
Superplastic Creep	Grain Boundary by Vacancy Exchange	$\sim 100 (b/d)^2$	2
Harper-Dorn in Al Single and Polycrystals	Volume by Vacancy Exchange	1.35×10^{-11}	1

Major emphasis, however, should be given to the technologically interesting mechanisms that supercede climb and viscous drag mechanisms at low values of σ/G. Evidence is yet somewhat inconclusive in this range, and the following issues need clarification: (1) The nature and origin of the creep observed at low stresses in Al by Harper and Dorn. (2) The details and the laws for the superplastic creep mechanism. (3) The transitional value of σ/G at which the viscous drag and climb mechanisms are replaced by superplasticity. (4) The transition from the superplastic creep to Coble or Nabarro creep at low values of σ/G.

Although a good start has been made in determining substructural changes attending creep by the climb mechanism, some issues need further clarification concerning disposition and densities of dislocations, the subgrain sizes, and the misorientation of subgrains. The principle of kinetic reciprocity suggests that all substructural details are significant to the steady-state creep rates, but no adequate experimental confirmation of this concept has yet been presented. More needs to be learned about stress-induced migration of subgrain boundaries and their contribution to the creep rates. Data on the substructures developed during creep of alloys undertaking the viscous-glide mechanism is almost nonexistant. Such information should do much to clarify the reasons for differences in transient creep for these two types of behavior and their different responses on drop-in-stress tests. More needs to be learned about the substructural details during creep of dispersion strengthened alloys, particularly with reference to the high values of n they exhibit.

In conclusion, high-temperature creep is dependent on a host of interrelated complex phenomena. The portals to the eventual solution of

this problem have now been opened sufficiently to permit rapid progress over the near future. The guiding information must inevitably be obtained from better and more complete mechanical data. Because high-temperature creep is often highly sensitive to structure and substructure, however, electron-microscopy coupled with additional microscopic tools of examination will prove to be invaluable aids in unraveling this complex subject. On this basis, more realistic theories of high temperature creep might eventually be built. Whereas current theories are based on assumed substructures (which are not always compatible with observations), new theories must "predict" the substructure as well as the mechanical behavior.

ACKNOWLEDGEMENTS

The authors express their appreciation to the United State Atomic Energy Commission for their support of this research effort through the Inorganic Materials Research Division of the Lawrence Radiation Laboratory of the University of California, Berkeley, California. They also thank Mr. Kamal Amin, Research Assistant at L.R.L. Berkeley, for his contributions of analyses on transient creep.

REFERENCES

1. T. Hazlett and R.D. Hansen; Trans. ASM, 47, 508 (1954).
2. B.M. Alexander, M.H. Dawson, and H.P. Kling; J. Appl. Phys., 22, 439 (1951).
3. A.K. Mukherjee and J.E. Dorn; J. Inst. Met., 93, 397 (1964-65).
4. J.G. Harper and J.E. Dorn, Acta Met., 5, 654 (1967).
5. H. Laks, C.D. Wiseman, O.D. Sherby, and J.E. Dorn; J. Appl. Mech., 24, 207 (1957).
6. E.M. Howard, W.L. Barmore, J.D. Mote, and J.E. Dorn; Trans AIME, 227, 1061 (1963).
7. L. Raymond and J.E. Dorn; Trans. AIME, 230, 560 (1964).
8. O.D. Sherby, T.A. Trozera, and J.E. Dorn; Proc. ASTM, 56, 789 (1956).
9. Private communication from G. A. Webster and J. E. Dorn.
10. G.A. Webster and B.J. Piearcey; Metal Sci. J., 1, 97 (1967).
11. E.R. Gilbert and D.E. Munson; Trans. AIME, 233, 429 (1965).
12. J. Glen; J. Iron and Steel Institute, 189, 333 (1958).
13. F.R.N. Nabarro; Report of a Conference on the Strength of Solids, p. 75. The Physical Society, London (1948).
14. C. Herring; J. Appl. Phys., 21, 437 (1950).
15. G.B. Gibbs; Phil. Mag., 13, 589 (1966).
16. F.H. Buttner, E.R. Funk, and H. Udin; Trans AIME, 194, 401 (1952).

17. E.R. Funk, H. Udin, and J. Wulff; Trans. AIME, 191, 1206 (1951).

18. A.O. Greenough; Phil. Mag., 43, 1075 (1952).

19. A.L. Pranatis and G.M. Pound; Trans. AIME, 203, 664 (1955).

20. H. Udin, A.J. Shaler, and J. Wulff; Trans. AIME, 185, 186 (1949); also, H. Udin; Trans. AIME, 191, 63 (1951).

21. E.R. Hayward and A.P. Greenough; J. Inst. Metals, 88, 217 (1959-60).

22. A.T. Price, H.A. Holl, and A.P. Greenough; Acta Met., 12, 49 (1964).

23. E.D. Hondros; Phys. Stat. Sol., 21, 375 (1967).

24. N.R. Borch and J.R. Hauber; Trans. AIME, 242, 1933 (1968).

25. R.B. Jones; Nature, 207, 70 (1965).

26. H. Jones and G.M. Leak; Acta Met., 14, 21 (1966).

27. B. Ya. Pines, R.I. Bazyura, and V.P. Khizhkovyi; Fiz. Metallov Metallovedenie (USSR), 23, [1] 185 (1967).

28. A.K. Mukherjee, J.E. Bird, and J.E. Dorn; Trans. ASM, 62, 155 (1969).

29. I.S. Servi and N.J. Grant; Trans. AIME, 191, 909 (1951).

30. J. Weertman; J. Mech. and Phy. Solids, 4, 230 (1956).

31. J. Weertman; J. Appl. Phys., 27, 832 (1956).

32. J. Weertman and P. Shahinian; Trans. AIME, 206, 1223 (1956).

33. C.M. Sellars and A.G. Quarrell; J. Inst. Met., 90, 329 (1961-62).

34. K. Monma, H. Suto, and H. Oikawa; J. Japan Inst. Metals, 28, 253 (1964).

35. J. Weertman; Trans. AIME, 218, 207 (1960).

36. P. Feltham; Proc. Phys. Soc., 66B, 865 (1953).

37. P. Feltham and J.D. Meakin; Acta Met., 7, 614 (1959).

38. C.R. Barrett and O.D. Sherby; Trans. AIME, 230, 1322 (1964).

39. K. Monma, H. Suto, and H. Oikawa; J. Japan Inst. Metals, 28, 258 (1964).

40. S. Dushman, L.W. Dunbar, and H. Huthsteiner; J. Appl. Phys. 15, 108 (1944).

41. R.P. Carreker, Jr.; J. Appl. Phys., 21, 1289 (1950).

42. G.R. Leverant, F.V. Lenel, and G.S. Ansell; Trans. ASM, 59, 890 (1966).

43. R.P. Carreker and R.W. Guard, "Creep of Silver Wires," General Electric Co. Report No. 55-RL-1414 (Nov. 1955).

44. C.R. Barrett and O.D. Sherby; Trans. AIME, 233, 1116 (1965).

45. S.K. Schröder, A.J. Giannuzzi, and G. Gorsha; Acta. Met., 16, 469 (1968).

46. D. McLean and K.F. Hale in Structural Processes in Creep, p. 19, Iron and Steel Institute, London (1961).

47. O.D. Sherby; Acta Met., 10, 135 (1962).

48. P. Feltham, in ref. 46, p. 82.

49. D. McLean; Met. Reviews, 7, 481 (1962).

50. Y. Ishida, C.Y. Cheng and J.E. Dorn; Trans. AIME, 236 964 (1966).

51. S. Karashima, H. Oikawa, and T. Watanabe; Acta Met., 14, 791 (1966).

52. T. Watanabe and S. Karashima; Trans. Japan Inst. Metals, 9, Supplement, 242 (1968).

53. A.H. Clauer, B.A. Wilcox, and J.P. Hirth, "Creep Behavior of Molybdenum Single Crystals," to be published in Acta Met. (1969).

54. W.V. Green, M.C. Smith and D.M. Olson; Trans. AIME, 215, 1061 (1959).

55. W.V. Green; Trans. AIME, 233, 1818 (1965).

56. O.D. Sherby; Trans. AIME, 212, 708 (1958).

57. W.V. Green; Trans. AIME, 215, 1057 (1959).

58. G.W. King and H.G. Sell; Trans. AIME, 233, 1104 (1965).

59. W.D. Klopp, W.R. Witzke, and P.L. Raffo; Trans. AIME, 233, 1860 (1965).

60. P.N. Flagella, "High Temperature Creep-Rupture Behavior of Unalloyed Tungsten," Third High-Temperature Technology Symposium, Asilomar, California (1967).

61. K.R. Wheeler, E.R. Gilbert, F.L. Yaggee, and S.A. Duran, unpublished data.

62. J.E. Flinn and F.A. Duran; Trans. AIME, 236, 1056 (1966).

63. W.J. McG. Tegart; Acta Met., 9, 614 (1961).

64. R.B. Jones and J.E. Harris, Joint International Conference on Creep, p.1-1, Inst. of Mech. Eng., London (1963).

65. J.E. Flinn and D.E. Munson; Phil. Mag., 10, 861 (1964).

66. W.J. McG. Tegart and O.D. Sherby; Phil. Mag., 3, 1287 (1958).

67. J.E. Flinn and E.R. Gilbert, "Steady State Creep Behavior of HCP Metals at High Temperatures," TMS Paper No. A68-40, A.I.M.E. (1968).

68. J. Weertman; J. Appl. Phys., 28, 1185 (1957).

69. J. Weertman; J. Appl. Phys., 28, 362 (1957).

70. J. Weertman; Trans. ASM, 61, 681 (1968).

71. R.M. Bonesteel and O.D. Sherby; Acta Met., 14, 385 (1966).

72. S. Karashima, T. Motomiya, and H. Oikawa; Tech. Repts. of Tohoku Univ. (Japan), 33, 193 (1968).

73. C.R. Barrett and W.D. Nix; Acta. Met., 13, 1247 (1965).

74. K. Monma, H. Suto, and H. Oikawa; J. Japan Inst. Metals, 28, 304 (1964).

75. F. Garofalo, O. Richmond, W.F. Domis, and F. von Gemmingen, ref. 64 , p. 1-31.

76. F. Garofalo, W. Domis, and F. Gemmingen; Trans. AIME, 230, 1460 (1964).

77. R. Lagneborg and R. Attermo, "Creep of Austenitic 20% Cr-35% Ni Stainless Steels," J. Matls. Sci., to be published.

78. R.G. Davies; Trans. AIME, 227, 665 (1963).

79. C.Y. Cheng, A. Karim, T.G. Langdon, and J.E. Dorn; Trans. AIME, 242, 890 (1968).

80. S. Karashima, H. Oikawa, and T. Watanabe; Trans. AIME, 242, 1703 (1968).

81. A. Lawley, J. A. Coll, R. W. Cahn; Trans. AIME, 218, 166 (1960).

82. R. G. Davies; Trans. AIME, 227, 22 (1963).

83. A. Fuchs and B. Ilschner, Acta Met., 17, 701 (1969).

84. C. Rossard and P. Blain, Publication IRSID, Series A, No. 174, St. Germain-en-Laye, France (1958).

85. R. Jackson, H. J. Carvalhinhos, and B. B. Argent; J. Inst. Met., 96, 210 (1968).

86. D. M. Schwartz, J. B. Mitchell, and J. E. Dorn; Acta Met., 15, 485 (1967).

87. B. Y. Chirouze, D. M. Schwartz, and J. E. Dorn; Trans. ASM, 60, 51 (1967).

88. J. A. Hren and O. D. Sherby; J. Appl. Matls. Res., 4, 41 (1965).

89. A. H. Cottrell, Dislocations and Plastic Flow in Crystals, p. 136, Clarendon Press, Oxford (1953).

90. H. Suzuki; Sci. Rep. Res. Inst. Tohoku Univ. (Japan), 7A, 194 (1955).

91. R. L. Fleischer; Acta Met., 9, 996 (1961); 11, 203 (1963).

92. A. H. Cottrell, S. C. Hunter, and F. R. N. Nabarro, Phil. Mag., 44, 1064 (1953).

93. J. Friedel; Dislocations, p. 410. Pergamon Press, London (1964).

94. L. Darken, Trans. AIME, 174, 184 (1948).

95. R. Horiuchi, H. Yoshinaga, and S. Hama; Trans. Japan Inst. Met., 6, 123 (1965).

96. H. Asada, R. Horiuchi, H. Yoshinaga, and S. Nakamoto, Trans. Japan Inst. Met., 8, 159 (1967).

97. R. R. Vandervoort, A. K. Mukherjee, and J. E. Dorn; Trans. ASM, 59, 930 (1966).

98. N. Brown and D. R. Lenton, Acta Met., 17, 669 (1969).

99. R. R. Vandervoort and W. L. Barmore, Proceedings of the Sixth Plansee Seminar, Reutte-Tyrol, Austria, June, 1968, to be published.

100. R. G. Davies, Trans. AIME, 221, 1280 (1961).

101. A. J. R. Soler-Gomez and W. J. McG. Tegart, Acta Met., 12, 961 (1964).

102. A. K. Mukherjee, J. Appl. Phys., 39, 2201 (1968).

103. P. A. Flinn, Trans. AIME, 218, 145 (1960).

104. J. H. Westbrook, in Mechanical Properties of Intermetallic Compounds, J. H. Westbrook (ed.), p. 1. J. Wiley, New York (1960).

105. A. Lawley, in Intermetallic Compounds, J. H. Westbrook (ed.), p. 464. J. Wiley, New York (1967).

106. R. Lowrie, Trans. AIME, 194, 1093 (1952).

107. G. S. Ansell and J. Weertman, Trans. AIME, 215, 838 (1959).

108. S. Tekahashi, K. Iida, and M. Adachi, Trans. Nat. Res. Inst. Metals, 6 [6], 29 (1964).

109. B. A. Wilcox and A. H. Clauer, Trans. AIME, 236, 570 (1966).

110. T. D. Gulden and J. C. Shyne, Trans. AIME, 227, 1088 (1963).

111. P. Guyot, Acta Met., 14, 955 (1966).

112. S. Tekahashi and M. Adachi, Trans. Japan Inst. Metals, 8, 133 (1967).

113. A. H. Claver and B. A. Wilcox, Metal Sci. J., 1, 86 (1967).

114. B. A. Wilcox and A. H. Claver, Metal Sci. J., 3, 26 (1969).

115. G. S. Ansell, in Oxide Dispersion Strengthening, Vol. 47 of A.I.M.E. Conference Series, p. 61. Gordon and Breach, New York (1968).

116. A. D. Kurtz, B. L. Averbach, and M. Cohen, Acta Met., 3, 442 (1955).

117. E. Lifshin, in Trans. 2nd Nat. Conf. on Electron Microprobe Analysis, Paper 23. M.I.T. Press, Cambridge (1967).

118. F. Garofalo, ref. 122, p. 95.

119. A. B. Kuper, D. Lazarus, J. R. Manning, and C. T. Tomizuka, Phys. Rev., 104, 1536 (1956).

120. R. Hultgren, R. L. Orr, P. D. Anderson, and K. K. Kelley, Selected Values of Thermodynamic Properties of Metals and Alloys, p. 719. J. Wiley, New York (1963).

121. H. Conrad, in Mechanical Behavior of Materials at Elevated Temperatures, J.E. Dorn (ed.), p. 218. McGraw-Hill, New York (1961).

122. F. Garofalo, Fundamentals of Creep and Creep Rupture in Metals, p. 27. McMillan, New York (1965).

123. P. Shahinian and J. R. Lane, Trans. ASM, 45, 177 (1953).

124. C. R. Barrett, J. L. Lytton, and O. D. Sherby, Trans. AIME, 239, 170 (1967).

125. L. M. T. Hopkin, Progress in Applied Materials Research, 7, p. 33 (1967).

126. V. P. Gupta and P. R. Strutt, Canad. J. Phys., 45, 1213 (1967).

127. J. D. Livingston, Acta Met., 10, 229 (1962).

128. A. H. Clauer, B. A. Wilcox, and J. P. Hirth; "Dislocation Substructure Induced by Creep in Molybdenum Single Crystals", to be published in Acta Met.

129. T. E. Mitchell, Progress in Applied Materials Research, 6, 117 (1964).

130. E. J. Nielsen and P. R. Strutt; Trans. AIME, 242, 2245 (1968).

131. F. H. Hammad and W. D. Nix, Trans. ASM, 59, 94 (1966).

132. D. McLean, Met. Reviews, 6 (1962).

133. D. McLean, Canad. J. Phys., 45, 973 (1967).

134. D. McLean; Trans. AIME, 242, 1193 (1968).

135. D. McLean, in Proceedings of Sixth International Conference for Electron Microscopy, Kyoto, 1966, p. 295.

136. I. S. Servi and N. J. Grant, Trans. AIME, 191, 917 (1951).

137. H. Busboom, Master's Report, Jan., 1963, Dept. of Materials Science, Stanford University, Stanford, California.

138. D. McLean and M. H. Farmer, J. Inst. Metals, 83, 1 (1954-55).

139. A. Goldberg, J. Iron and Steel Inst., 204, 268 (1968).

140. C. R. Barrett, W. D. Nix, and O. D. Sherby, Trans. ASM, 59, 3 (1966).

141. S. K. Mitra and D. McLean, Metal Sci. J., 1, 192 (1967).

142. R. Guard, Creep and Recovery, p. 251. American Society for Metals, Cleveland (1957).

143. C. R. Barrett, Acta Met., 13, 1088 (1965).

144. D. H. Warrington, private communication.

145. D. L. Klarstrom, E. J. Nielsen, P. R. Strutt, and R. A. Dodd, "Substructure in α-Cu/Al Single Crystals Deformed in High Temperature Creep", presented at A.I.M.E. Spring Meeting, Philadelphia (May, 1969).

146. C. S. Roberts, Trans. AIME, 197, 732 (1953).

147. J. W. Suiter and W. A. Wood, J. Inst. Metals, 81, 181 (1952-53).

148. A. R. Chaudhuri, H. C. Chang, and N. J. Grant, Trans. AIME, 203, 682 (1955).

149. D. McLean and M. H. Farmer, J. Inst. Metals, 85, 41 (1956-57).

150. J. A. Ramsey, J. Inst. Metals, 80, 167 (1951-52).

151. F. Garofalo, ref. 122, p. 126.

152. F. Garofalo, R. W. Whitmore, W. F. Domis, and F. von Gemmingen, Trans. AIME, 221, 310 (1961).

153. R. Lagneborg, Metal Sci. J., 3, 18 (1969).

154. G. B. Greenough, C. M. Bateman, and E. M. Smith, J. Inst. Metals, 80, 545 (1951-52).

155. W. A. Rachinger, J. Inst. Metals, 81, 817 (1952-53).

156. J. G. Harper, L. A. Shepard, and J. E. Dorn, Acta Met., 6, 509 (1958).

157. L. N. Larikov, V. M. Tyshkevich, and L. F. Chernaya; Ukr. Fiz. Zh. 12 [6], 973 (1967); data also summarized in Diffusion Data, 1 [3], 46 (Dec. 1967).

158. R. L. Andelin, J. D. Knight, and M. Kahn, Trans. AIME, 233, 19 (1965).

159. A. W. Mullendore and N. J. Grant; Trans. AIME, 200, 973 (1954).

160. D. Hardwick, C. M. Sellars, and W. J. McG. Tegart, J. Inst. Metals, 90, 21 (1961-62).

161. W. D. Jenkins, T. G. Digges, and C. R. Johnson, J. Research Nat. Bur. Stand., 53, 329 (1954).

162. R. C. Gifkins, J. Inst. Metals, 86, 15 (1957-58).

163. E.N. da C. Andrade, J. Iron and Steel Inst., 171, 217 (1952).

164. R. C. Gifkins, J. Inst. Metals, 87, 255 (1958-59).

165. N. J. Grant and A. G. Bucklin, Trans. ASM, 45, 151 (1953).

166. H. Hirst, Proc. Australas. Inst. Min. Met., 121, 29 (1941).

167. G. J. Richardson, C. M. Sellars, and W. J. McG. Tegart, Acta Met., 14, 1225 (1966).

168. R. C. Gifkins, Acta Met., 15, 1074 (1967).

169. J. L. Lytton, C. R. Barrett, and O. D. Sherby, Trans. AIME, 233, 1399 (1965).

170. C. R. Barrett, Trans. AIME, 239, 1726 (1967).

171. Y. Ishida and D. McLean, J. Iron and Steel Inst., 205, 88 (1967).

172. A. K. Head, Phil. Mag., 4, 295 (1959).

173. J. C. M. Li, Discussions of the Faraday Society, 38, 138 (1964).

174. P. M. Hazzeldine, J. de Physique, 27, Supplement C3, 210 (1966).

175. W. A. Wong, H. J. McQueen, and J. J. Jonas, J. Inst. Metals, 95, 129 (1967).

176. J. J. Jonas, H. J. McQueen, and D. W. Demianczuk; Deformation Under Hot Working Conditions, Spec. Report No. 108, p. 97. Iron and Steel Inst., London (1968).

177. Y. Ishida and M. H. Brown, Acta Met., 15, 857 (1967).

178. D. J. Dingley and K. F. Hale, Proc. Royal Soc., 295 A, 55 (1966).

179. J. J. Jonas, H. J. McQueen, and W. A. Wong, ref. 176, p. 49.

180. H. J. McQueen, W. A. Wong, and J. J. Jonas, Canad. J. Phys., 45, 1225 (1967).

181. L. A. Shepard and J. E. Dorn, "The Role of Subgrains in High Temperature Creep", First Technical Report, Series No. 108, Minerals Research Laboratory, Institute of Engineering Research, Univ. of California, Berkeley (1957).

182. G. R. Wilms, J. Inst. Metals, 83, 427 (1954-55).

183. W. A. Wood and J. W. Suiter, J. Inst. Metals, 80, 501 (1951-52).

184. O. D. Sherby, A. Goldberg, and J. E. Dorn, Trans. ASM, 46, 681 (1954).

185. J. W. Kelly and R. C. Gifkins, J. Inst. Metals, 82, 475 (1953-54).

186. I. S. Servi, J. T. Norton, and N. J. Grant, Trans. AIME, 194, 965 (1952).

187. D. McLean, J. Inst. Metals, 80, 507 (1951-52).

188. O. D. Sherby and J. E. Dorn, Trans. AIME, 197, 324 (1953).

189. D. McLean, J. Inst. Metals, 81, 287 (1952-53).

190. W. A. Rachinger, J. Inst. Metals, 80, 415 (1951-52).

191. R. C. Rau, S. F. Bartram, and P. N. Flagella, Trans. ASM, 61, 646 (1968).

192. L. J. Cuddy, Trans. ASM, 61, 647 (1968).

193. D. McLean and M. H. Farmer, J. Inst. Metals, 83, 1 (1954-55).

194. D. McLean, in Creep and Fracture of Metals at High Temperatures, p. 73. Her Majesty's Stationery Office, London (1956).

195. F. Garofalo, L. Zwell, A. S. Keh, and S. Weissman, Acta Met., 9, 721 (1961).

196. A. M. Gervais, J. T. Norton, and N. J. Grant, Trans. AIME, 197, 1166 (1953).

197. P. R. Strutt and R. W. Howe, "Substructure in Copper Single Crystals Deformed in High Temperature Creep", presented at A.I.M.E. Spring Meeting, Philadelphia (May, 1969).

198. C. Stein, J. Metals, 20, 63A (1968).

199. A. S. Keh and S. Weissman, in Electron Microscopy and Strength of Crystals, p. 231. J. Wiley, New York (1963).

200. J. J. Jonas, D. R. Axelrad, and J. L. Uvira, J. Japan Inst. Metals, 9, Supplement (1968).

201. R. N. Stevens, Met. Rev., 11, 129 (1966).

202. R. L. Bell and T. G. Langdon, "Grain Boundary Sliding - A Review", to be published as Proceedings on the Conference on Interfaces, Univ. of Melbourne (1969).

203. B. Fazan, O. D. Sherby and J. E. Dorn, Trans. AIME, 200, 919 (1954).

204. P. R. Strutt, A. M. Lewis, and R. C. Gifkins, J. Inst. Metals, 93, 71 (1964-65).

205. J. Intrater and E. S. Machlin, J. Inst. Metals, 88, 305 (1959-60).

206. K. E. Puttick and R. King, J. Inst. Metals, 80, 537 (1951-52).

207. S. K. Tung and R. Maddin, Trans. AIME 209, 905 (1957).

208. P. A. Turner, Ph.D. Thesis, Univ. of London (1965).

209. P. W. Davies, R. N. Stevens and B. Wilshire, J. Inst. Metals, 94, 49 (1966).

210. J. A. Martin, M. Herman and N. Brown, Trans. AIME, 209, 78 (1957).

211. H. Brunner and N. J. Grant, Trans. AIME, 218, 122 (1960).

212. R. C. Gifkins, J. Australian Inst. Met., 8, 148 (1963).

213. T. G. Langdon, Ph.D. Thesis, Univ. of London (1965).

214. E. E. Underwood, J. Metals, 14, 914 (1962).

215. W. A. Bakofen, I. R. Turner, and D. H. Avery, Trans. ASM, 57, 980 (1964).

216. D. H. Avery and W. A. Bakofen, Trans. ASM, 58, 551 (1965).

217. R. C. Gifkins, J. Inst. Metals, 95, 373 (1967).

218. G. Cook, discussion on paper by C. E. Pearson, J. Inst. Metals, 54, 134 (1934).

219. A. Ball and M. M. Hutchison, Metal Sci. J., 3, 1 (1969).

220. C. M. Packer and O. D. Sherby, Trans. ASM, 60, 21 (1967).

221. H. W. Hayden, R. C. Gibson, H. F. Merrick, and J. H. Brophy, Trans. ASM, 60, 3 (1967).

222. H. E. Evans, Scripta Met., 2, 157 (1968).

223. R. C. Gifkins, J. Amer. Ceramic Soc., 51, 69 (1968).

224. J. Friedel, ref. 94, p. 279 and 315.

225. R. L. Coble, J. Appld. Phys., 34, 1679 (1963).

226. J. E. Breen and J. Weertman, Trans. AIME, 203, 1230 (1955).

227. F. R. N. Nabarro, Phil. Mag., 16, 231 (1967).

228. J. E. Dorn, J. Mech. Phys. Solids, 3, 85 (1954).

229. G. A. Webster, A. P. D. Cox, and J. E. Dorn, "Relationship Between Transient and Steady-State Creep at Elevated Temperatures", to be published.

230. P. G. McVetty, Mech. Eng., 56, 149 (1934).

231. J. B. Conway and M. J. Mulliken, Trans. AIME, 236, 1496 (1966).

232. W. T. Evans and B. Wilshire, Trans. AIME, 242, 1303 (1968).

233. E. N. da C. Andrade, Proc. Royal Soc. 84A, 1 (1910).

234. E. R. Parker, Trans. ASM, 50, 85 (1958).

235. Unpublished data of ref. 53.

236. G. Brinson and B. Argent, J. Inst. Metals, 91, 293 (1962-63).

237. P. Feltham, in Proc. 2nd International Conference on Rheology, Oxford, July, 1953, p. 266. Butterworth, London (1954).

238. R. W. Bailey, J. I. M., 35, 27 (1926).

239. E. Orowan, J. West. Scot. Iron St. Inst., 54, 45 (1946-47).

240. S. K. Mitra and D. McLean, Proc. Roy. Soc., 295A, 288 (1966).

241. A. E. Bayce, W. D. Ludeman, L. A. Shepard and J. E. Dorn, Trans. ASM., 52, 451 (1960).

242. W. D. Ludman, L. A. Shepard and J. E. Dorn, Trans. AIME, 218, 923 (1960).

243. L. Raymond and J. E. Dorn, Trans. AIME, 230, 560 (1964).

244. O. D. Sherby, R. Frenkel, J. Nadeau and J. E. Dorn, J. of Metals, Feb., p. 275 (1954).

FIGURE CAPTIONS

Fig. 1. Common Types of Creep Curves. See Table I for references to actual examples.

Fig. 2. Comparison of Creep Data Obtained at High Temperatures and Low Stresses to Values Predicted Theoretically for Nabarro Creep.

Fig. 3. Steady-State Creep Rates of Nominally Pure FCC Metals Correlated by Eq. 4.

Fig. 4. Relation of the Power Law Stress Dependence, σ^n, of Steady-State Creep of FCC Metals to Stacking Fault Energy Γ. Brackets indicate the estimated accuracy of n and Γ/Gb. Solid line shows the "best fit" value of n.

Fig. 5. Steady-State Creep Rates of FCC Metals as Predicted from Eq. 5 Using the "Best Fit" Values of n (from Fig. 4).

Fig. 6. Steady-State Creep Rates of Nominally Pure BCC Metals Correlated by Eq. 4.

Fig. 7. Steady-State Creep Rates of Nominally Pure HCP Metals Correlated by Eq. 4.

Fig. 8. Steady-State Creep Rates of Binary Solid Solution Alloys Correlated by Eq. 4.

Fig. 9. Correlated Steady-State Creep Rates For FCC Metals and Solid Solution Alloys.

Fig. 10. Steady-State Creep Rates of Binary Solid Solution Alloys and Intermetallic Compounds Which Creep by The Viscous Glide Mechanism Correlated by Eq. 14.

Fig. 11. Steady-State Creep Rates of Dispersion-Strengthened Metals Correlated by Eq. 4.

Fig. 12. Comparison of the Activation Energies For Creep and Self Diffusion of Cu-Zn Solid Solution Alloys.

Fig. 13. Comparison of the Activation Energies For Creep and Self Diffusion of Ni-Cu Solid Solution Alloys.

Fig. 14. Comparison of the Activation Energies For Creep and Self Diffusion of Ni-Fe Solid Solution Alloys.

Fig. 15. Comparison of the Activation Energies For Creep and Self Diffusion of Ni-Cr Solid Solution Alloys.

Fig. 16. Comparison of the Activation Energies For Creep and Self Diffusion of Ni-Cr-ThO_2 Dispersion-Strengthened Alloys.

Fig. 17. Comparison of the Activation Energies For Creep and Self Diffusion of Ni-Au Solid Solution Alloys.

Fig. 18. Effect of Phase Transformations on Creep by the Dislocation-Climb Mechanism.

Fig. 19. Effect of Grain Size on Steady-State Creep Rate at Constant Temperature and Stress.

Fig. 20. Stress Dependence of Dislocation Density ρ. Data are from references 99, 153, 46, 73, 83, 171, 113, 169, 170, 126, 128, 129.

Fig. 21. Stress Dependence of Steady-State Creep Subgrain Size. Data from references 136-140, 83, 141, 142, 126, 143, 144, 75.

Fig. 22. An Idealized Schematic Drawing of the Arrangement of the Subgrains into Bands During Creep of Mo Single Crystals [from Clauer, Wilcox, and Hirth[128]].

Fig. 23. Contribution of Creep Strain Due to Grain Boundary Shearing to Total Strain, χ vs. σ/G.

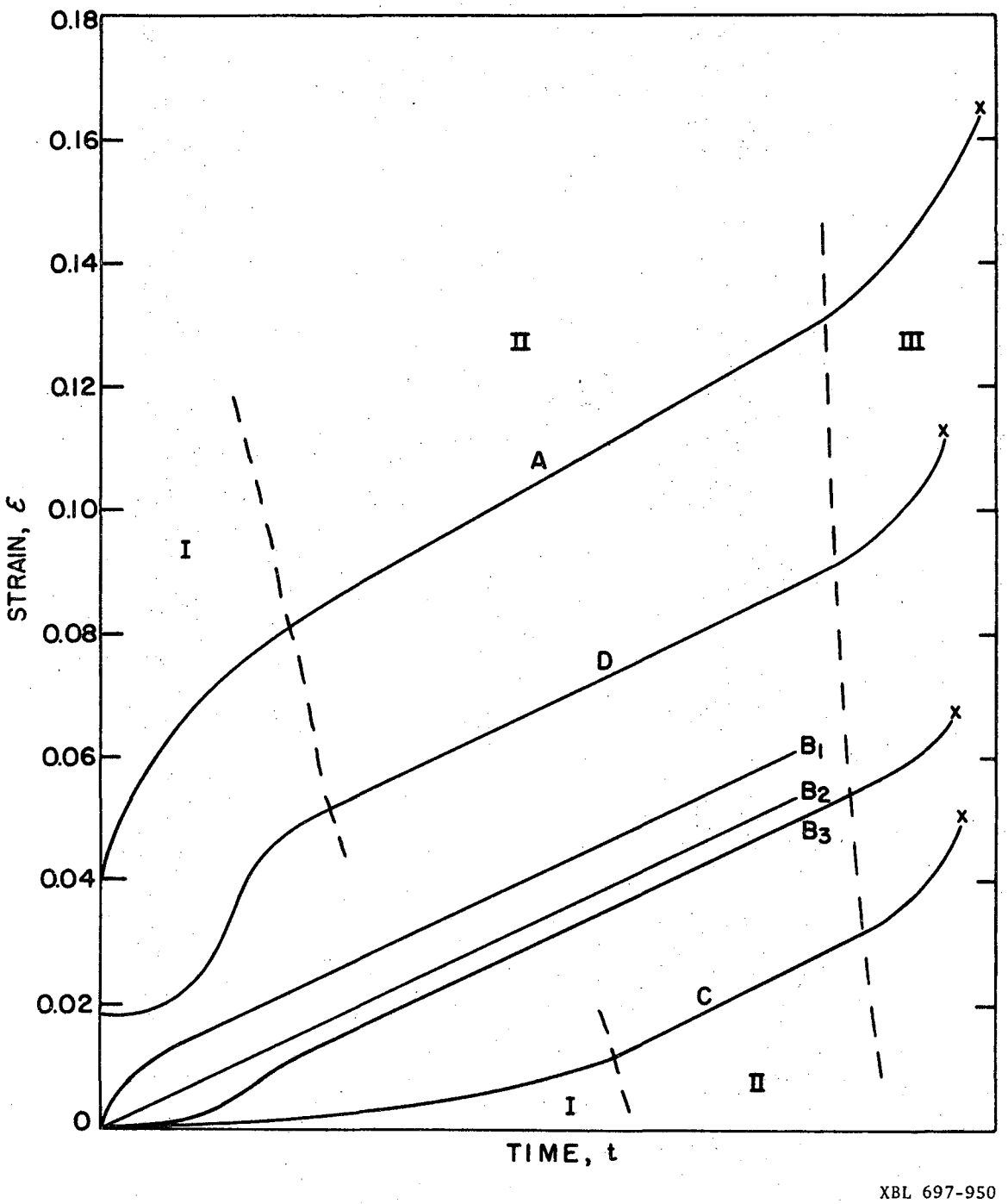
0.18
0.16
0.14
0.12
0.10
0.08
0.06
0.04
0.02
0
STRAIN, ε
TIME, t
I
II
III
A
D
B1
B2
B3
C
I
II
XBL 697-950

FIG. 1

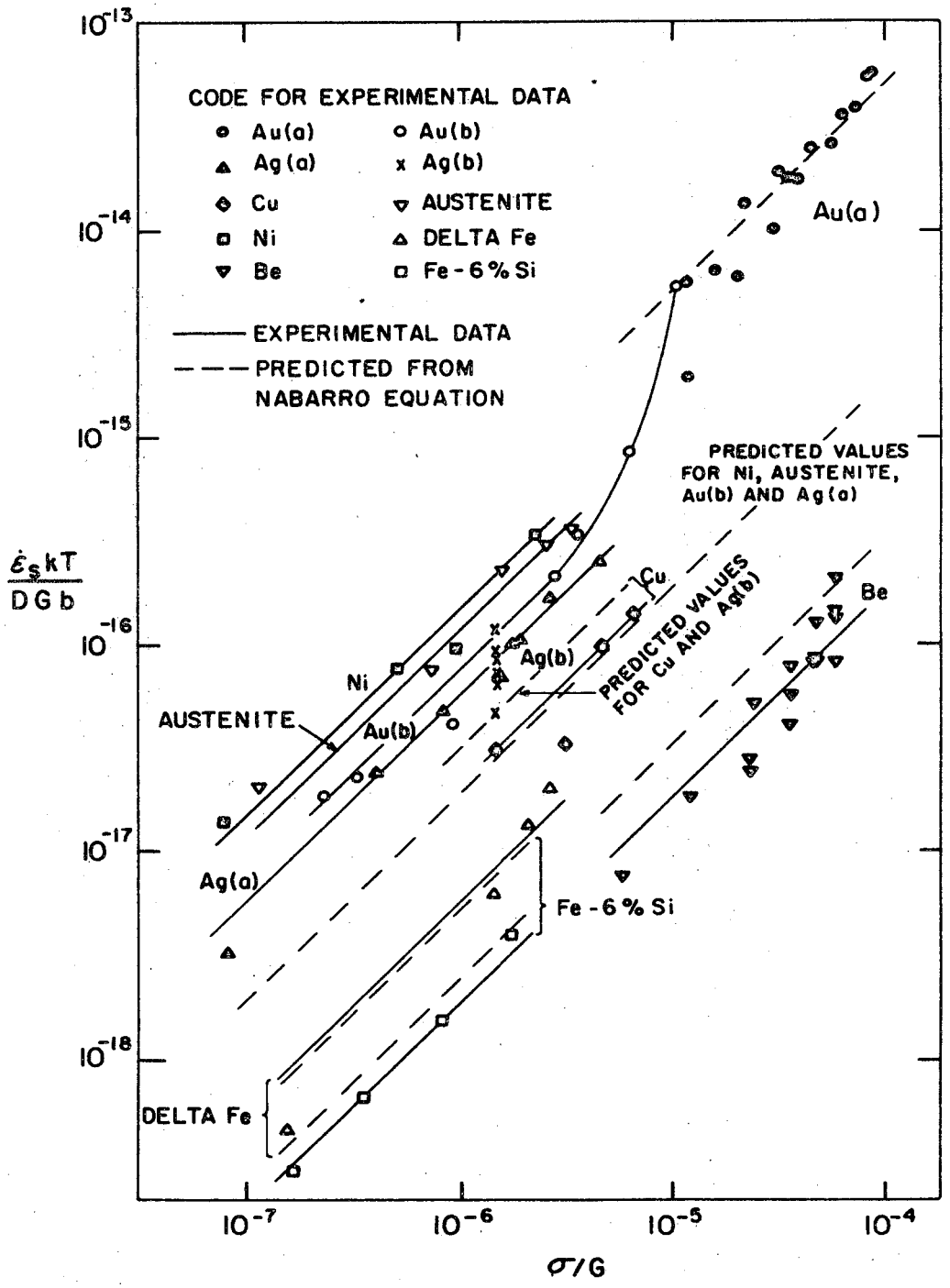

XBL 697-955

FIG. 2

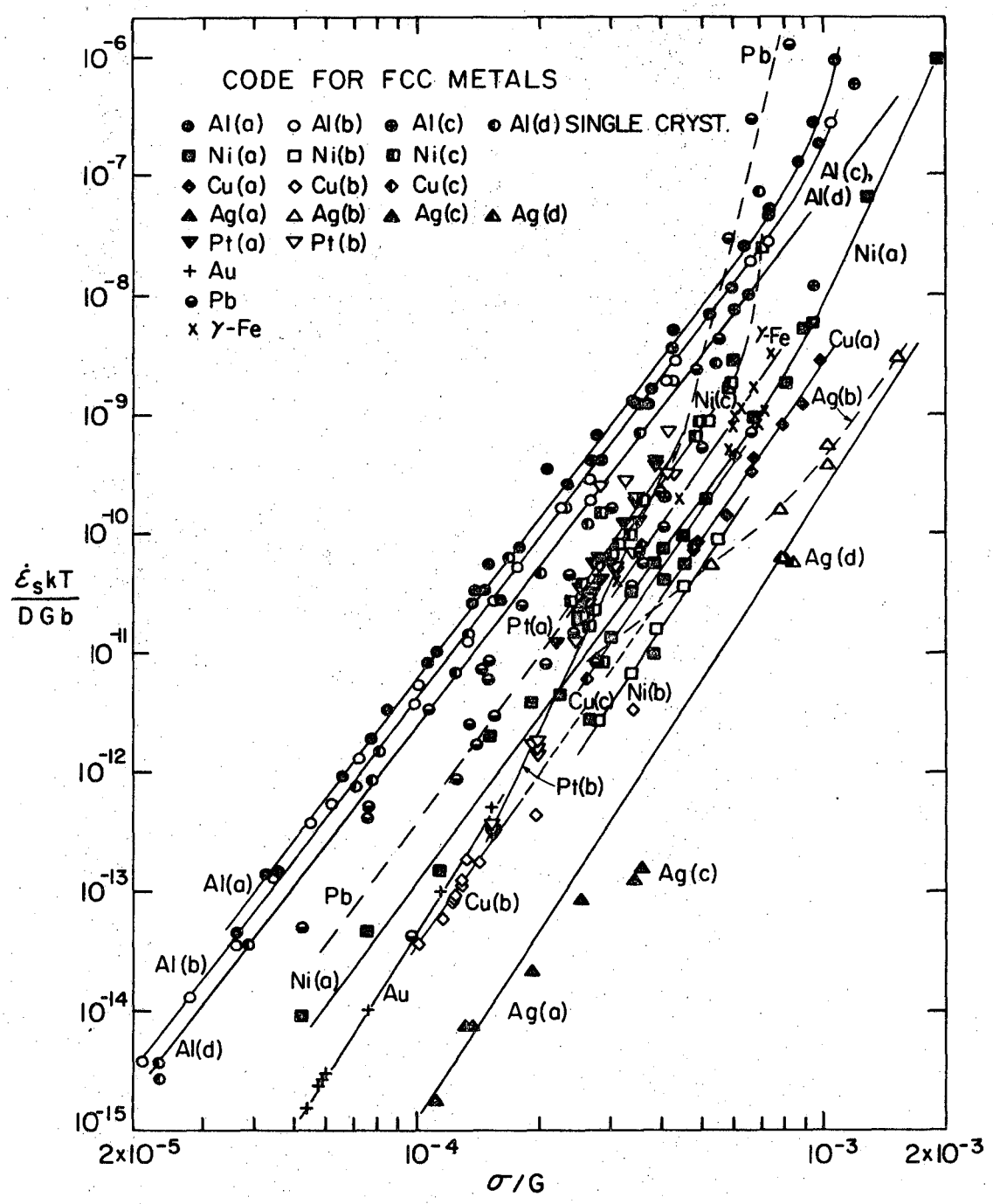

XBL 697-947

Fig. 3

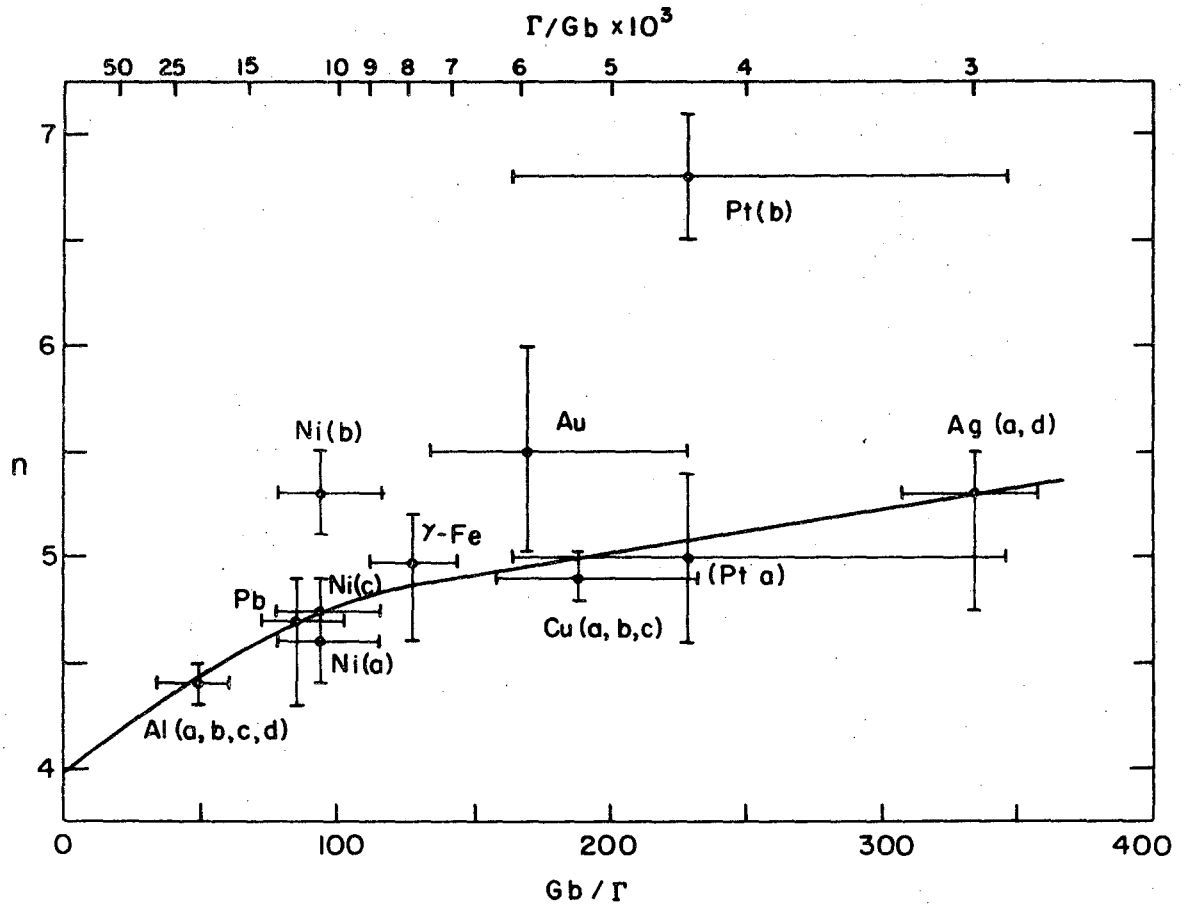
Γ/Gb x10³
50 25 15 10 9 8 7 6 5 4 3
7
6
5
4
n
Pt(b)
Au
Ag (a, d)
Ni(b)
γ-Fe
(Pt a)
Pb
Ni(c)
Cu (a, b,c)
Ni(a)
Al (a, b, c, d)
0
100
200
300
400
Gb / Γ
XBL 697-953

FIG. 4

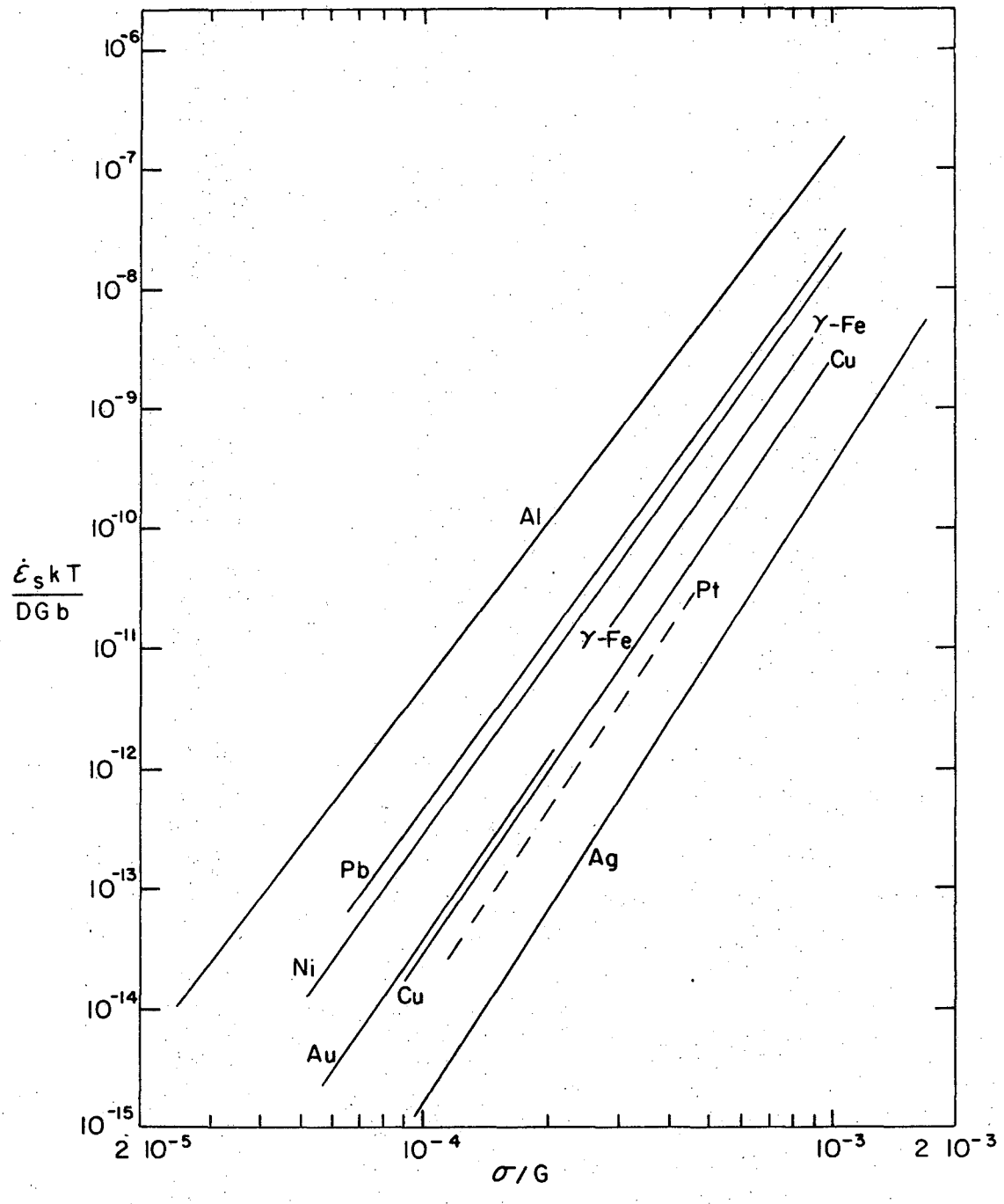

XBL 697-912

FIG. 5

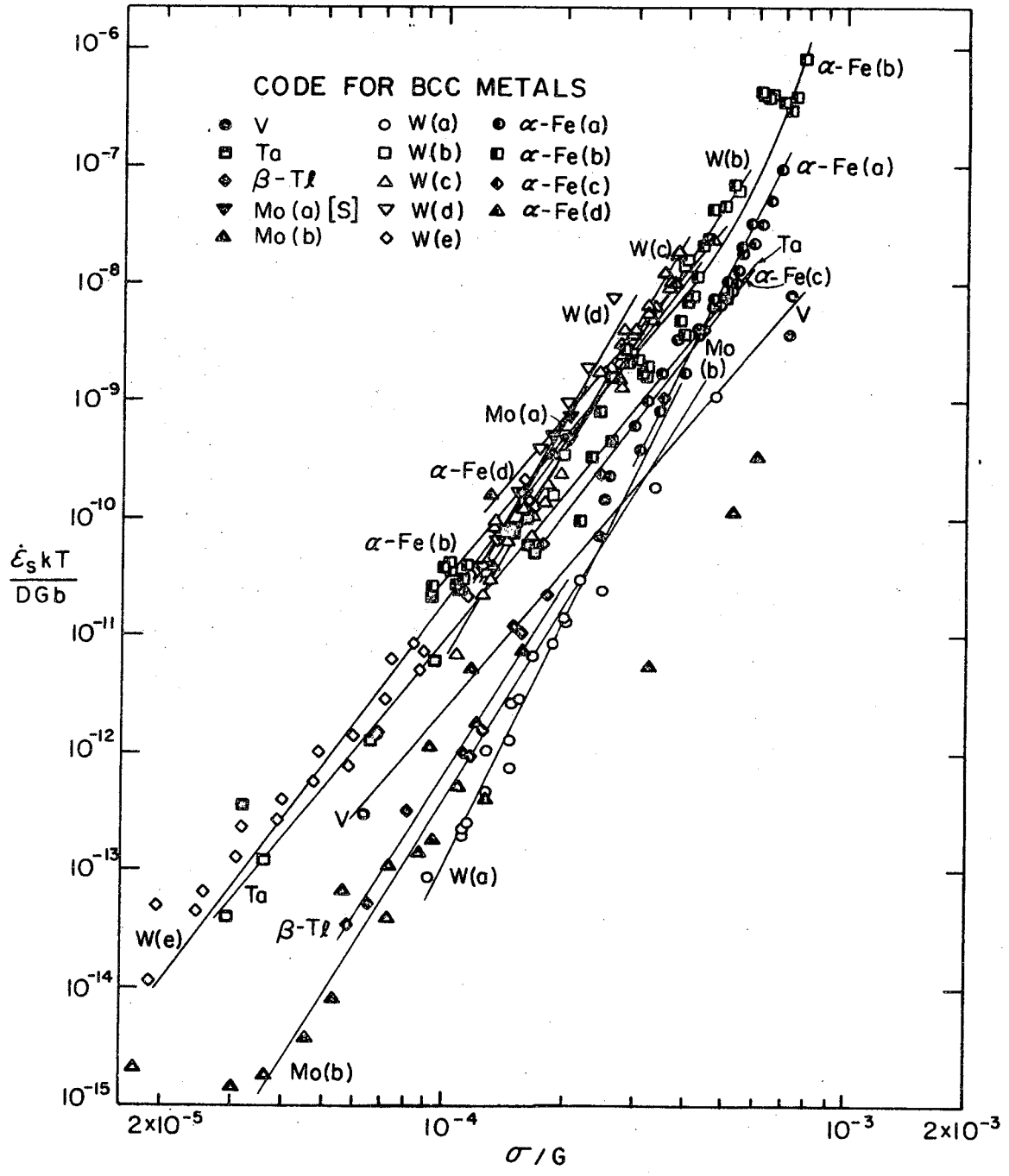

XBL 697-911

FIG. 6

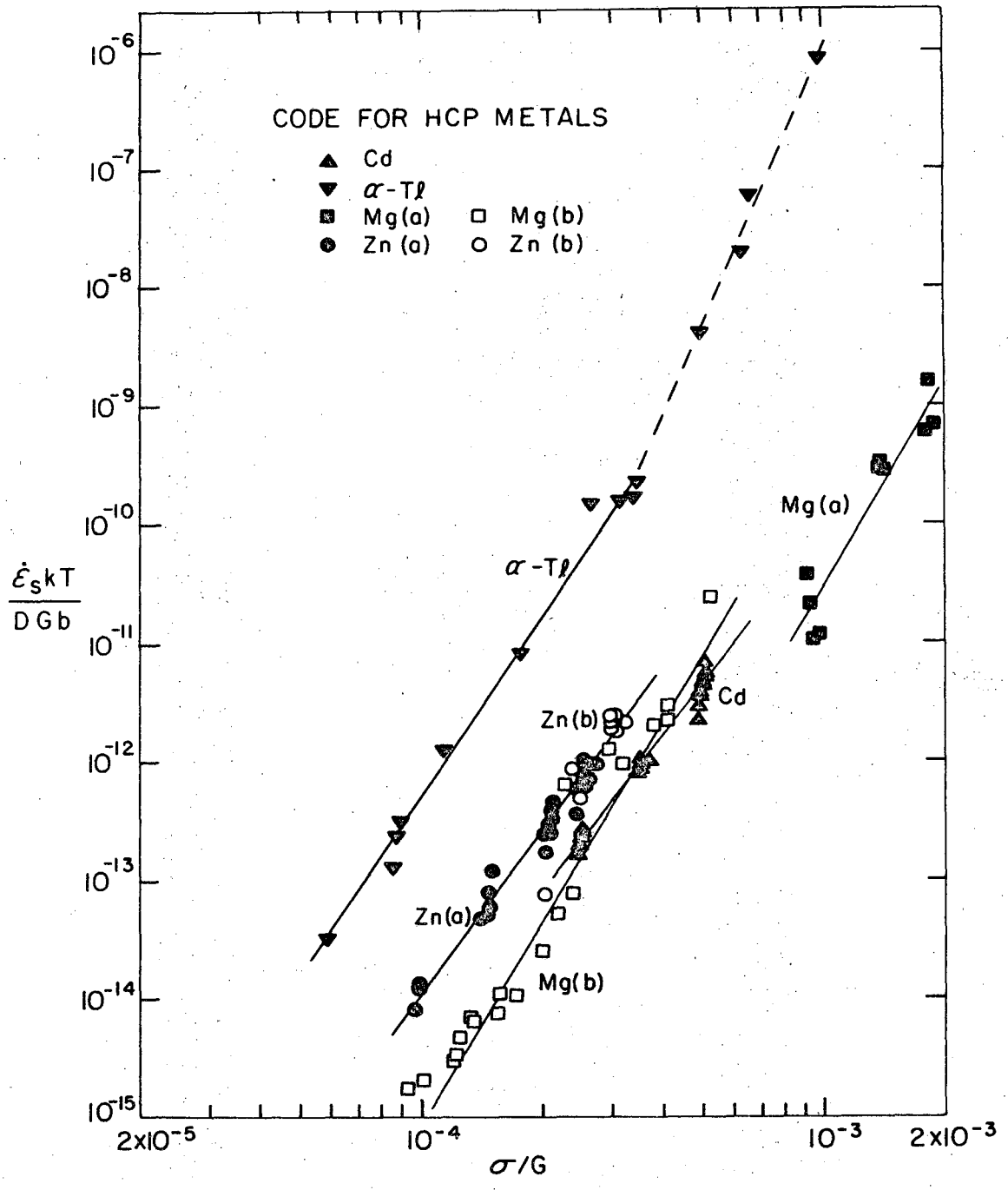

XBL 697-909

FIG. 7

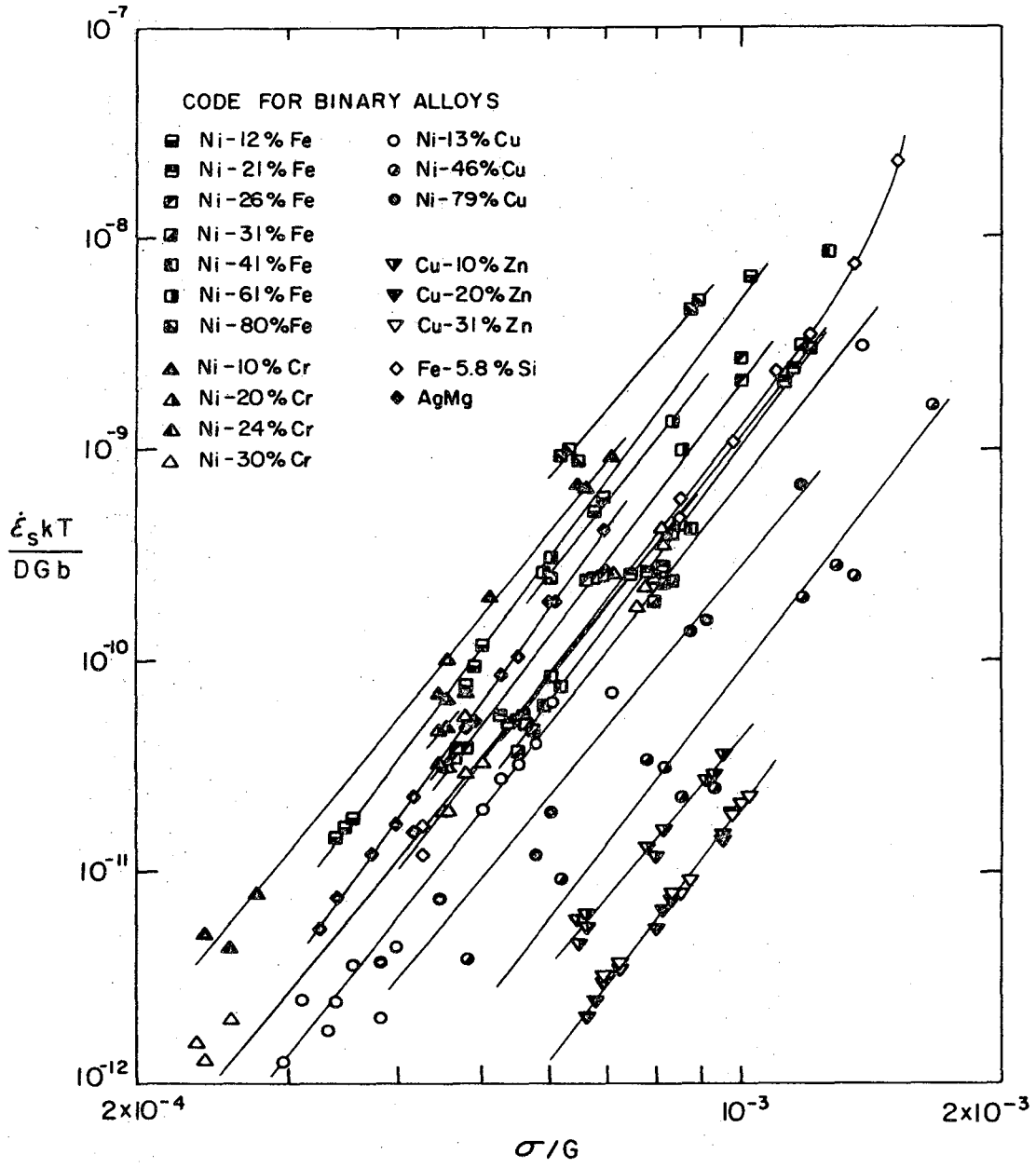

XBL 697-945

FIG. 8

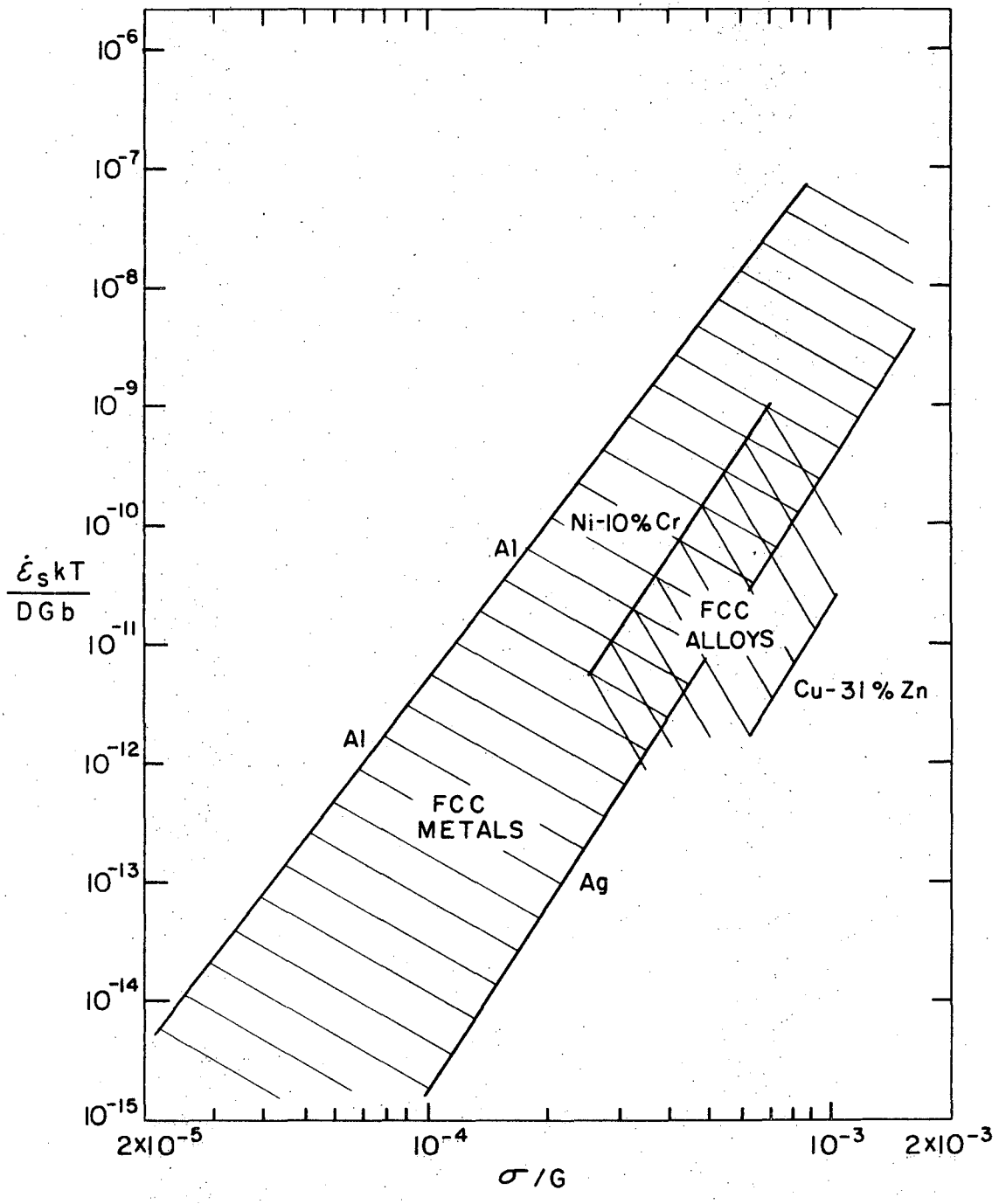

XBL 697-908

Fig. 9

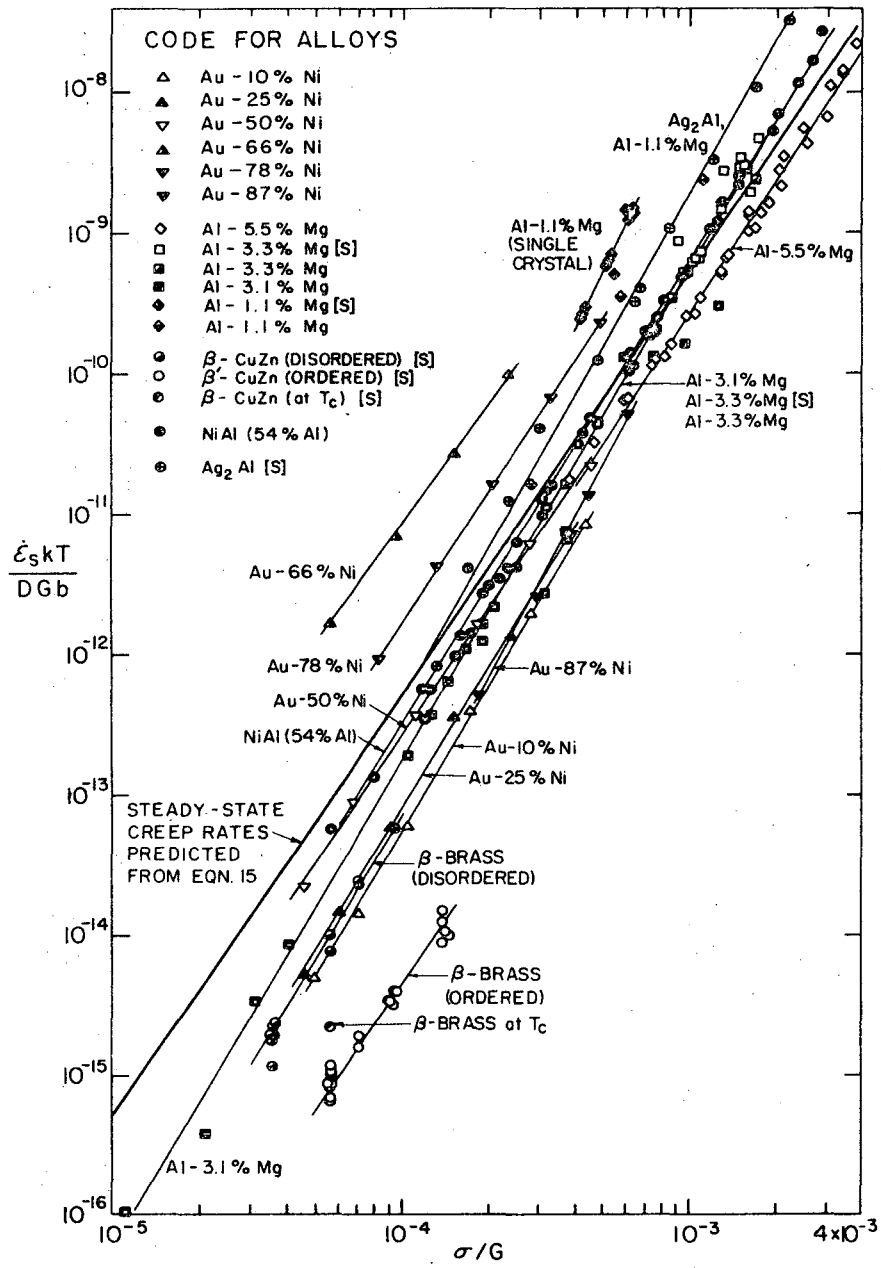

XBL 697-948

FIG. 10

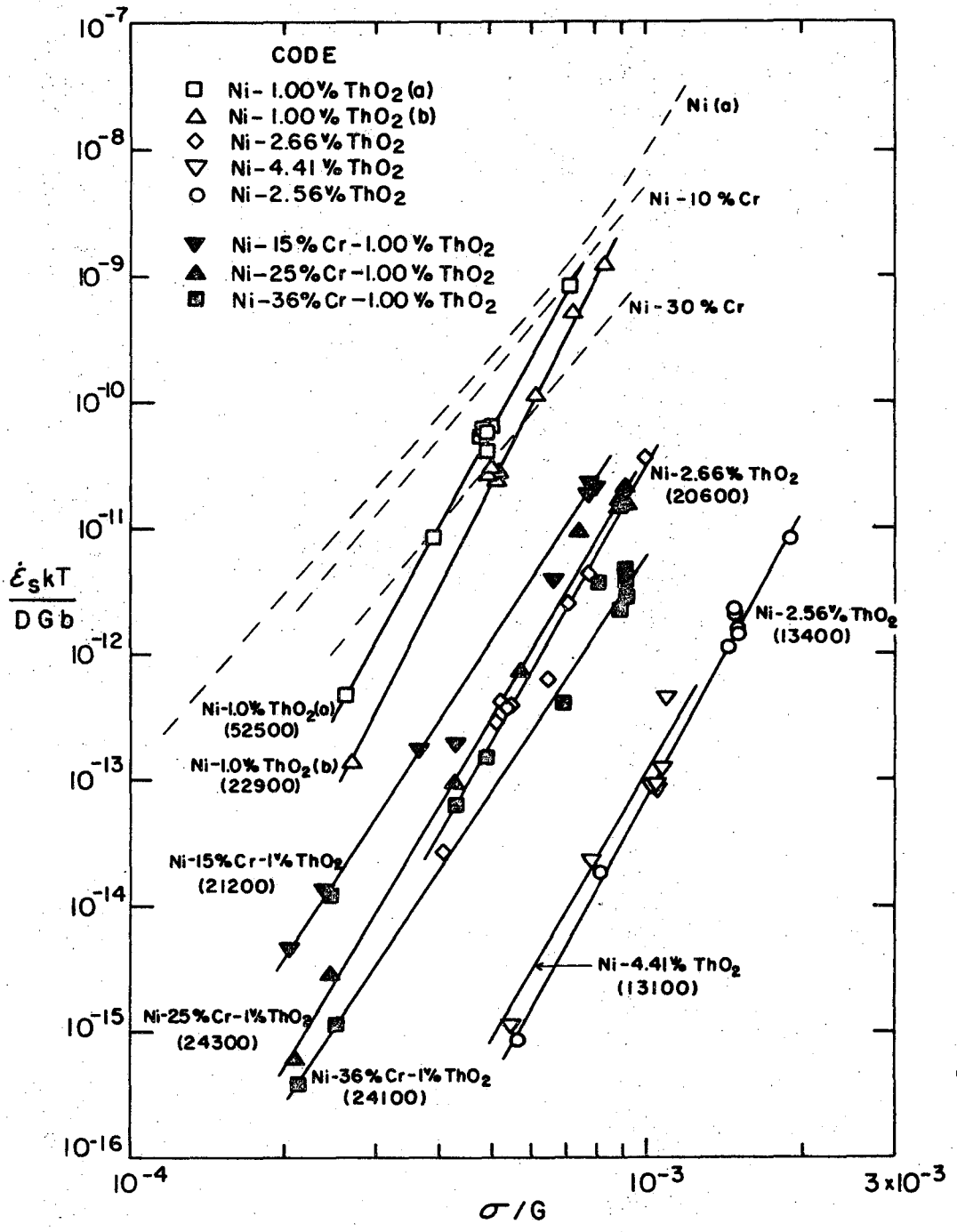

XBL 697-952

FIG. 11

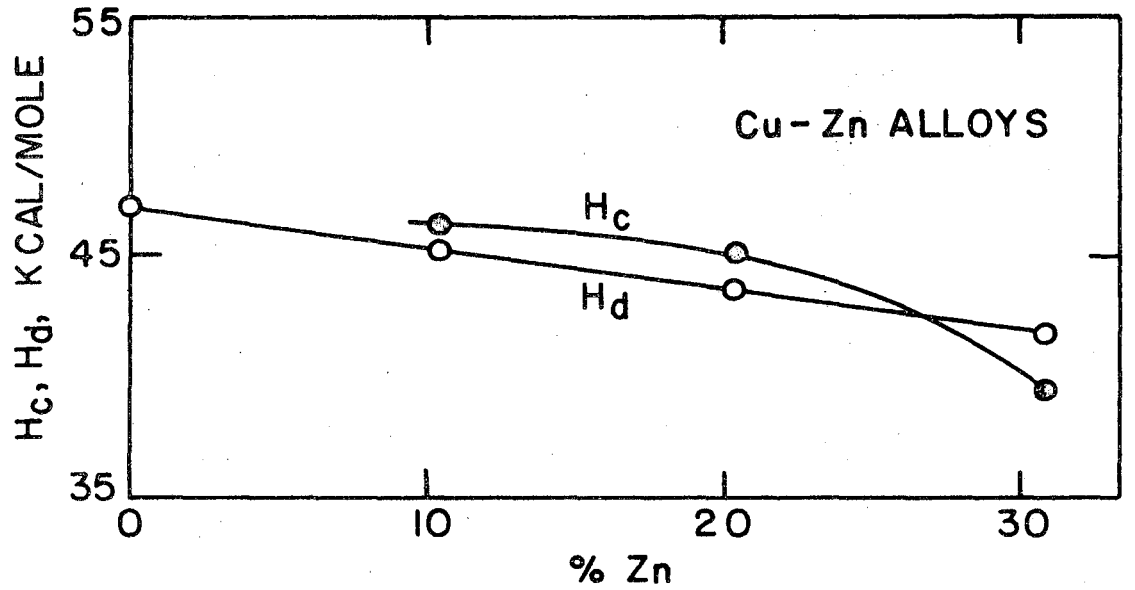

XBL 697-899

Fig. 12

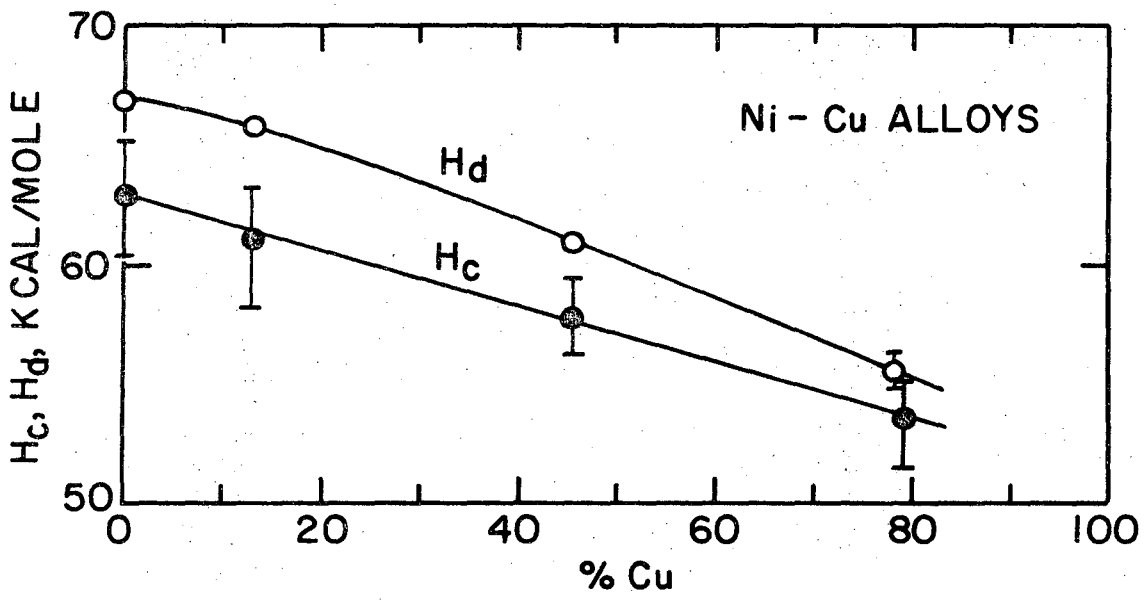

XBL 697-900

Fig. 13

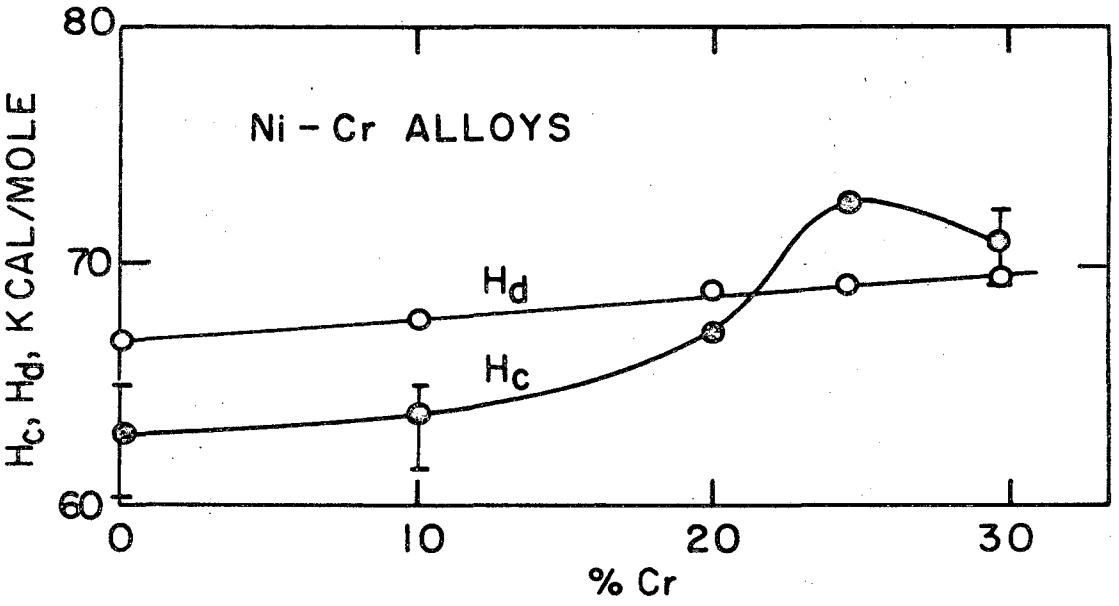

XBL 697-898

Fig. 14

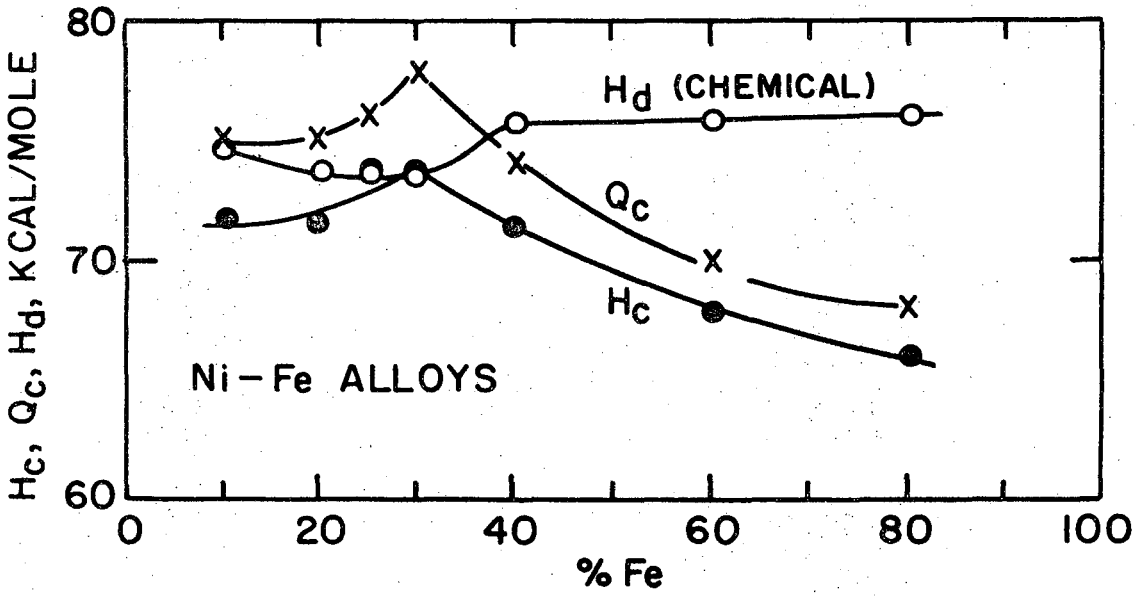

XBL 697-896

FIG. 15

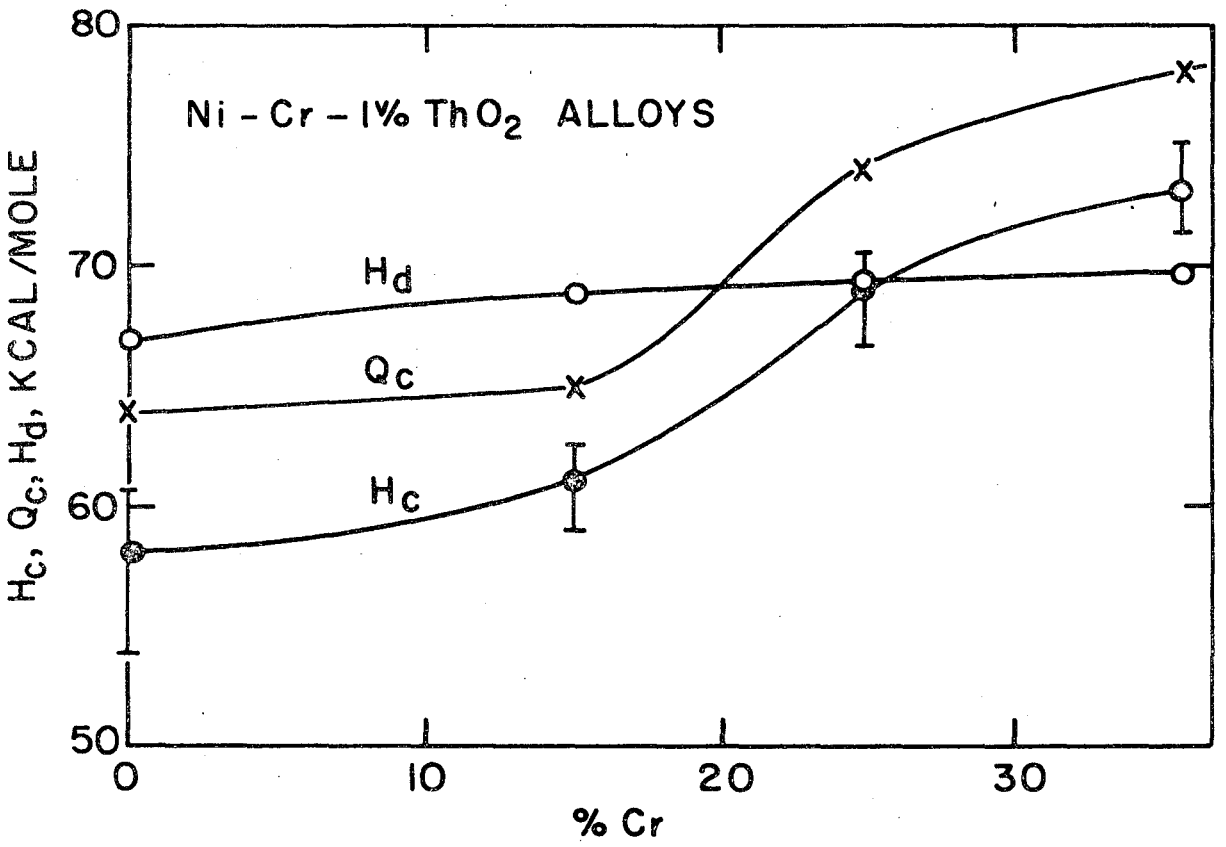

XBL 697-897

Fig. 16

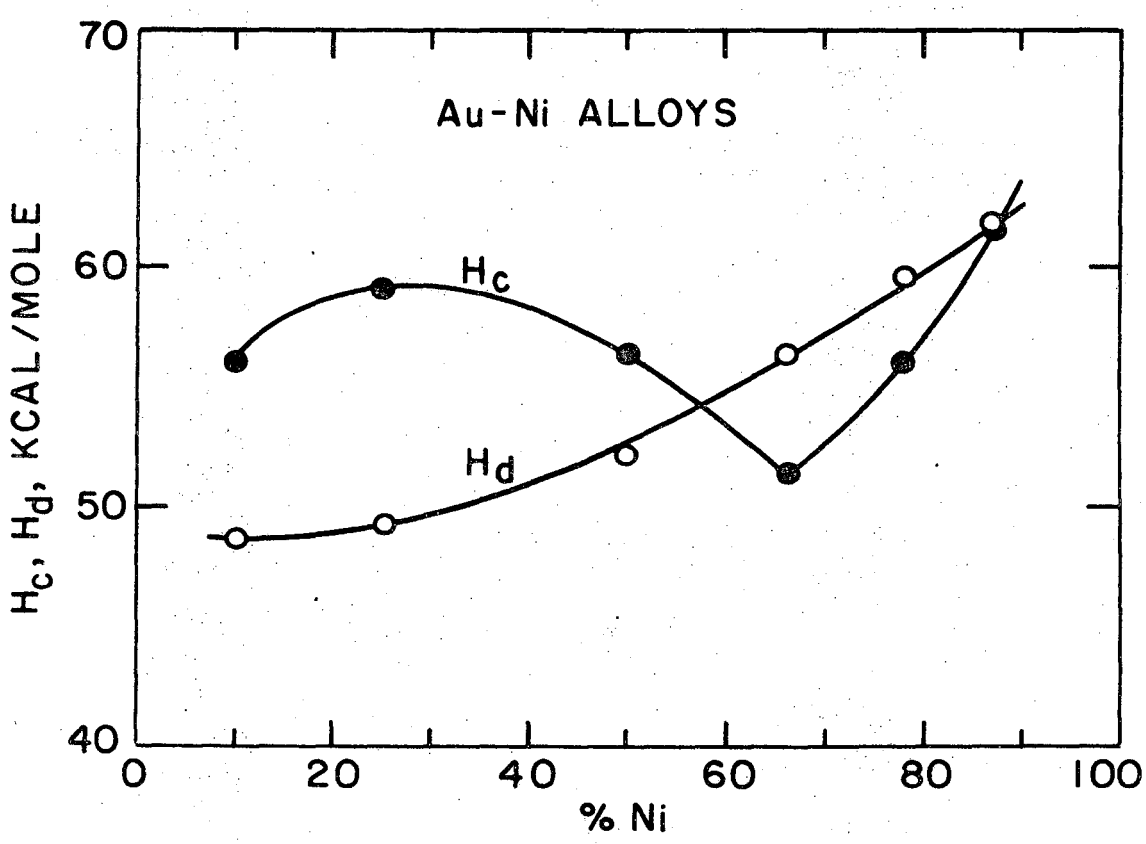

XBL 697-906

FIG. 17

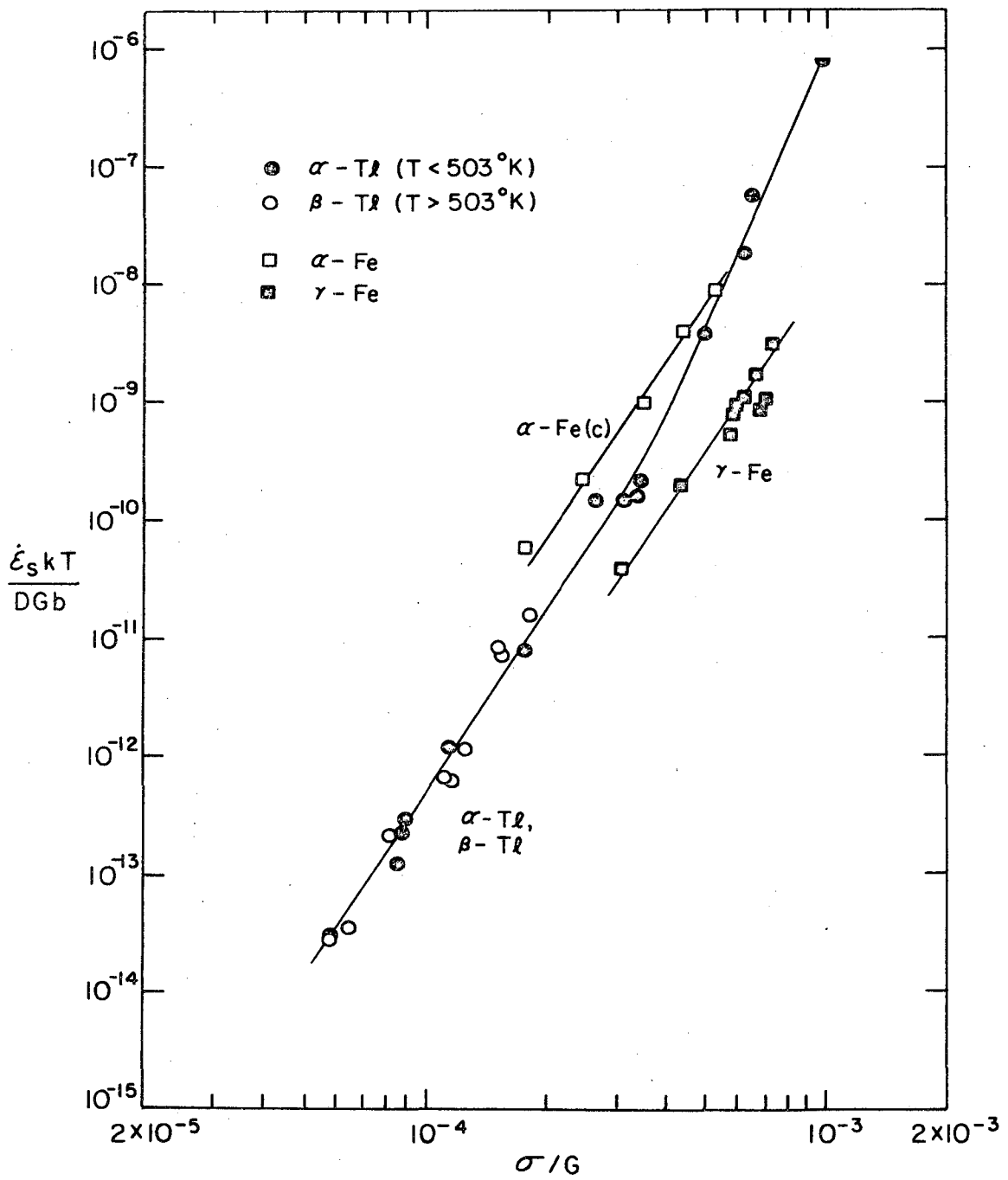

XBL 697-910

FIG. 18

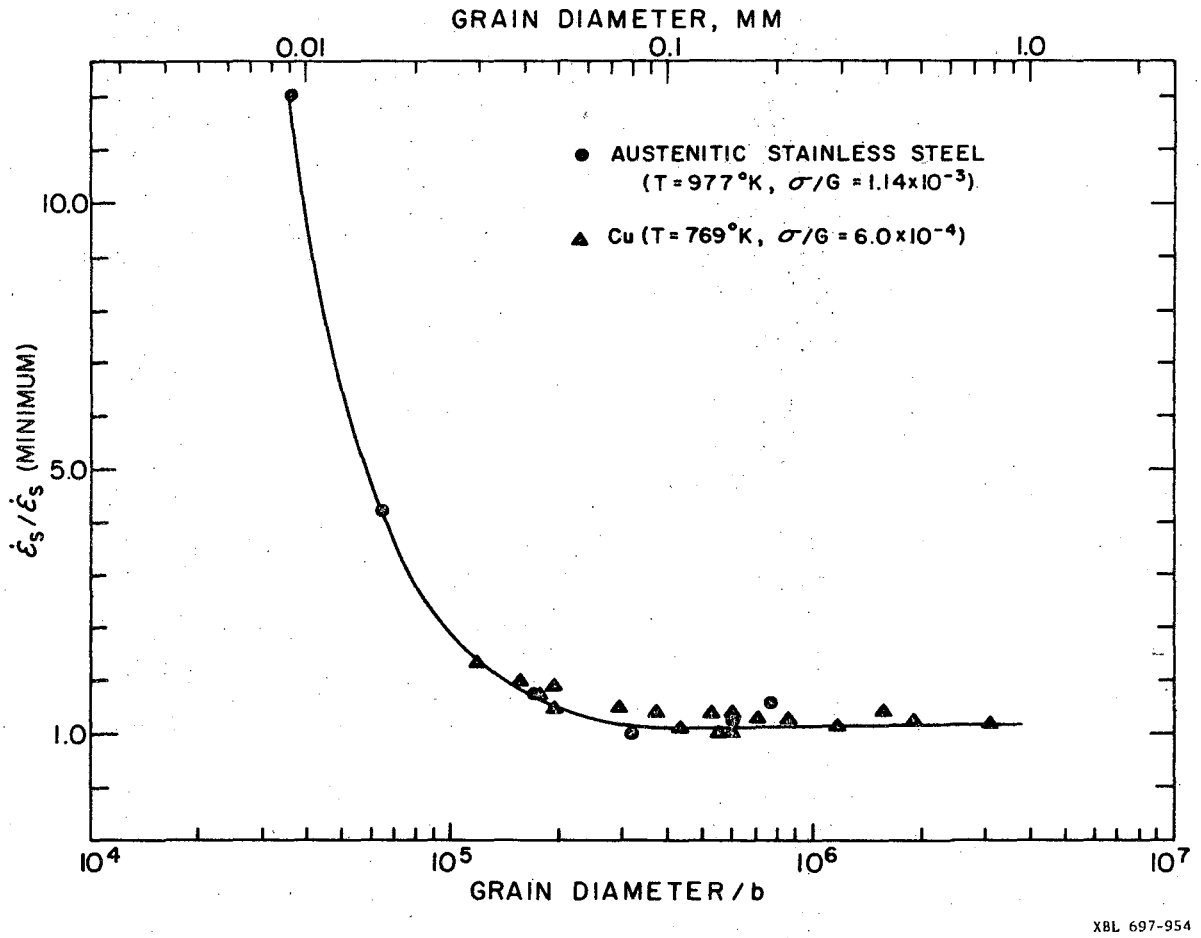
GRAIN DIAMETER, MM
0.01
0.1
1.0
AUSTENITIC STAINLESS STEEL
(T = 977°K, σ/G = 1.14x10⁻³)
Cu (T = 769°K, σ/G = 6.0x10⁻⁴)
10.0
5.0
1.0
$\dot{\varepsilon}_s/\dot{\varepsilon}_s$ (MINIMUM)
10^4
10^5
10^6
10^7
GRAIN DIAMETER / b
XBL 697-954

FIG. 19

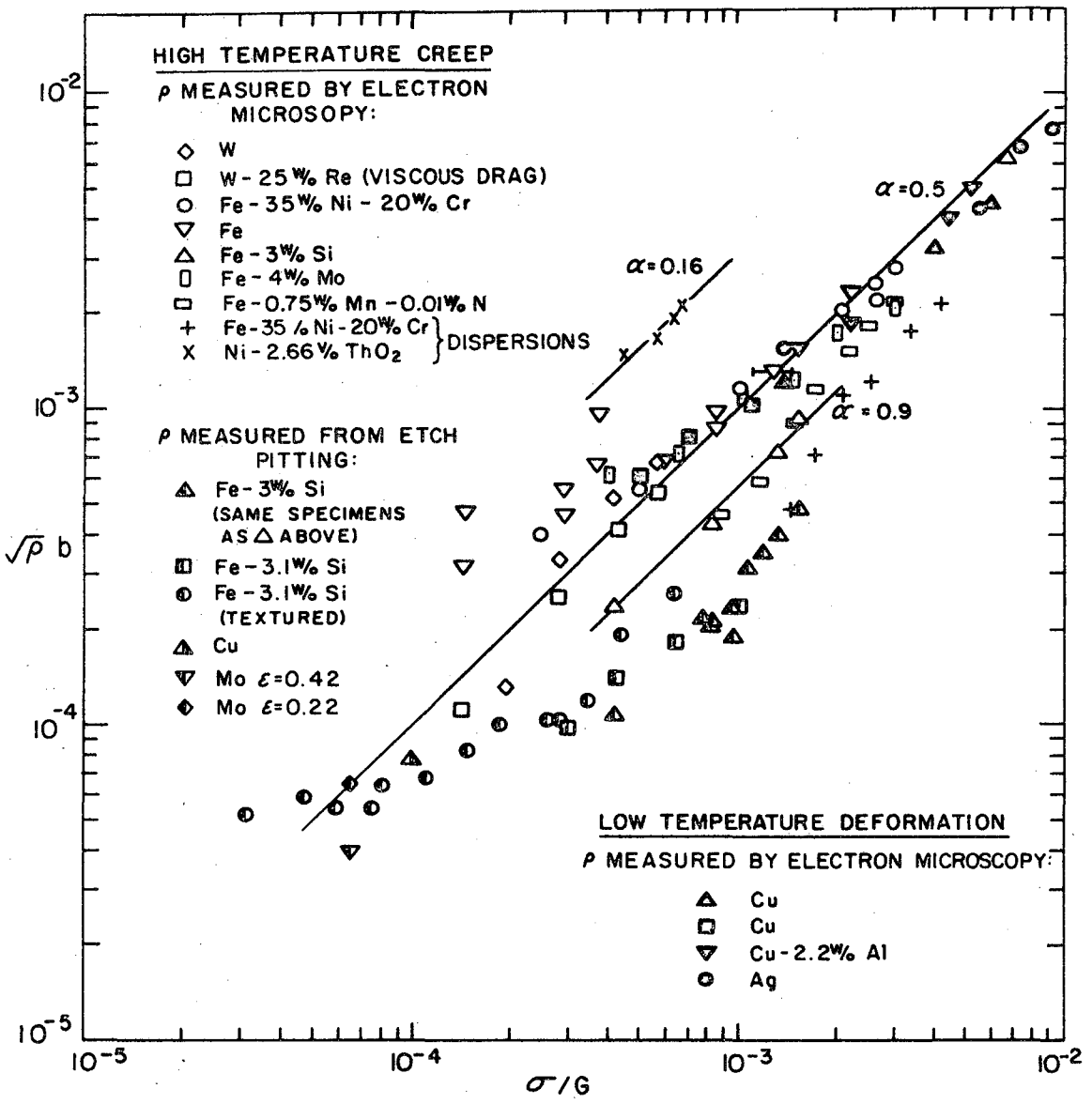

XBL 697-1041

FIG. 20

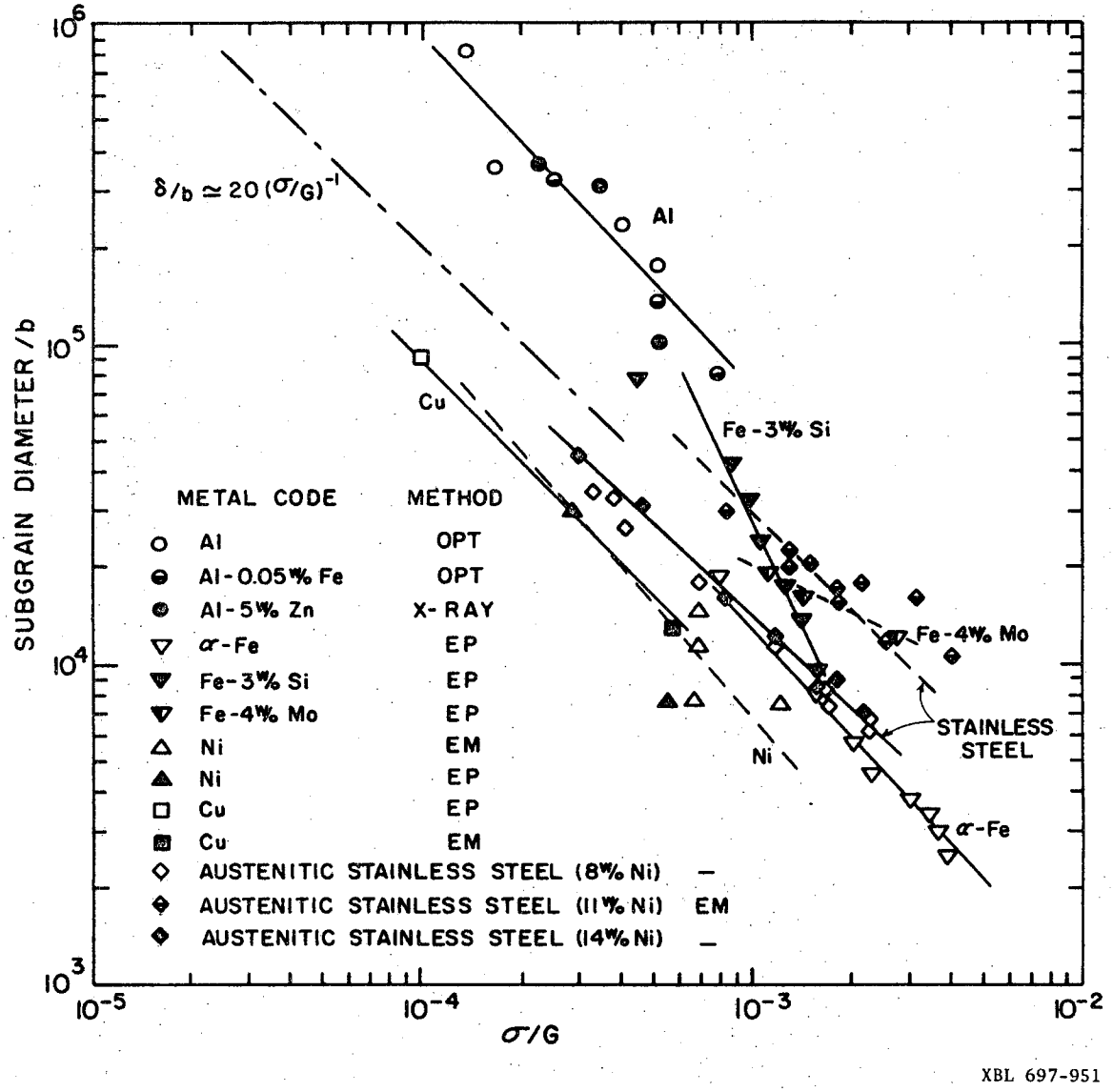

XBL 697-951

FIG. 21

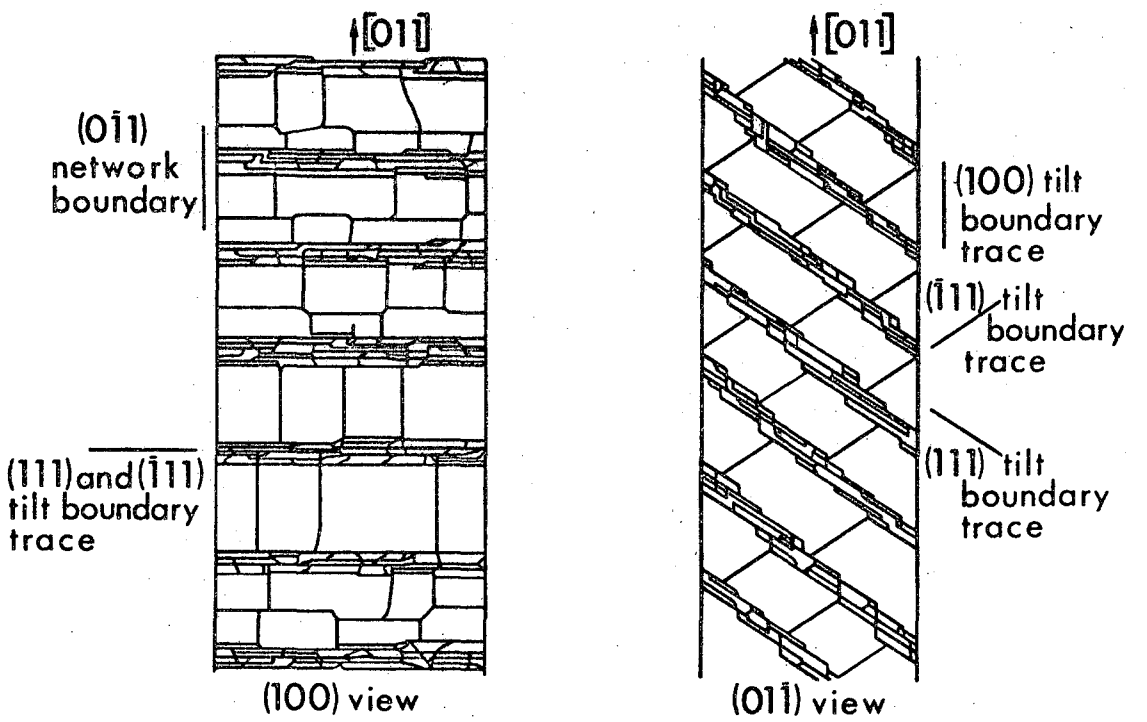

XBL 697-960

FIG. 22

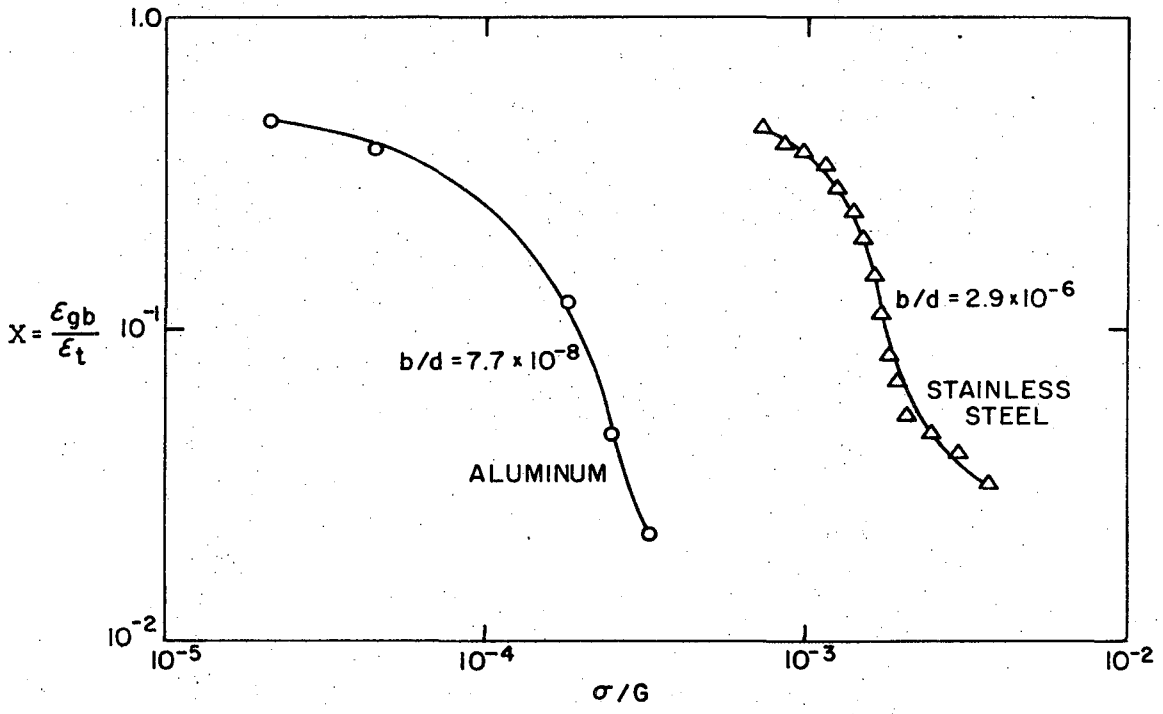

XBL 697-1042

FIG. 23

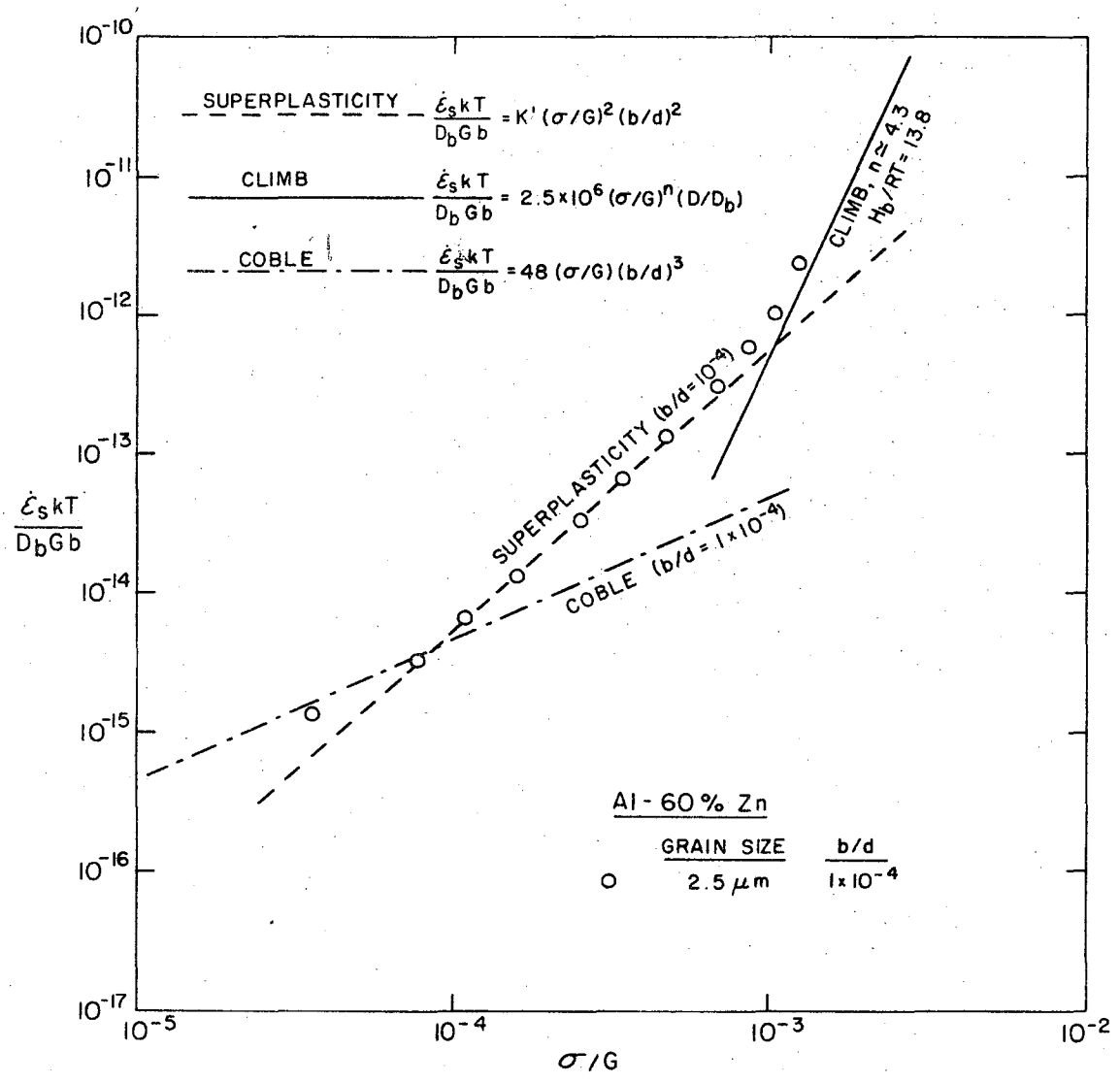

XBL 697-1046

FIG. 24

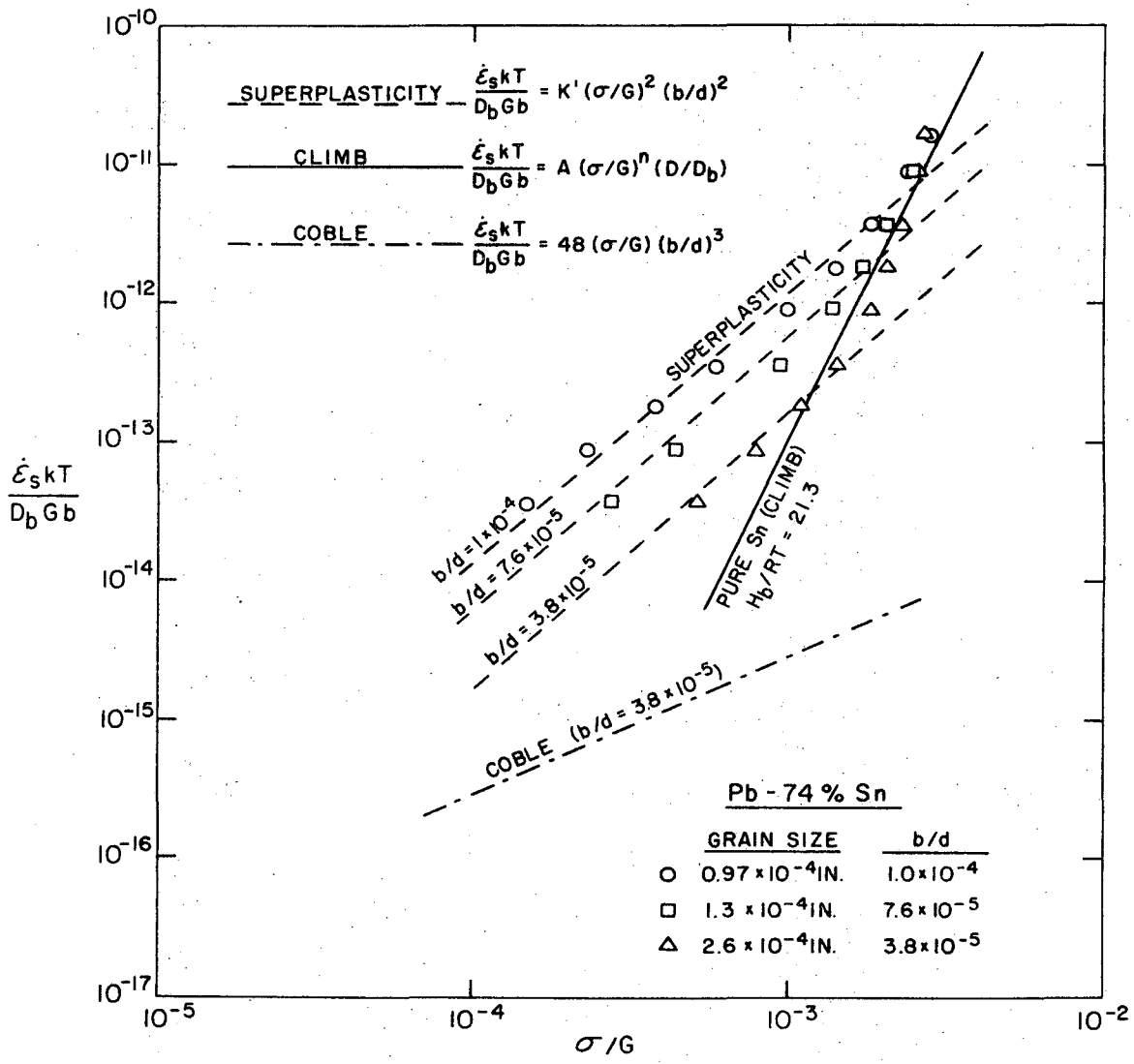

XBL 697-1047

FIG. 25

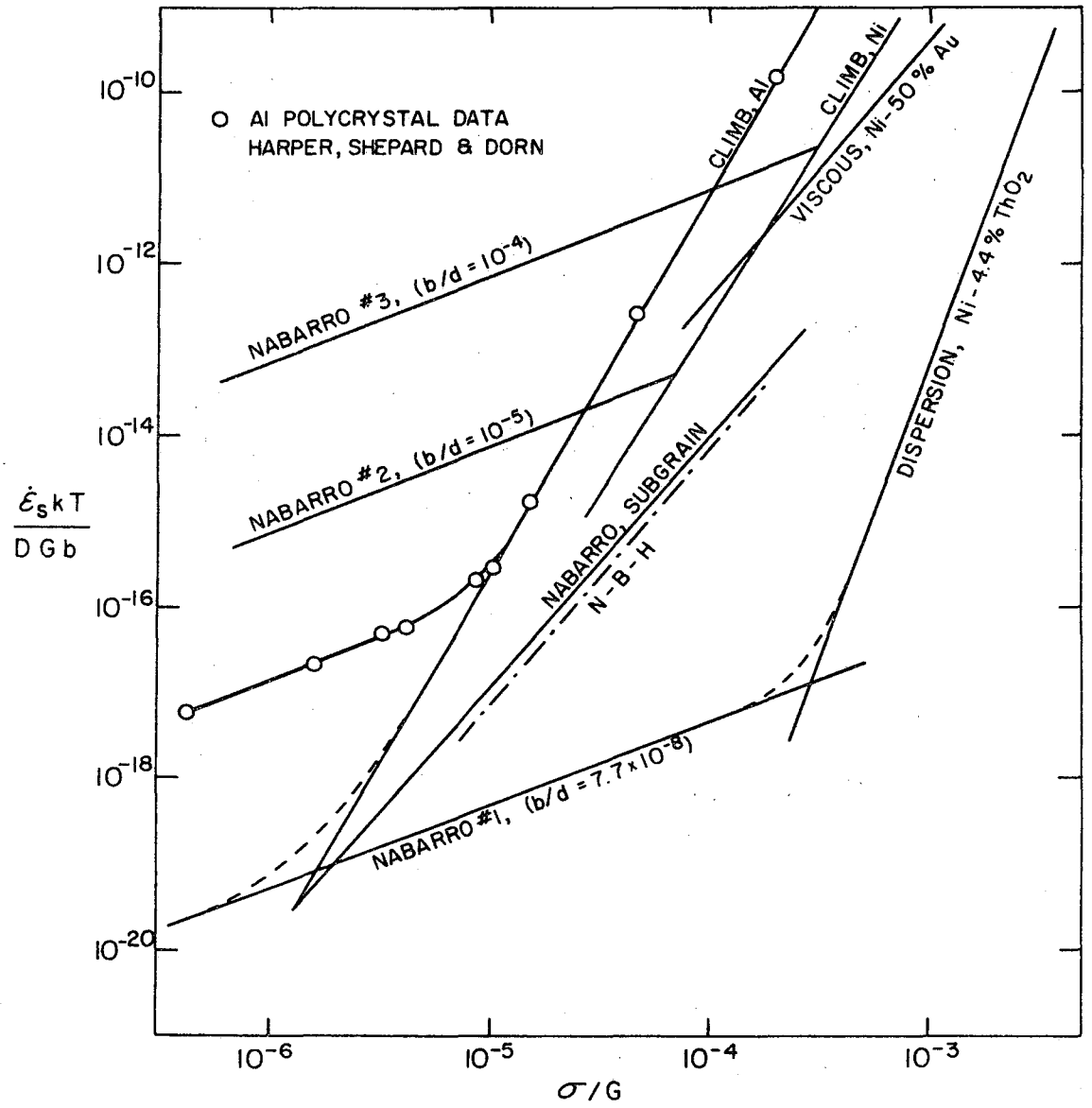

XBL 697-1045

FIG. 26

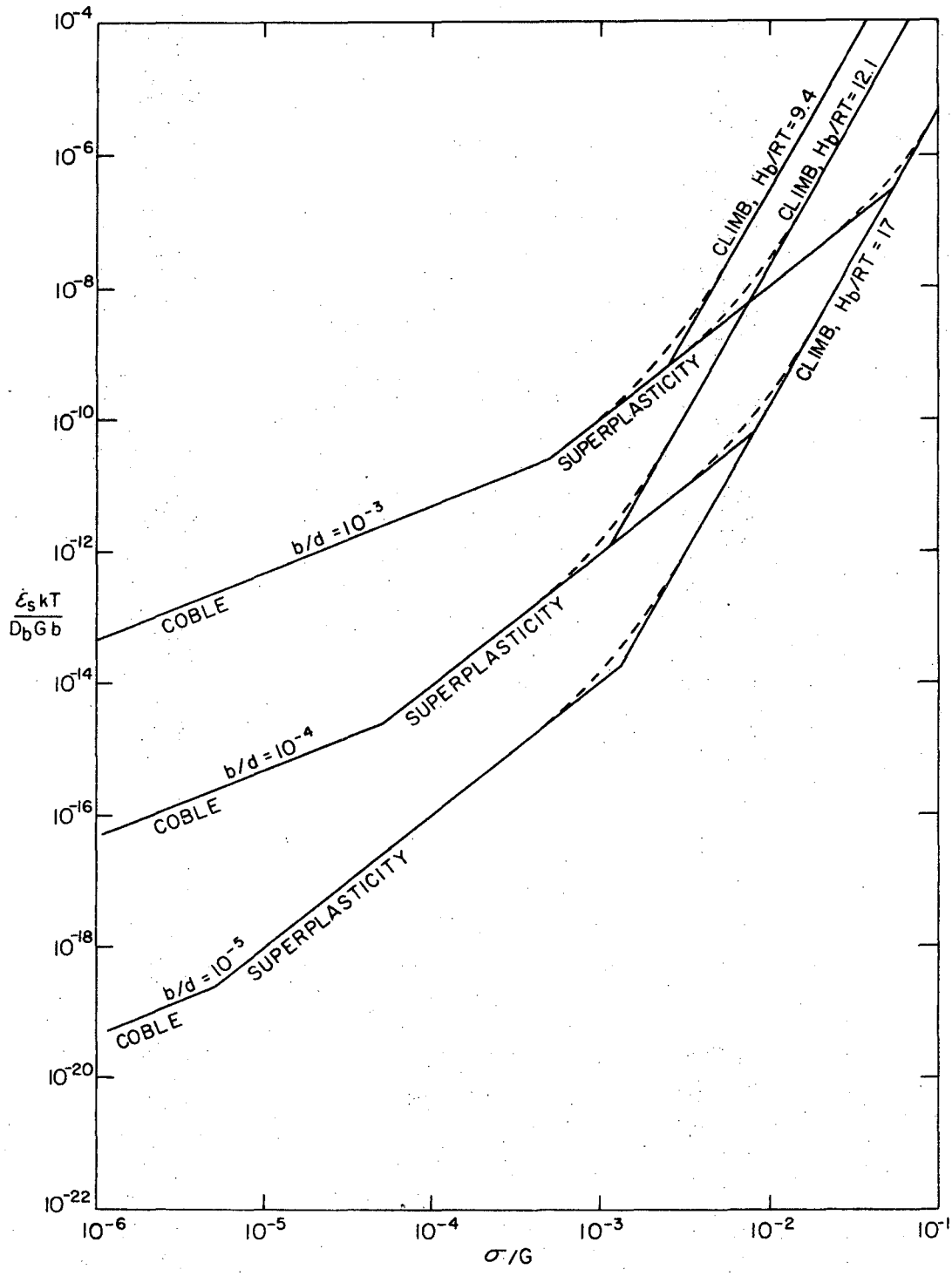

XBL 697-1044

FIG. 27

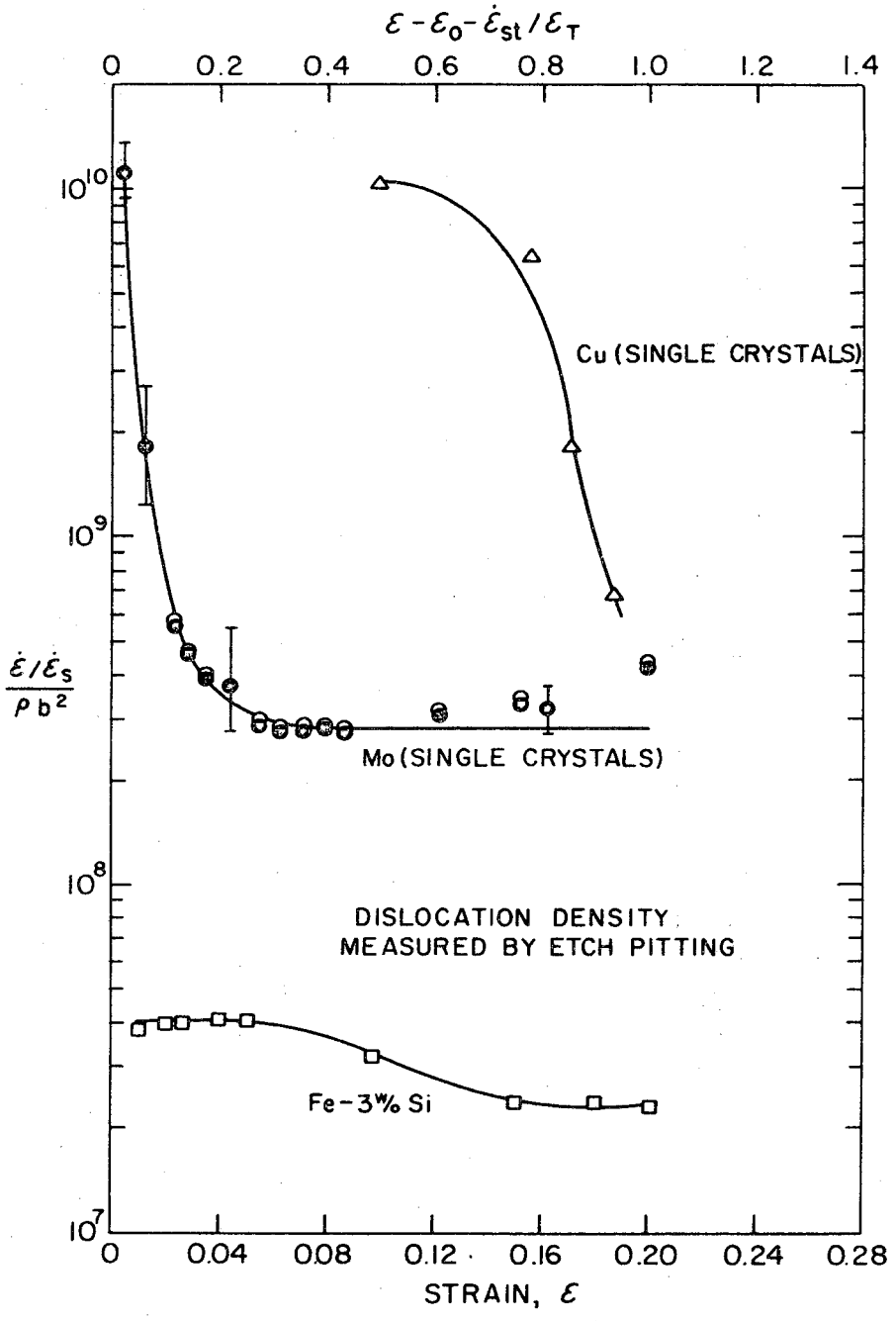

XBL 697-918

FIG. 28

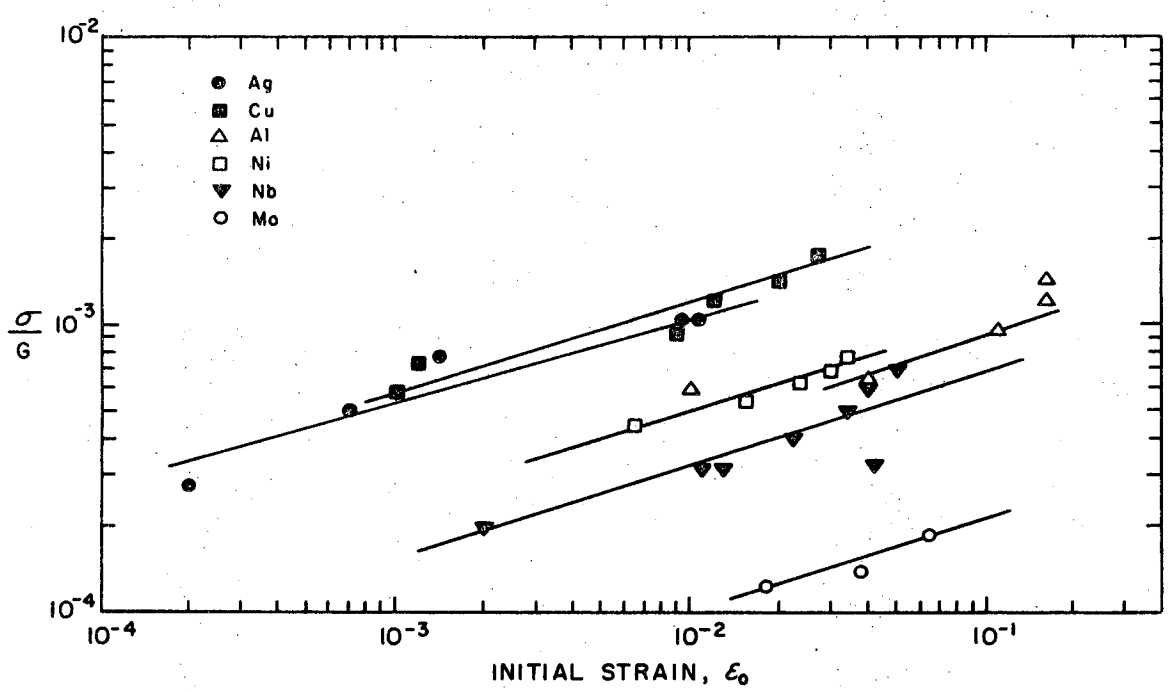

XBL 697-916

FIG. 29

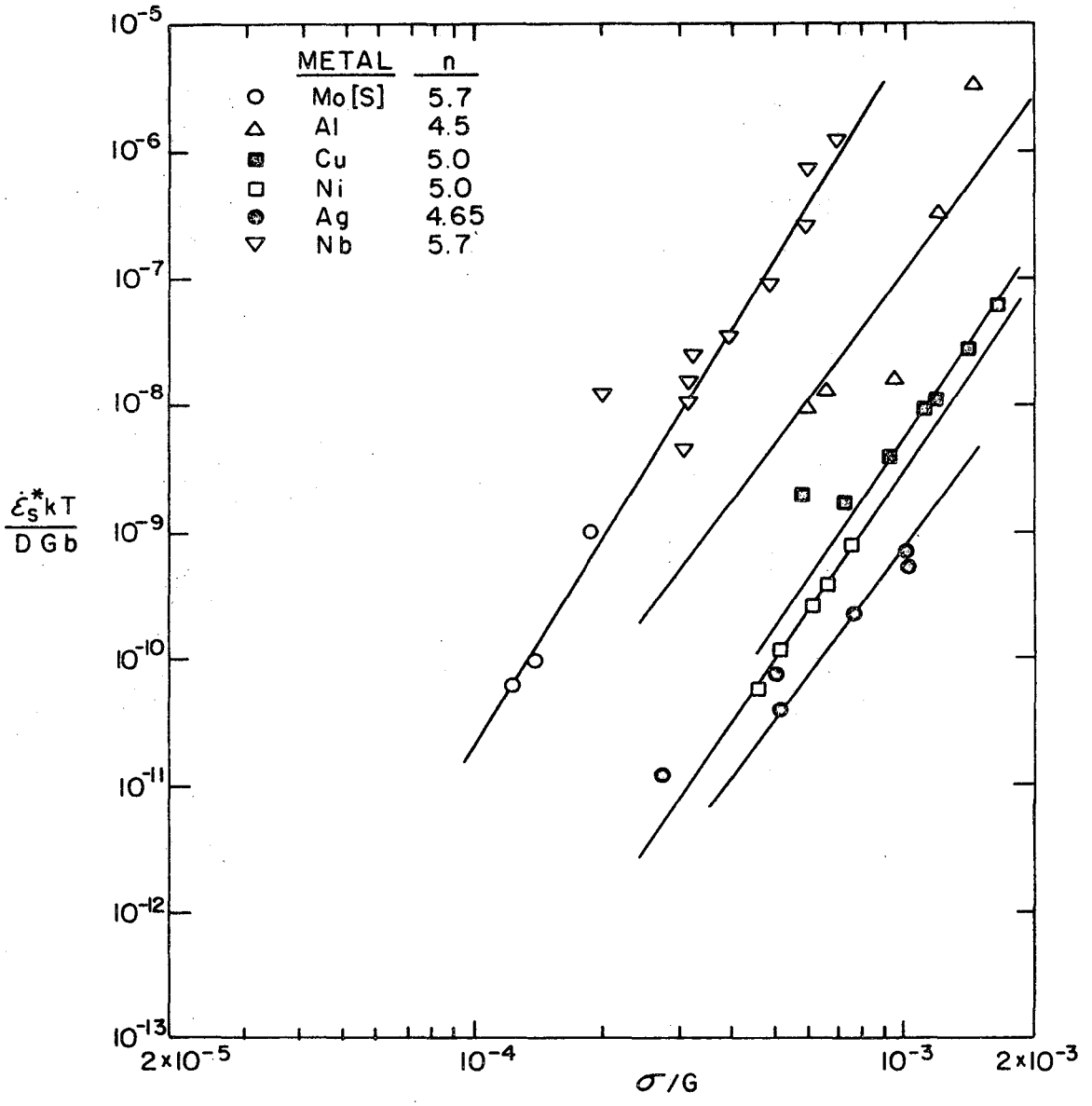
METAL n
Mo[S] 5.7
Al 4.5
Cu 5.0
Ni 5.0
Ag 4.65
Nb 5.7
$\frac{\dot{\varepsilon}_s^* kT}{DGb}$
10^{-5}
10^{-6}
10^{-7}
10^{-8}
10^{-9}
10^{-10}
10^{-11}
10^{-12}
10^{-13}
2×10^{-5}
10^{-4}
10^{-3}
2×10^{-3}
σ/G
XBL 697-919

FIG. 30

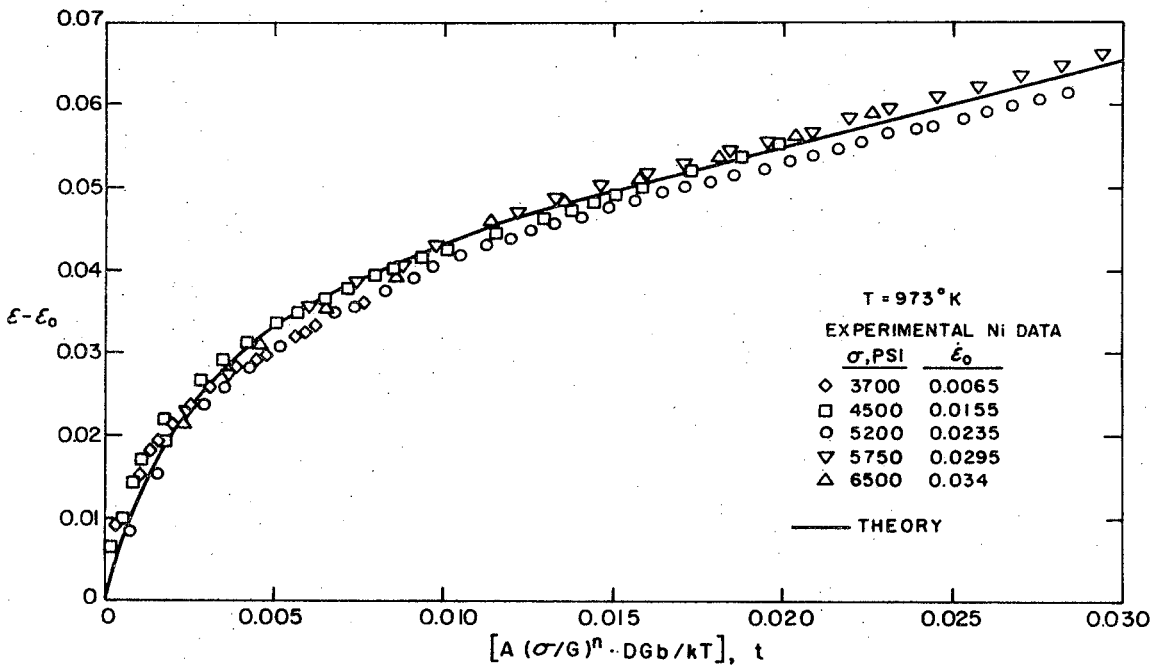
0.07
0.06
0.05
0.04
0.03
0.02
0.01
0
$\varepsilon - \varepsilon_o$
0
0.005
0.010
0.015
0.020
0.025
0.030
$[A(\sigma/G)^n \cdot DGb/kT]$, t
T = 973°K
EXPERIMENTAL Ni DATA
σ, PSI
$\dot{\varepsilon}_o$
◇ 3700 0.0065
□ 4500 0.0155
○ 5200 0.0235
▽ 5750 0.0295
△ 6500 0.034
THEORY
XBL 697-915

FIG. 31

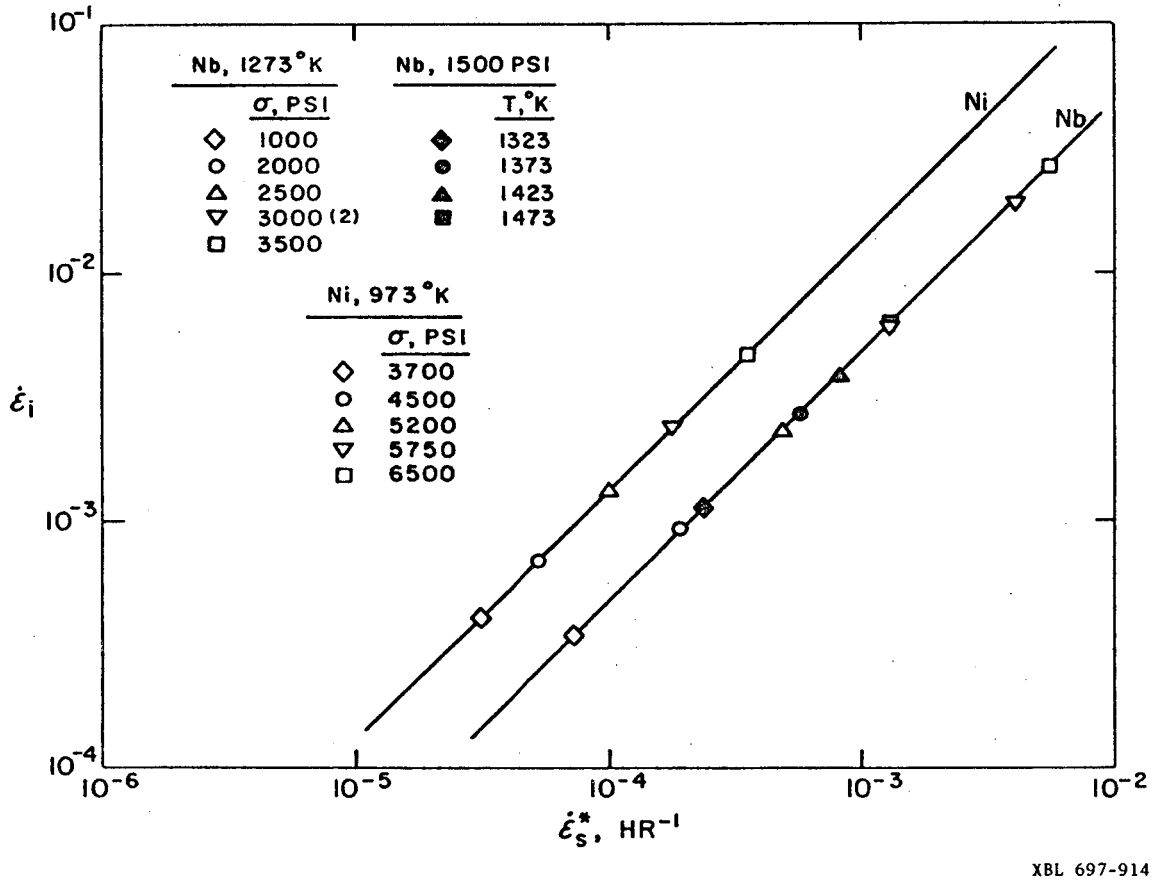
Nb, 1273°K
σ, PSI
1000
2000
2500
3000 (2)
3500
Nb, 1500 PSI
T, °K
1323
1373
1423
1473
Ni, 973°K
σ, PSI
3700
4500
5200
5750
6500
Ni
Nb
$\dot{\varepsilon}_i$
$\dot{\varepsilon}_s^*$, HR^{-1}
10^{-1}
10^{-2}
10^{-3}
10^{-4}
10^{-6}
10^{-5}
10^{-4}
10^{-3}
10^{-2}
XBL 697-914

FIG. 32

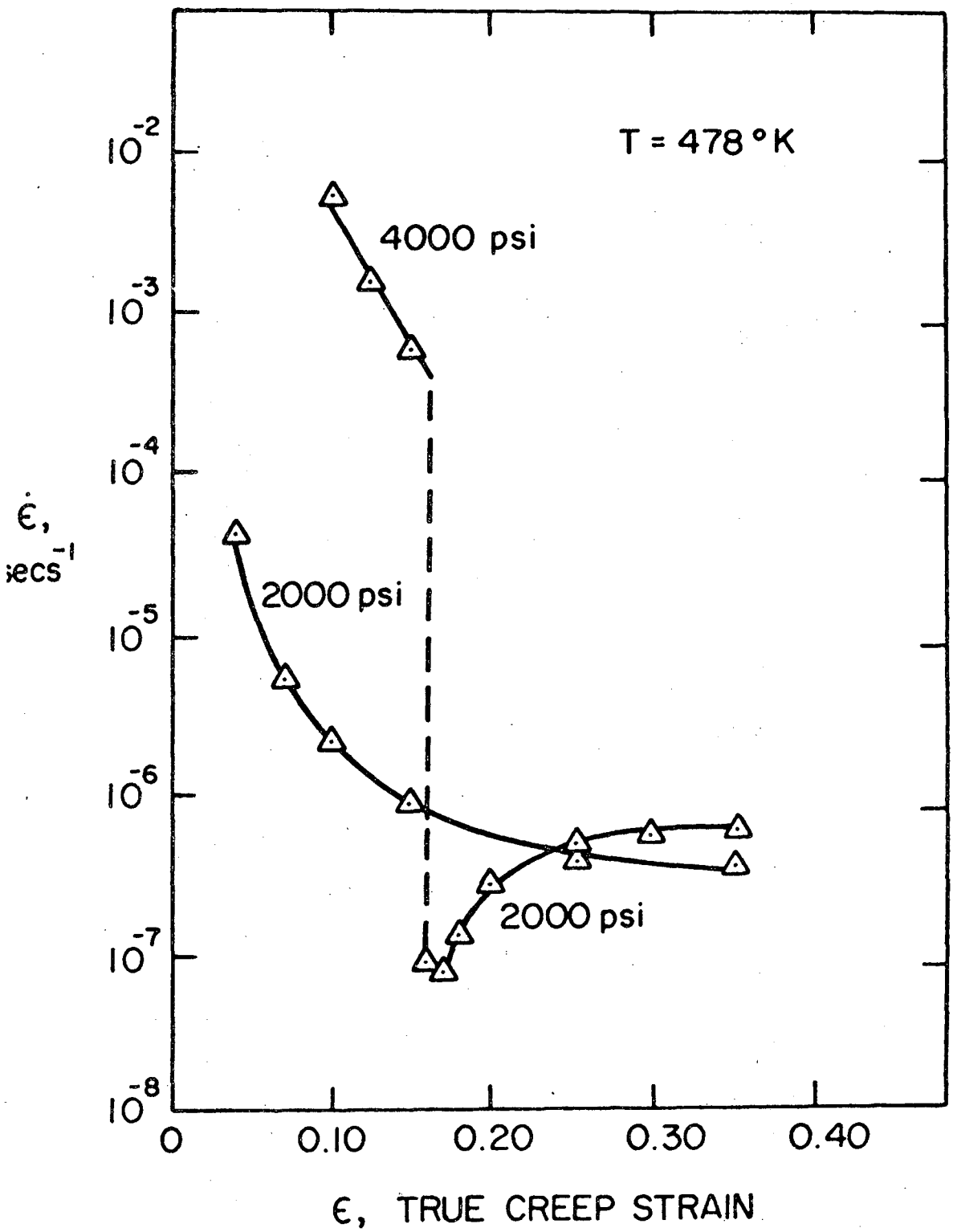
T = 478 °K
4000 psi
2000 psi
2000 psi
10^{-2}
10^{-3}
10^{-4}
10^{-5}
10^{-6}
10^{-7}
10^{-8}
$\dot{\epsilon}$, secs^{-1}
0
0.10
0.20
0.30
0.40
ϵ, TRUE CREEP STRAIN
XBL 688-1499

FIG. 33

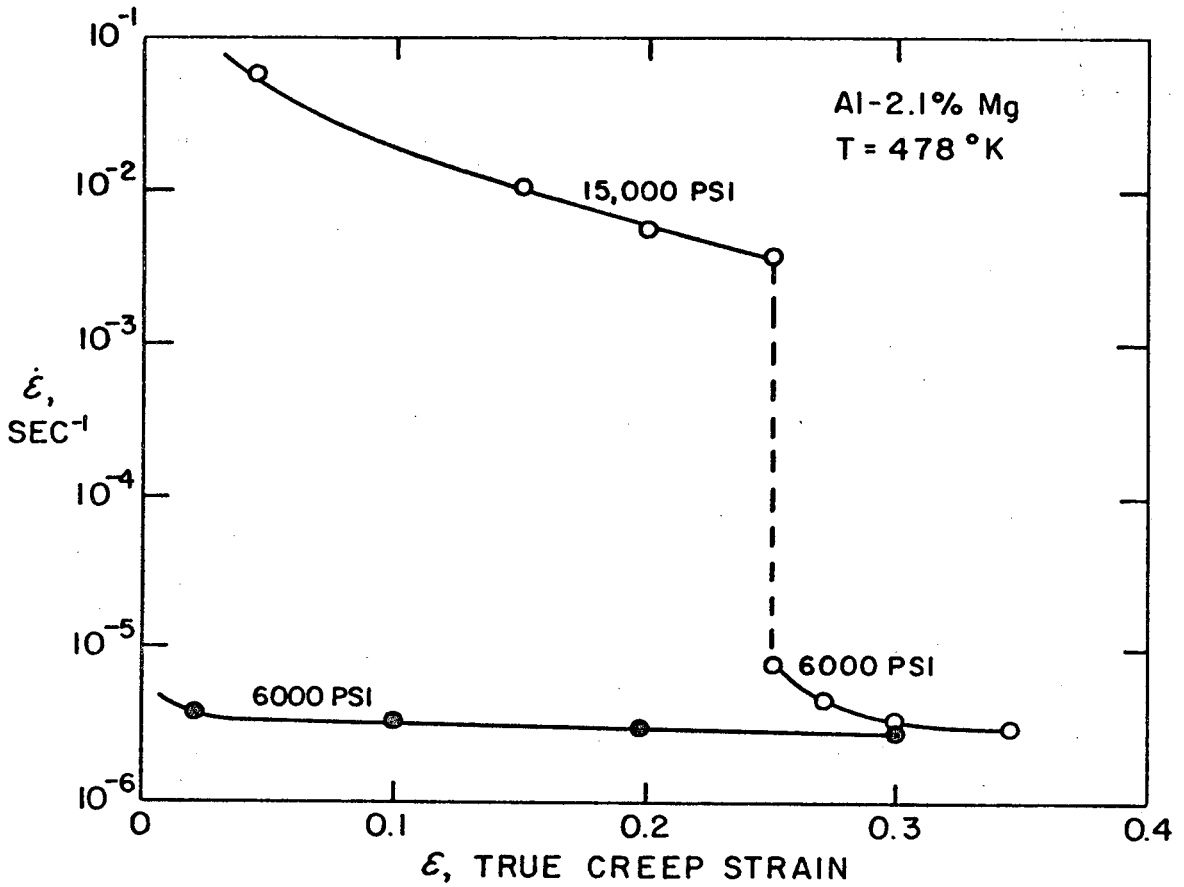
Al-2.1% Mg
T = 478 °K
15,000 PSI
6000 PSI
6000 PSI
$\dot{\varepsilon}$, SEC^{-1}
10^{-1}
10^{-2}
10^{-3}
10^{-4}
10^{-5}
10^{-6}
0
0.1
0.2
0.3
0.4
ε, TRUE CREEP STRAIN
XBL 697-956

FIG. 34

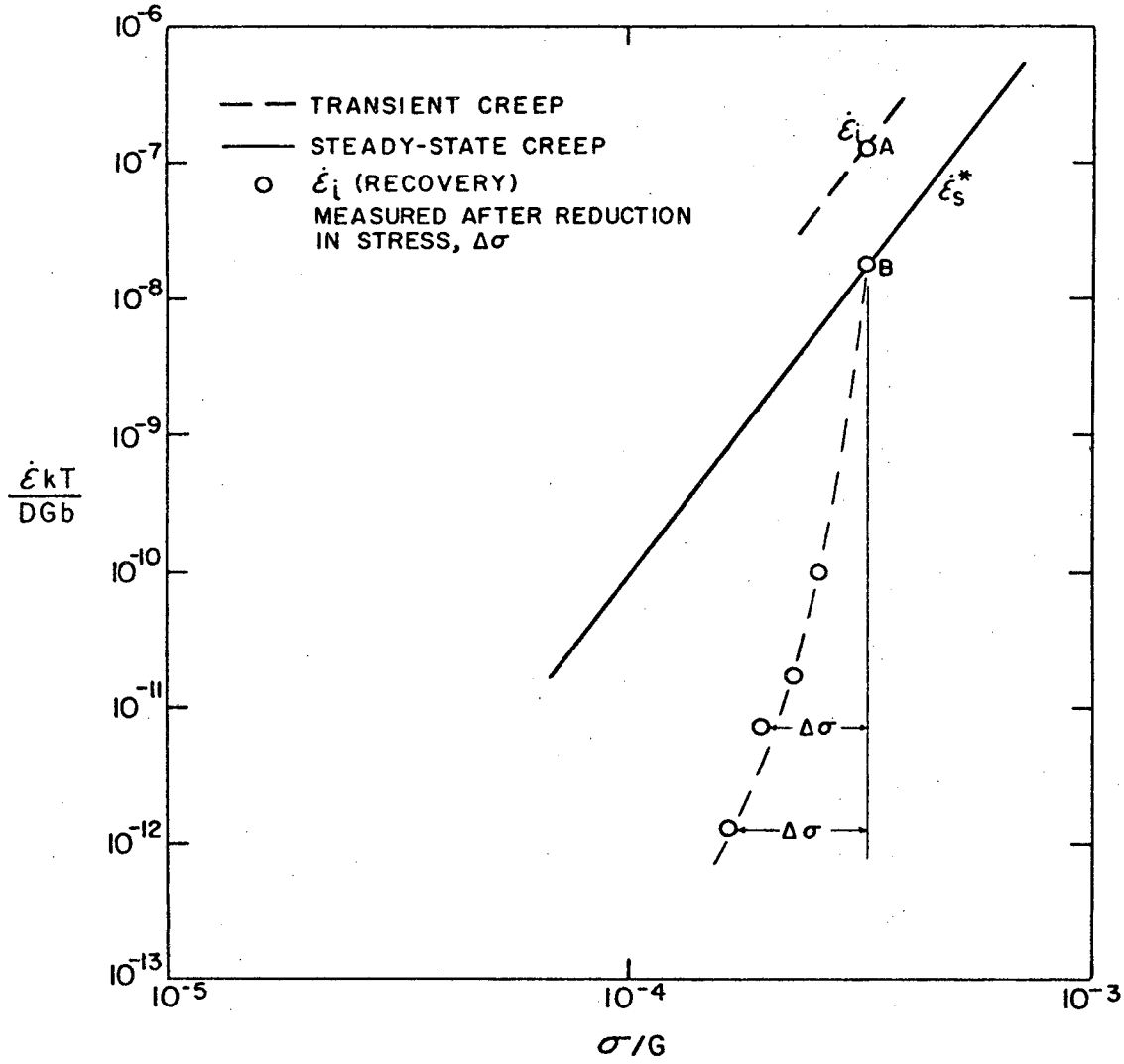

XBL 697-1043

FIG. 35

APPENDIX: Shear modulus, diffusivity and stacking fault energy values used in analyses of this paper.

I. Shear Modulus.

The unrelaxed shear modulus of most metals can be represented at temperatures above about one-third of the Debye temperature by

$$G = G_o - G_T T \tag{A1}$$

or

$$G = G_o \left(1 - \beta \frac{T}{T_m}\right) \tag{A2}$$

where G is the shear modulus, T is the absolute temperature, T_m is the melting point of the metal, and G_o, G_T, and β are material constants. The values of G_o, G_T, and β for all of the pure metals and for many of the alloys* considered in this paper are tabulated in Table A1.

Unless noted otherwise all values have been calculated from elastic compliances of single crystals using the relation

$$G = \sqrt{c_{44} \cdot 1/2 \, (c_{11}-c_{12})} \tag{A3}$$

According to anisotropic dislocation theory this value of G is a reasonably accurate approximation to the isotropic shear modulus for glide dislocations in cubic and HCP crystals[49A-51A].

For the metals Fe, Ta, V, Be, α-Tl, and the Ni-Fe alloys, G was calculated from the temperature dependence of the unrelaxed Young's modulus, E, using the relation

$$G = E \times \left[\frac{G^*}{E}\right]_{300°K} \tag{A4}$$

---

*Alloy compositions are stated in terms of atomic percent unless otherwise noted.

TABLE A1: Shear Modulus Values for Metals and Alloys at High Temperatures.

Metal	G_o 10^{11} dynes/cm^2	G_T 10^8 dynes/cm^2	B	References for G	D
Al	3.022	1.60	0.520	1A	2A
Cu	4.740	1.70	0.487	3A	4A
Au	2.766	0.84	0.406	3A	5A
γ-Fe	9.574	4.27	0.807	6A	7A
Pb	0.994	0.883	0.534	8A	9A
Ni(1)	8.412	2.69	0.552	10A	11A
Pt(2)	6.457	1.40	0.443	12A,6A	13A
Ag	3.043	1.27	0.515	3A	14A
α-Fe(3)					
Fe-6% Si	-(4)	-(4)	-	15A	16A
δ-Fe(3)	7.215	2.62	0.657	15A	16A
Mo	13.520	2.05	0.438	17A	18A
Ta(2)	~6.950	~0.87	~0.41	19A,20A	21A
B-Tl	0.767	0.903	0.678	6A	22A
V	0.502	0.73	0.316	23A,24A	25A
W	16.559	1.84	0.404	26A	27A,28A
Be	15.7	2.26	0.223	6A,29A	30A
Cd(2)	3.60	2.15	0.354	31A,6A	32A
Mg(2)	1.92	0.86	0.480	33A,6A	34A
α-Tl	0.55	0.326	0.342	35A,6A	22A
Zn	5.981	3.37	0.390	36A	37A
Cu-10.3% Zn(5)	3.949	1.41	0.462	38A	-

Metal	G_o 10^{11}dynes/cm^2	G_T 10^8dynes/cm^2	B	References for G	D
Cu-20.3% Zn[5]	4.177	1.47	0.441	38A	-
Cu-30.7% Zn[5]	4.374	1.52	0.413	38A	39A
Ni-(10 to 30)% Cr	8.80	2.4	0.457	40A	-
Ni- 10% Fe[1]	8.76	2.54	0.498	41A,42A	-
Ni- 20% Fe[1]	8.30	2.73	0.564	41A,42A	-
Ni- 25% Fe[1]	8.33	2.04	0.420	43A,42A	-
Ni- 30% Fe[1]	7.84	2.44	0.533	41A	-
Ni- 40% Fe[1]	7.20	2.15	0.510	41A,42A	-
Ni- 60% Fe[1]	6.74	1.75	0.446	41A	-
Ni- 80% Fe [1][5]	6.8	2.	0.51	-	-
AgMg (50% Mg)	2.830	0.75	0.29	44A	45A
β - CuZn(47.5% Zn)	-[4]	-[4]	-	46A	-
Ag_2Al (33% Al)	3.670	1.75	0.477	47A	-
NiAl	6.462	1.21	0.358	48A	-

1. Valid for paramagnetic metal only.
2. Estimated from single crystal elastic compliances; value of G_T chosen so as to be compatable with measurements of E_T for polycrystals.
3. Based upon measurements of E of randomly oriented Fe-6$^a/_o$ Si (at pct).
4. Variation of G with temperature is nonlinear due to ferromagnetic or ordering reaction.
5. Elastic compliances obtained by interpolation of experimental data.

where G* represents the value of G calculated from single crystals at 300°K using Eq. A3. (An average value of G*/E = 1/2.9 was used for all of the Ni-Fe alloys). For γ-Fe, β-Tl, NiAl, and all of the Ni-Cr alloys, G was calculated from the temperature dependence of the unrelaxed Young's modulus assuming that

$$G = \frac{E}{2(1 + \nu)} \tag{A5}$$

and Poisson's ratio, ν, is equal to about 1/3. The variation of G with temperature for α-Fe is shown in Fig. A1. It has been derived from measurements of E on randomly oriented, polycrystalline Fe-6% Si[15A].

For Ni-Cu alloys the elastic modulus was calculated from a weighted average of the moduli of Cu and Ni since investigations[42A,52A,53A] on the elastic compliances of single crystals show that this is an excellent approximation at high temperatures:

$$G \text{ (Ni-Cu alloys)} = N_{Ni}G_{Ni} + N_{Cu}G_{Cu} \tag{A6}$$

N stands for atomic fraction in this equation. The modulus of pure Al was used for all of the Al-Mg alloys since room temperature measurements[53A] of E in Al - 0 to 10% Mg alloys show that E is independent of composition. The shear modulus of Au-Ni alloys at 860°C was estimated using the assumption that the variation of G with composition is similar to that measured at room temperature[54A]. The modulus, in dynes/cm^2, was calculated from the expression:

$$G = \sqrt{(3.084 + 2.36\, N_{Ni} + 3.83\, N_{Ni}^2)(1.068 + 0.712\, N_{Ni} + 1.29\, N_{Ni}^2)}\ \times 10^{11} \tag{A7}$$

II. Diffusivity

The tracer diffusivities of all of the pure metals and a few alloys were obtained directly from the references given in Table A1.

The diffusivity of α-Fe has not been measured experimentally below 700°C. To permit analysis of creep data obtained at $T \geq 500°C$, the tracer diffusivity measurements of Lai and Borg[19A] were extrapolated to lower temperatures using the approximate relation:

$$D^{*}_{\alpha\text{-Fe}} \simeq (1.4\ e^{-56500/RT})(10^{-0.45\left\{1 + \tanh\left[17(10^{3}/T - 0.96)\right]\right\}}) \quad (A8)$$

The solid line in Fig. A2 illustrates this extrapolation. The extrapolation to low temperatures was based upon the assumption that $H_d \simeq 56.5$ Kcal/mole at temperatures very much higher or lower than T_c, the ferromagnetic Curie temperature. Measurements of the activation enthalpy for creep, H_c, of α-Fe at $T \ll T_c$[55A] show that this is a reasonable assumption. Extrapolation of $D^{*}_{\alpha\text{-Fe}}$ could have alternatively been made by assuming the diffusivity in iron parallels the elastic strain energy associated with vacancy motion as Borg[56A] has suggested (see heavy dashed line of Fig. A2). However, steady-state creep rates of α-Fe at $T \ll T_c$ correlate poorly if this assumption is made.

The tracer diffusivities of Cu-10.3% Zn and Cu-20.3% Zn alloys were estimated from experimental data on tracer diffusivities in pure Cu[4A], in a Cu-26.4% alloy[57A], and in a Cu-31% Zn alloy[39A]. The tracer diffusivities of Ni-Cu alloys[58A] and Ni-Cr alloys[59A] were obtained from the data of Monma, Suto and Oikawa, after their results were replotted and extrapolated to lower temperatures in an internally consistent manner. All tracer diffusivities which were obtained by interpolation or from a reconsideration of experimental data are shown in Table A2.

TABLE A2: Tracer Diffusivities of Binary Alloys Used For Analysis of Creep Data.

Alloy, A	A-B % B	D_o^A cm^2/sec	H_d^A Kcal/mole	D_o^B Cm^2/sec	H_d^B Kcal/mole
Cu	10.3 Zn	0.24	45.4	0.44	44.0
Cu	20.3 Zn	0.28	43.7	0.56	42.4
Ni	13.0 Cu	1.8	66.0	0.54	59.9
Ni	45.4 Cu	1.8	61.9	0.44	55.6
Ni	78.5 Cu	1.8	58.4	0.40	51.3
Ni	10.0 Cr	1.9	68.0	1.1	65.1
Ni	19.9 Cr	1.9	69.2	1.9	67.7
Ni	24.2 Cr	1.9	69.3	2.5	68.5
Ni	29.7 Cr	1.9	69.5	3.2	69.4

Tracer diffusivity data were not available for many of the Ni-Fe alloys. Since these alloys are nearly ideal solid solutions, the diffusivity was approximated using chemical interdiffusivity data[60A].

The chemical interdiffusivity, $\tilde{D}$, of Au-Ni alloys at 860°C was obtained by interpolation of experimental measurements made at 850 and 875°C[61A]. The resulting values are shown in Fig. A3. The interdiffusivity in vacancy excess NiAl (54% Al) was assumed to be

$$\tilde{D} = 1\ e^{-64{,}500/RT} \qquad (A9)$$

since H_c = 64.5 Kcal/mole. As shown in Fig. 4 this assumed value is in reasonable agreement with tracer diffusivity measurements made on other non-stoichiometric NiAl compounds[62A]. The interdiffusivity of Ag_2Al was likewise assumed to agree with H_c:

$$\tilde{D} = 1\ e^{-32{,}900/RT} \qquad (A10)$$

The interdiffusivity of Al-Mg alloys was approximated by the tracer diffusivity of pure Al, for scattered experimental data[63A] indicates that this assumption introduces little error. The chemical interdiffusivity for β-CuZn was calculated from Eq. 11 of the text using tracer diffusivity data[64A] and a crudely estimated value of $\partial \ln a_{Cu}/\partial \ln N_{Cu}$ from Fig. A5[65A].

III. Stacking Fault Energy.

The stacking fault energy in dimensionless units Γ/Gb for FCC metals and alloys was estimated from published data as shown in Table A3. Some of the measurements of Γ/Gb were made at room temperature while others were made at temperatures close to those encountered during high-temperature creep. Currently available evidence suggests that stacking-fault width

is relatively insensitive to temperature in FCC metals which do not undergo FCC - HCP phase transformations at elevated temperatures[84A].

TABLE A3: Stacking Fault Energies for FCC Metals and Alloys.

Method of Measurement:
A. Extended node measurements.
B. Estimated from size of stacking fault tetrahedra and Frank dislocation loops.
C. Estimated from deformation textrue.
D. Comparison of shrinkage rates of faulted and unfaulted dislocation loops.
E. Estimated from τ_{III} $(\dot{\varepsilon})$.
F. Estimated from annealing twin frequency and twin boundary energy at 1100°C; value of G at 1100°C used to compute Γ/Gb.

Metal Alloy	$\frac{\Gamma}{Gb} \times 10^3$	Approximate Value of Γ	Source of Data	Method of Measurement
Al	20.5 ± 4	150	66A-68A	D
Ni	10.7 ± 2	210	69A-70A	A,C
Pb	9.4 ± 1.4	30	71A	E
γ-Fe	$\sim 8 \pm 1$	75	72A	F
Au	5.9 ± 1.5	50	73A-74A	B
Cu	5.3 ± 1	55	73A-75A	A,B
Pt	$\sim 4.4 \pm 1.5$	75	76A	C
Ag	3.0 ± 0.2	23	77A-81A	A
Cu-10% Zn	1.63	17	82A-84A	A; Γ values have been corrected in manner suggested by ref. 84A
Cu-20% Zn	1.92	20	82A-84A	
Cu-30% Zn	3.56	37	82A-84A	
Ni-13% Cu	7.4	133	85A	C; Γ values have been proportionately scaled to obtain $\Gamma/Gb \times 10^3$ = 10.7 for pure Ni & 5.3 for pure Cu
Ni-46% Cu	5.55	85	85A	
Ni-79%	8.0	100	85A	
Ni-10% Cr	9.2	180	86A	C; $\Gamma/Gb \times 10^3$ values have been scaled to obtain a value of 10.7 for pure Ni
Ni-20% Cr	7.7	150	86A	
Ni-24% Cr	6.5	130	86A	
Ni-30% Cr	4.65	93	86A	

Metal Alloy	$\frac{\Gamma}{Gb} \times 10^3$	Approximate Value of Γ	Source of Data	Method of Measurement
Ni-12% Fe	7.35	97	72A	F
Ni-21% Fe	7.65	88	72A	F
Ni-26% Fe	5.87	82	72A	F
Ni-31% Fe	6.45	73	72A	F
Ni-41% Fe	5.53	60	72A	F
Ni-61% Fe	3.25	36	72A	F
Ni-80% Fe	5.04	53	72A	F

REFERENCES FOR APPENDIX

1A. P. M. Sutton, Phy. Rev., 91, 816 (1953).

2A. T. S. Lundy and J. F. Murdock, J. Appld. Phy., 33, 1671 (1962).

3A. Y. A. Chang and L. Himmel, J. Appld. Phys., 37, 3567 (1956).

4A. A. Kuper, H. Letaw, L. Slifkin and C. Tomizuka, Phy. Rev., 98, 1870 (1955).

5A. H. M. Gilbert and D. Lazarus, J. Phys. Chem. Solids, 26, 2081 (1965).

6A. W. Köster, Z. Metallkunde, 39, 1 (1948).

7A. B. Sparke, D. W. James, and G. M. Leak, J. Iron and Steel Inst., 203, 152 (1965).

8A. Unpublished data of L. C. Cardinal and S. D. Hart; presented by J. Weertman, Trans. ASM, 61, 681 (1968).

9A. N. H. Nachtrieb and G. S. Handler, J. Chem. Phys., 23, 1569 (1955).

10A G. A. Alers, J. R. Neighbours, and H. Sato, J. Phys. Chem. Solids, 13, 40 (1960).

11A R. Hoffman, F. Pickus and R. Ward, Trans. AIME, 206, 483 (1956).

12A R. E. MacFarlane, J. A. Rayne, and C. K. Jones, Phys. Letters, 18, 91 (1965).

13A F. Cattaneo, E. Germagnoli, and F. Grasso, Phil. Mag. 7, 1373 (1962).

14A C. Tomizuka and E. Sonder, Phy. Rev., 103, 1182 (1956).

15A J. L. Lytton, J. Appld. Phys., 35, 2397 (1964).

16A D. Y. F. Lai and R. J. Borg, Trans. AIME, 233, 1973 (1965).

17A J. M. Dickinson and P. E. Armstrong, J. Appld. Phys., 38, 602 (1967).

18A J. Askill, in Diffusion in BCC Metals, p. 247, Amer. Soc. Met., Metals Park (1965).

19A W. V. Green, Trans. AIME, 233, 1818 (1965).

20A F. H. Featherston and J. R. Neighbours, Phys. Rev. 130, 1324 (1963).

21A R. L. Eager and D. B. Langmuir, Phy. Rev., 89, 911 (1953).

22A G. A. Shirn, Acta Met., 3, 87 (1955).

23A P. E. Armstrong and H. L. Brown, Trans. AIME, 230, 962 (1964).

24A G. A. Alers, Phys. Rev., 119, 1532 (1960).

25A R. F. Peart, J. Phys. Chem. Solids, 26, 1853 (1965).

26A D. I. Bolef and J. de Klerk, J. Appld. Phys., 33, 2311 (1962).

27A K. G. Kreider and G. Bruggeman, Trans. AIME, 239, 1222 (1967).

28A L. N. Larikov, V. M. Tyshkevich, and L. F. Chernaya, Ukranskii Fizicheskii Zhurnal, 12, 986 (1967).

29A J. F. Smith and C. L. Arbogast, J. Appld. Phys., 31, 99 (1960).

30A J. M. Dupouy, M. Maik, Mlle. Mathie, and Y Adda, Beryllium Technology, Vol. 1, AIME Met. Soc. Conf. Vol. 33. New York: Gordon and Breach (1966), p. 307.

31A C. W. Garland and J. Silverman, Phys. Rev., 119, 1218 (1960).

32A F. Wajda, G. Shirn and H. Huntington, Acta. Met., 3, 39 (1955).

33A L. J. Slutsky and C. W. Garland, Phys. Rev., 107, 972 (1957).

34A P. Shewmon, Trans. AIME, 206, 918 (1960).

35A R. W. Ferris, M. L. Shepard, and J. F. Smith, J. Appld. Phys., 34, 768 (1963).

36A G. A. Alers and J. R. Neighbours, J. Phys. Chem. Solids, 7, 58 (1958).

37A G. Shirn, E. Wajda and H. Huntington, Acta. Met., 1, 513 (1953).

38A G. A. Rayne, Phys. Rev., 115, 63 (1959).

39A J. Hino, C. Tomizuka, and C. Wert, Acta. Met., 5, 41 (1957).

40A T. Ya. Benieva and I. G. Polotskii, Phys. Met. Metallog. 12 [4], 107 (1961).

41A W. Köster, Z. Metall., 35, 194 (1943).

42A J. Sakurai, M. Fujii, Y. Nakamura, and H. Takaki, J. Phys. Soc. Japan, 19, 308 (1964).

43A I. L. Eganyan and Ya. P. Selisskii, Sov. Phys.-Dokl., 12, 269 (1967).

44A C. H. Cheng, J. Phys. Chem. Solids, 28, 413 (1967).

45A H. A. Domian and H. I. Aronson, Diffusion in B.C.C. Metals. Metals Park: Amer. Soc. for Metals, 1965, p. 209.

46A G. M. McManus, Phys. Rev., 129, 2004 (1963).

47A Y. A. Chang, J. Phys. Chem. Solids, 28, 2117 (1967).

48A R. J. Wasilewski, Trans. AIME, 236, 445 (1966).

49A J. P. Hirth and J. Lothe, Theory of Dislocations. New York: McGraw-Hill, 1968, Chapter 13.

50A L. J. Teutonico, Phil. Mag., 15, 959 (1967).

51A E. Aerts, P. Delavignette, R. Seims, and S. Amelinckx, J. Appld. Phys., 33, 3078 (1962).

52A A. F. Orlov and S. G. Fedotov, Phys. Metals Metallog., 22 [1] (1966).

53A W. Köster and W. Rauscher, "Relations Between the Modulus of Elasticity of Binary Alloys and Their Structure", National Advisory Committee for Aeronautics (U.S.A.), Tech. Memo. No. 1321 (Nov., 1951).

54A B. Golding, S. C. Moss, and B. L. Averbach, Phys. Rev., 158, 637 (1967).

55A T. Watanabe and S. Karashima, Trans. Japan Inst. Metals, 9, Supplement 242 (1968).

56A R. J. Borg, J. Appld. Phys., 35, 567 (1964).

57A M. C. Inman, D. Johnston, W. L. Mercer, and R. Shuttleworth, Proc. 2nd Radioisotope Conference, Oxford, 1954; J.E. Johnston (ed), p. 85. Academic Press, New York (1954).

58A K. Monma, H. Suto, and H. Oikawa, J. Japan Inst. Metals, 28, 192 (1964).

59A ibid., p. 188.

60A J. I. Goldstein, R. E. Hanneman, and R. E. Ogilvie, Trans. AIME, 233, 812 (1965).

61A J. E. Reynolds, B. L. Averbach, and M. Cohen, Acta Met., 5, 29 (1957).

62A A. E. Berkowitz, F. E. Jaumot, and F. C. Nix, Phys. Rev., 95, 1185 (1954).

63A H. Bückle, Z. Electrochem, 49. 238 (1943).

64A A. B. Kuper, D. Lazarus, J. R. Manning, and C. T. Tomizuka, Phys. Rev., 104, 1536 (1956).

65A R. Hultgren, R. L. Orr, P. D. Anderson, and K. K. Kelley, Selected Values of Thermodynamic Properties of Metals and Alloys, p. 719 J. Wiley, New York (1963).

66A P. S. Dobson, P. J. Goodhew, and R. E. Smallman, Phil. Mag., 16, 9 (1967).

67A J. P. Tartour and J. Washburn, Phil Mag, 18, (1968).

68A V. C. Kannan and G. Thomas, J. Appl. Phys., 38, 4076 (1967).

69A P. Humble, M. H. Lorretto and L. M. Clarebrough, Phil. Mag., 15, 297 (1967).

70A B. E. P. Beeston, I. L. Dillamore and R. E. Smallman, Met. Sci. J., 2, 12 (1968).

71A G. F. Bolling, L. E. Hays, and H. W. Weidersich, Acta Met., 10, 185 (1962).

72A W. Charnock and J. Nutting, Metal. Sci. J., 1, 123 (1967).

73A T. Jøssang and J. P. Hirth, Phil. Mag., 14, 657 (1966).

74A P. Humble, R. L. Segall, and A. K. Head, Phil. Mag., 15, 281 (1967).

75A P. R. Thorton, T. E. Mitchell, and P. B. Hirsch, Phil. Mag., 7 1349 (1962).

76A I. L. Dillamore, R. E. Smallman, and W. T. Roberts, Phil. Mag., 9, 517 (1964).

77A P. C. J. Gallagher and J. Washburn, Phil. Mag., 14, 971 (1966).

78A L. M. Clarebrough, R. L. Segall, and M. H. Loretto, Canad. J. Phys., 45, 1135 (1967).

79A L. K. Ives, and A. W. Ruff, Jr., Phys. Stat. Sol., 27, 117 (1968).

80A M. Wilkens, M. Rapp, and K. Differt, Z. Metallkunde, 57, 746 (1966).

81A S. Major, Jr., Japan J. Appld. Phys., 7, 574 (1968).

82A A. Howie and P. R. Swann, Phil. Mag., 6, 1215 (1961).

83A G. Thomas, J. Aust. Inst. Met., 8, 80 (1963).

84A P. C. J. Gallagher, "Influence of Alloying, Temperature and Related Effects on the Stacking Fault Energy", presented at Spring Conf. AIME (May 14, 1969).

85A J. Harris and B. Masters; data presented by R. E. Smallman, I. L. Dillamore and P. S. Dobson, J. de Physique, 27, Supple. C3, 86 (1966).

86A B. E. P. Beeston and L. K. France, J. Inst. Metals, 96, 105 (1968).

APPENDIX FIGURE CAPTIONS

A1. Shear Modulus of α-Fe (data from E measurements of randomly oriented Fe - 6% Si).

A2. Tracer Diffusivity and Elastic Strain Energy for Vacancy Diffusion in Para- and Ferromagnetic α-Fe.

A3. Chemical Interdiffusivity $\tilde{D}$ of Au-Ni Alloys at 860°C.

A4. A Comparison of Tracer Diffusivity in NiAl (54% Al) with the Value of Chemical Interdiffusivity Assumed for Creep Data Analyses (Eq. A9).

A5. Temperature Dependence of $\partial \ln a_{Cu} / \partial \ln N_{Cu}$ for β-CuZn.

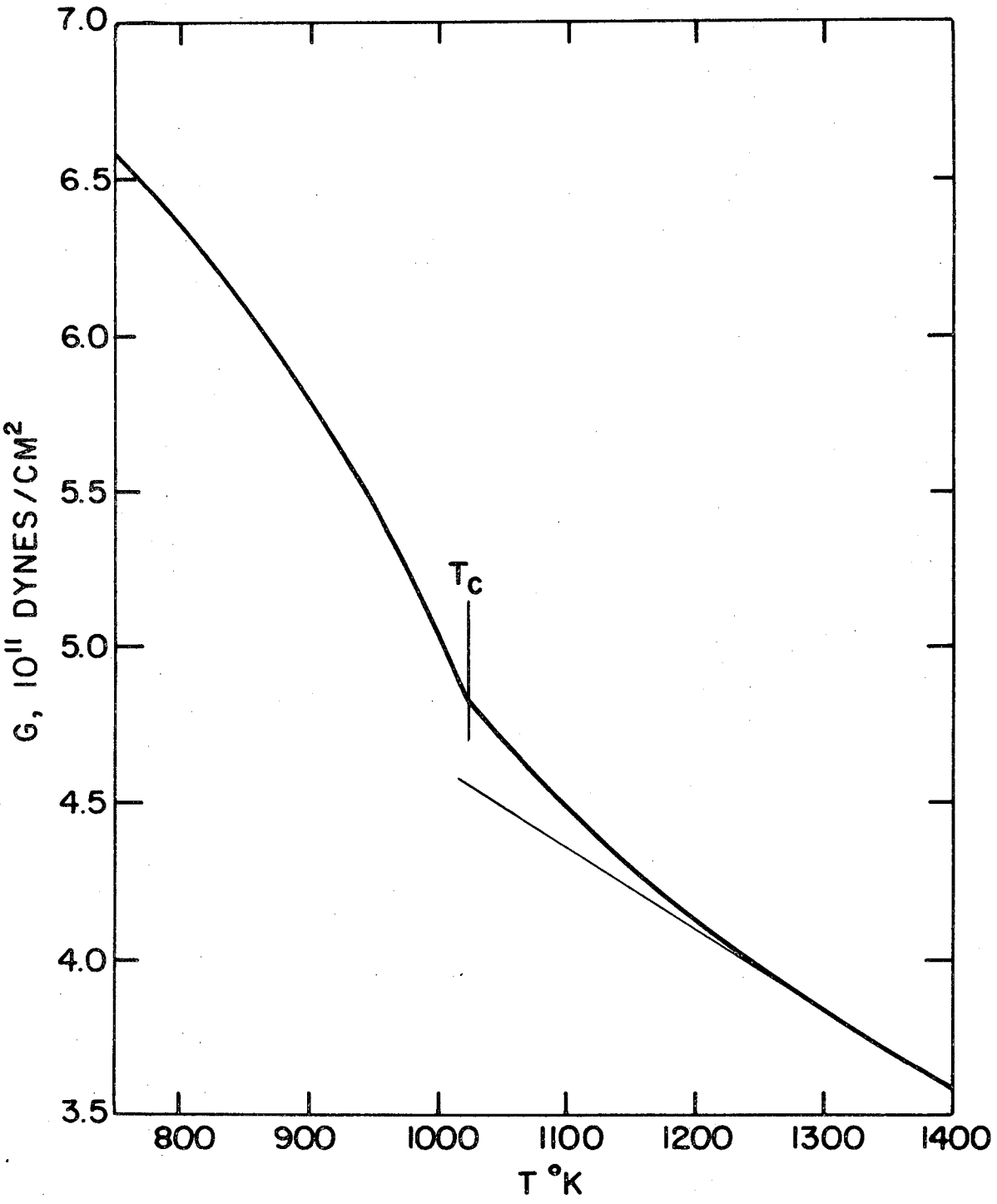

XBL 697-901

Fig. A1

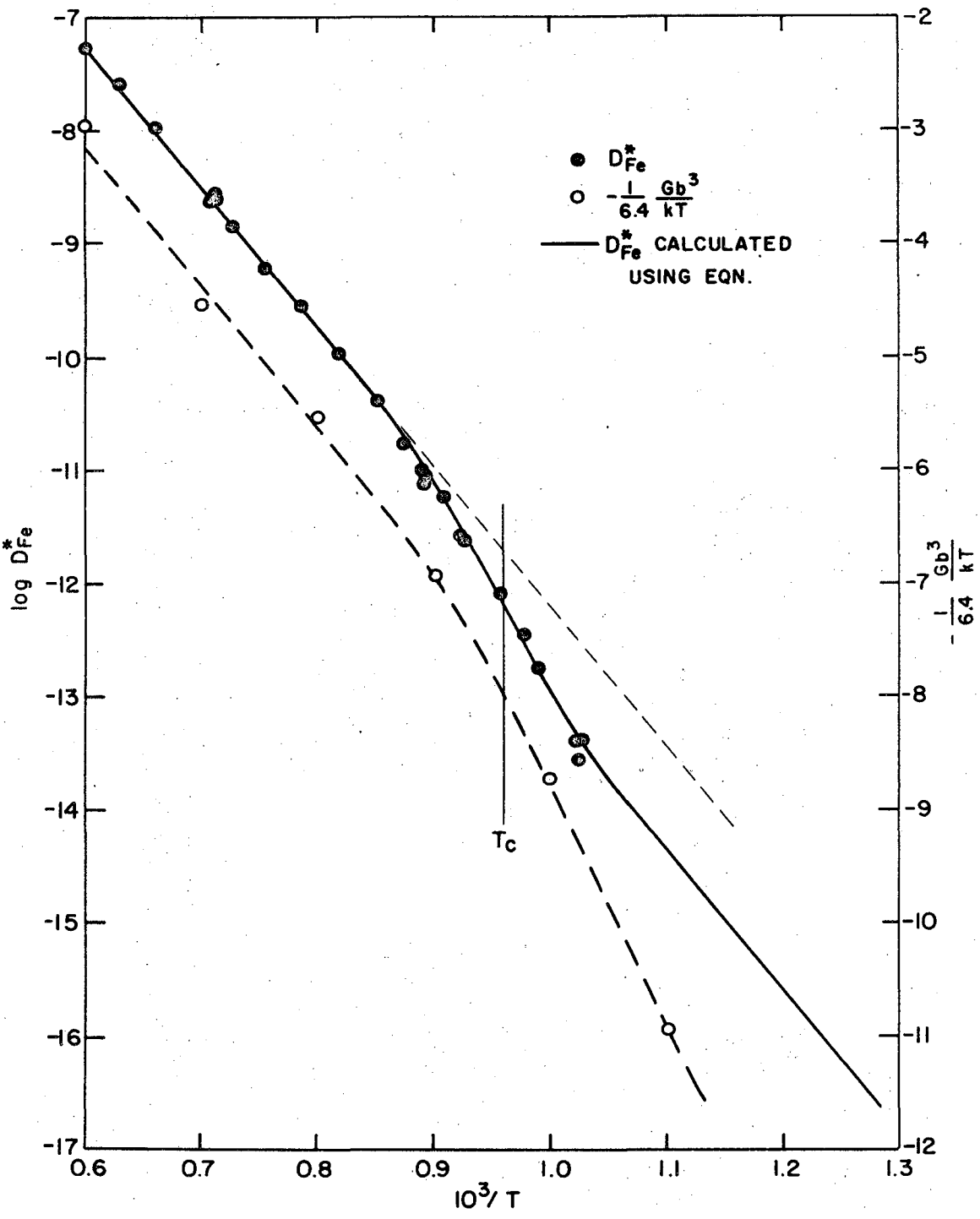

XBL 697-902

Fig. A2

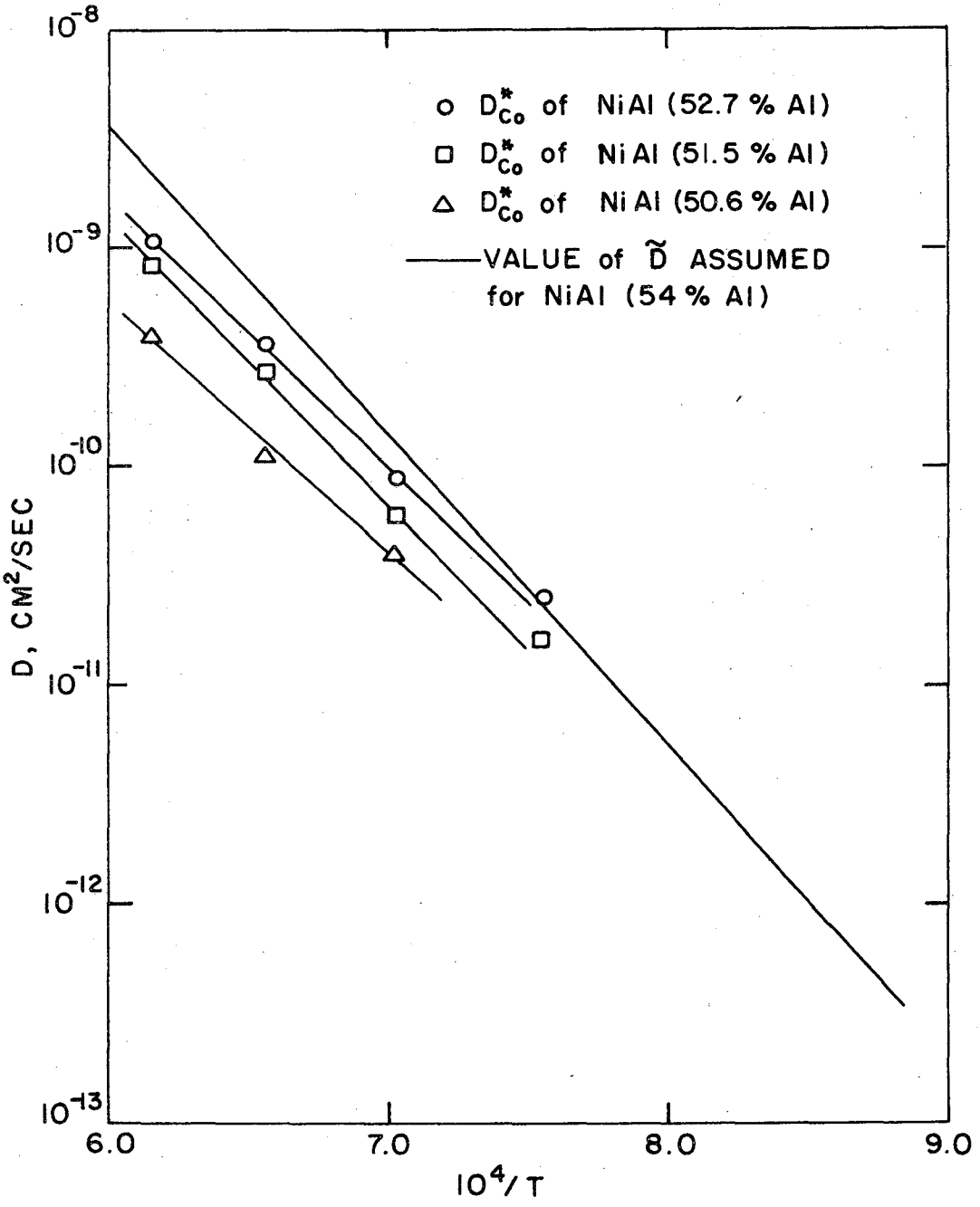

XBL 697-903

Fig. A3

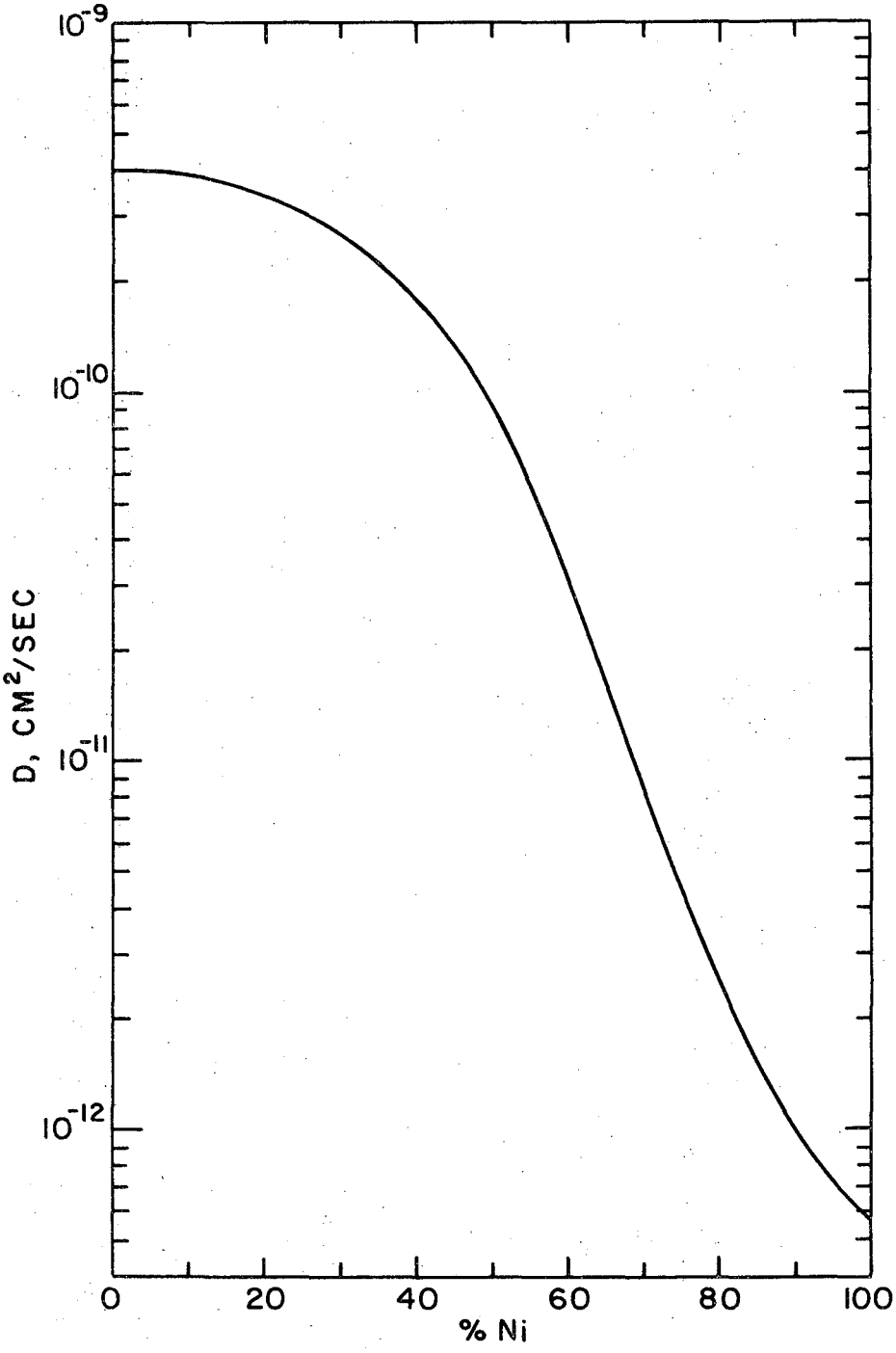

Fig. A4

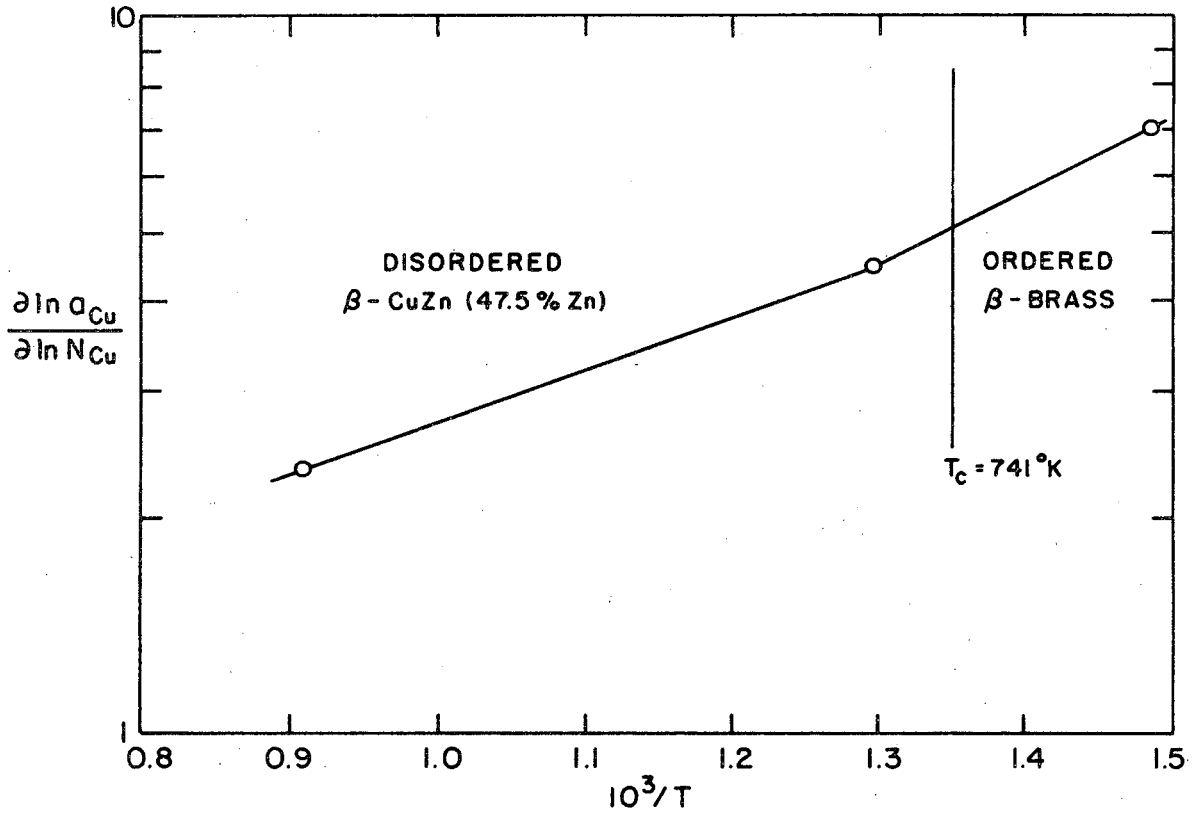

XBL 697-905

Fig. A5

TECHNICAL INFORMATION DIVISION
LAWRENCE RADIATION LABORATORY
UNIVERSITY OF CALIFORNIA
BERKELEY, CALIFORNIA 94720